SATURATION AND FOAMING OF THERMOPLASTIC NANOCOMPOSITES USING SUPERCRITICAL CO_2

William Carl Strauss, B.S.

Thesis Prepared for the Degree of

MASTER OF SCIENCE

UNIVERSITY OF NORTH TEXAS

May 2005

APPROVED:

Nandika A. D'Souza, Major Professor
Witold Brostow, Committee Member
Richard F. Reidy, Committee Member
Donald Purinton, Committee Member
Mike Kaufman, Chair of the Department of Materials Science and Engineering
Sandra L. Terrell, Dean of the Robert B. Toulouse School of Graduate Studies

Strauss, William C., *Saturation and foaming of thermoplastic nanocomposites using supercritical CO_2*. Master of Science (Materials Science and Engineering), May 2005, 118 pp., 8 tables, 46 illustrations, references, 143 titles.

Polystyrene (PS) nanocomposite foams were prepared using supercritical fluid (SCF) CO_2 as a solvent and blowing agent. PS was first in-situ polymerized with a range of concentrations of montmorillonite layered silicate (MLS). The polymerized samples were then compression molded into 1 to 2mm thick laminates. The laminates were foamed in a batch supercritical CO_2 process at various temperatures and pressures from 60°-85°C and 7.6-12MPa. The resulting foams were analyzed by scanning electron microscopy to determine effect of MLS on cellular morphology. Differential scanning calorimetry was used to determine the impact of nanocomposite microstructure on glass transition of the foamed polymer. X-ray diffraction spectra suggested that the PS/MLS composite had an intercalated structure at both the 1% and 3% mixtures, and that the intercalation may be enhanced by the foaming process.

ACKNOWLEDGEMENTS

Dr. D'Souza, for providing me with guidance and training to pursue this research, and for continually motivating me towards success in graduate school and in life.

Dr. Reidy, for his teaching and advice on everything from phase diagrams to draught beer, and especially for the use of his laboratory and supercritical reactor.

Dr. Brostow, for his authority on the subjects of polymers and thermodynamics.

Dr. Purinton, for mentoring me in my career as well as in academics, and for always helping me to stay focused on the important things in life.

David Garrett, for his training and assistance with electron microscopy.

Alberta Caswell, who has made my experience in the Materials Science and Engineering Department an enjoyment each semester.

Greg Wolf, and Applied Aerodynamics, Inc., for tuition assistance and for the flexible work schedule I needed to complete this thesis.

My parents, who have come with me every step of the way, even through the many storms that they might have warned me against.

My sisters, for their never-ending faith and constant encouragement.

My friends, who have given me the time and space I have needed to complete this work, as well as the times and places to get away from it all.

Eryn, for love and support, and for listening for hours about things like montmorillonite.

Natalie, my daughter and greatest inspiration;

May Providence shape me into the father she needs me to be.

TABLE OF CONTENTS

LIST OF TABLES

LIST OF FIGURES

LIST OF PREVIOUSLY PUBLISHED MATERIALS

Sections 3.1-3.3, 4.1, and 4.4: Reprinted with permission of Sage Publications Ltd, from "Supercritical CO_2 Processed Polystyrene Nanocomposite Foams," W. Strauss and N.A. D'Souza, *Journal of Cellular Plastics*, Vol. 40, pp229-241, Copyright (© SAGE Publications, 2004).

Figures 3, 4: Reprinted with permission of Springer Science and Business Media, Copyright (© Springer-Verlag Berlin Heidelberg, 1999).

Figures 5, 10: Reprinted with permission of Elsevier, Copyright (© Butterworth-Heinemann, 1994).

Figure 9: Reprinted with permission of John Wiley & Sons, Inc, Copyright (© John Wiley & Sons, Inc, 1992).

Figure 11: Reprinted with permission of John Wiley & Sons, Inc , Copyright (© John Wiley & Sons, Inc, 2002).

Figure 12: Reprinted with permission of John Wiley & Sons, Inc , Copyright (© John Wiley & Sons, Inc, 1976).

Figure 14: Reprinted with permission of John Wiley & Sons, Inc , Copyright (© John Wiley & Sons, Inc, 1992).

Figure 15: Reprinted with permission of John Wiley & Sons, Inc , Copyright (© John Wiley & Sons, Inc, 1994).

Figures 16, 29: Reprinted with permission of Dr. Zhang Yi, Copyright (© Zhang Yi, 1997).

Figure 18: Reprinted with permission of John Wiley & Sons, Inc, Copyright (© John Wiley & Sons, Inc, 1998).

Figure 30: Reprinted with permission of American Chemical Society, Copyright (© American Chemical Society, 1989).

Figure 31: Reprinted with permission of Dr. Michael F. Vincent, Copyright (© Michael F. Vincent, 1997).

Figure 32: Reprinted with permission of Elsevier, Copyright (© Elsevier Science B.V., 2001).

Figure 33: Reprinted with permission of Dr. Xiangmin Han, Copyright (© Xiangmin Han, 2000).

Figure 34: Reprinted with permission of John Wiley & Sons, Inc , Copyright (© John Wiley & Sons, Inc, 2001).

Figure 35: Reprinted with permission of John Wiley & Sons, Inc , Copyright (© John Wiley & Sons, Inc, 1982).

Figure 36: Reprinted with permission of John Wiley & Sons, Inc , Copyright (© John Wiley & Sons, Inc, 1994).

1. INTRODUCTION

1.1. Polymer Foams

Polymer foams are a relatively young family of synthetic materials, the first vinyl foams having been developed in the 1930s. Since their discovery, however, foam manufacturing has grown into a multi-billion dollar industry worldwide. According to the US 1997 economic census, the value of just the polystyrene foam products manufactured in the United States at that time was approximately 5 billion dollars.[1] By 2006, the US domestic market for plastic foam stock alone will be over 8 billion pounds annually.[2] Foams have become such an integral part of modern life that they are often taken for granted; nonetheless, it is difficult to imagine upholstery or bedding without foam cushions, refrigerators or ice chests without foam insulation, life preservers or buoys without foam flotation. Plastic foams are used in virtually every sector of technology, and while the major traditional markets for foam materials continue to be packaging, insulation, cushioning, and safety, new foam materials and applications are continually being developed.

Foam materials are categorized by several different criteria. Morphologically they are generally divided into either closed-cell or open-cell. Closed-cell foams contain discrete voids, or bubbles, that do not interconnect with each other. Open-cell foams, on the other hand, contain interconnected voids within a strut-like structure. Closed-cell foams exhibit superior properties for applications such as insulation, flotation, food packaging, and load bearing structures. Open-cell foams are well suited for porous

applications such as sponges and filters, or for compressible applications such as cushions or soft packaging. Physically, foams are divided into flexible and rigid, although this distinction is primarily a function of the plasticity of the polymer foam precursor. Flexible and semi-flexible foams contain polymer with a glass transition (T_g) below their service temperature, while rigid foams have a T_g above their service temperature. Structural foams are a subcategory of rigid, closed-cell foams, developed specifically for maximum mechanical properties. The foam discussed in this work is a structural foam with added nano-scale reinforcement to further improve mechanical, as well as other properties.

Foams are also categorized by manufacturing process. The common premise of foam manufacture is the coalescence and expansion of a gas phase (or "blowing agent") supersaturated within a liquid phase of foam precursor. Differences between the various specific foaming methods lie in the sources and types of the blowing agents used. Of these agents, two primary classes exist: chemical and physical. Chemical blowing agents are reactive components that generate gas when activated, either through mixing and/or heating. Frequently used chemical agents are organic nitrogen compounds such as azodicarbonamide, which when reacted generates nitrogen gas. The chemical reaction is exothermic, and the hot, high pressure nitrogen gas generated is not by itself conducive to the growth of stable foam microstructure. For that reason, polymers used with chemical foaming processes are typically thermosetting, cross-linking resins that can cure at high temperatures during the foaming process, effectively freezing the bubbles of nitrogen in place.[3]

Thermoplastic materials, which have become popular for their short processing times and ease of recycling, are primarily foamed using physical blowing agents. Physical blowing agents are preferably inert, and with a low boiling point so as to provide the most vapor pressure for foam expansion at processing conditions. Physical blowing is a two step process: first, blowing agent is introduced into the polymer precursor through mixing and/or diffusion (often at high pressures) followed by foam expansion via either a decrease in process pressure (quench) or an increase in temperature. In many cases, blowing agent is introduced into the polymer in densified phase such as liquid or supercritical fluid (SCF) and the phase transition to gas is used to create the supersaturated conditions required for foam nucleation and growth. For many years, the most efficient and least expensive physical foaming processes involved the use of chlorofluorocarbons (CFCs) which are desirable for their low boiling temperatures, low flammability, low toxicity, and inert behavior. Unfortunately, CFCs are at the top of the list of ozone depleting substances (ODS) that have been judged harmful to the earth's atmosphere. In 1987, the landmark Montreal Protocol set into motion a worldwide phase-out of CFC usage. Alternative physical blowing agents include inert gasses such as CO_2 and N_2, as well as some hydrocarbons such as pentane and cyclopentane. It should be noted, however, that hydrocarbon usage also has a negative environmental impact, as well as contributing to foam flammability.[4] The emphasis of the current work is therefore to develop foam technology using carbon dioxide as a safe, environmentally friendly, physical blowing agent.

1.2. Nanocomposites

A nanocomposite may be defined as a composite mixture in which at least one of the dimensions of one of the component materials is in the nanometer range (10^{-9}m). As with other composite materials, polymer nanocomposites consist of a host material, or matrix, which is reinforced by a secondary phase, typically a fiber or platelet of another material that contributes, among other things, a higher level of rigidity to the net material when distributed throughout the matrix. One popular example of such nano-scale reinforcement is the carbon nanotube, each typically 1-2 nm in diameter while as much as 1,000,000 nm in length. In the current work, a nanocomposite is presented which is made up of a polystyrene matrix reinforced by surfactant-treated montmorillonite layered silicate (MLS). Each montmorillonite platelet is approximately 1nm thick and between 200-1000nm long. The ratio of length and/or width over thickness of a reinforcement is referred to as aspect ratio; high aspect ratio is one requirement of an effective composite reinforcement. It has been shown that polystyrene reinforced with low weight percentages of MLS (<9%) can be processed to exhibit an increase in mechanical properties such as tensile strength, modulus, and impact strength.[5] The minute size of nanocomposite reinforcements is the secret to their importance in the development of composite foams. Because the platelets are small in relation to the size of foam cells, they are able to rearrange themselves in the matrix material during the foaming process without inhibiting the development and expansion of the foam.[6] Prior to the discovery of nanocomposites, manufacture of foams with macro-scale fiber reinforcements was

attempted, but in those cases, the long fibers limited foam growth to high densities and had a detrimental effect on the overall physical properties of the resultant materials.

1.3. Nanocomposite Foams

Nanocomposite thermoplastic foams are a newly developed group of polymeric materials that have rapidly become a vital focus of materials research. The primary benefits of these foams lie in their unique combination of high strength to weight ratio, thermal stability, and tailorable electrical and chemical properties. They hold great potential for use in structural applications such as foam core panels, self-skinning molded parts, and impact tolerant structures for the aerospace industry, as well as in applications that take advantage of other properties such as low vapor permeability, controlled chemical release, and thermal insulation. Later uses might include insulated food packaging, biochemical hazard containment, or self medicated bone implants, to name a few.

Facilitating the development of nanocomposite foams is the technology of foam generation with supercritical CO_2 ($scCO_2$), which has become a popular topic of research over the past decade, and has been shown to have many attractive advantages over other physical foaming methods.[7,8,9,10] Because $scCO_2$ methods permit foaming of solid samples without requiring that they be completely melted or dissolved, carefully prepared nanocomposite thermoplastics may now be foamed without destroying their finely mixed microstructure. Also, the $scCO_2$ foaming process is environmentally benign, and involves no toxic chemicals.

While the potential for nanocomposite thermoplastic foams is seemingly endless and evermore appealing, their technical development is rigorous and multi-disciplinary. The optimization of nanocomposite foams requires a well rounded knowledge of thermodynamics, mass transfer, mechanics of materials, foam nucleation and growth, polymer processing, rheology, nanocomposite chemistry, and supercritical fluids. This thesis attempts to address these disciplines by first discussing individually the subjects of nanocomposite polymers, supercritical fluids, and thermoplastic foams, and subsequently integrating these three into the discussion of a new and original engineered material. At issue in the current work are the specific mechanical and thermal benefits of nanocomposite foam, as well as the benefits of a simple isochoric $scCO_2$ process for batch production of these foams.

1.4. Scope

The nanocomposite foam presented in this thesis is montmorillonite-reinforced polystyrene prepared by in-situ polymerization of styrene in the presence of surfactant-treated montmorillonite. Polystyrene was chosen for this study because it is a well-understood and readily synthesized polymer with abundant applications in industry. Secondly, its amorphous nature facilitates examination of the effects of nanocomposite microstructure on the foam morphology without requiring consideration of the possible effects of crystallinity within the polymer itself. Finally, in highly crystalline polymer systems, $scCO_2$ diffusion may be limited by the crystal structure.[11]

The basic foaming method used for this study is a constant temperature, variable pressure process that derives from previous work, first by Goel and Beckman[7,8], and

more recently by Zeng et al.[12] In the former work, very high pressures (25-35 MPa) and low temperatures (40°C) were used to successfully create microcellular polymethyl-methacrylate (PMMA) foams with cell diameters 1-10 μm. In the later work, relatively low pressures (8.3 MPa) and high temperatures (120°C) were used to successfully create macrocellular polystyrene/nanosilicate (PS+MLS) foams with cell diameters 10-50 μm. In this study, macrocellular foams are formed using low to moderate pressures (7.6-12 MPa) and temperatures (60°-85°C) in order to investigate the effects of MLS presence on foam nucleation, growth, and microstructure. Analysis techniques used for this investigation include differential scanning calorimetry (DSC), X-ray diffraction (XRD), scanning electron microscopy (SEM), and dynamic mechanical analysis (DMA).

2. LITERATURE REVIEW

2.1. Nanocomposites

The discovery of nanocomposite materials has been attributed to Okada et al. for their work with montmorillonite reinforced nylons at Toyota in 1989.[13] At the time, montmorillonite layered silicate (MLS) was already in use by the plastics industry as a filler, but its reinforcing potential could not be exploited because in their natural state, MLS platelets do not interact chemically with polymer molecules. Figure 1 shows schematically some of the ways in which nano-reinforcements can disperse in a polymer matrix. Because there are weak attractions between MLS platelets themselves, they will tend to coagulate if there is no interaction with the matrix. In this first case, macrostructures of MLS additive act as immiscible fillers in the polymer host. What the researchers at Toyota discovered, however, is that if the MLS is first treated with an organophilic surfactant prior to mixing with a polymer, the polymer molecular chains will be able to migrate in between the reinforcing platelets and interact with the surfactant molecules. This creates an intercalated dispersion, in which the MLS platelets still interact with each other while at the same time swelling to accommodate interactions with the polymer host. Intercalated dispersions of high aspect-ratio nanoparticles have been shown to considerably increase the mechanical and thermal properties of polymer systems.[13,14] In idealized nanocomposite dispersions, interaction between reinforcements and matrix are so great that individual reinforcements become completely exfoliated from one another and are evenly distributed throughout the composite mixture. Such exfoliated

systems are possible only if there is virtually no attraction between the reinforcing platelets (or if there is in fact a repulsion between them), but systems with a mixture of both intercalated and exfoliated behavior are quite common (Figure 1).

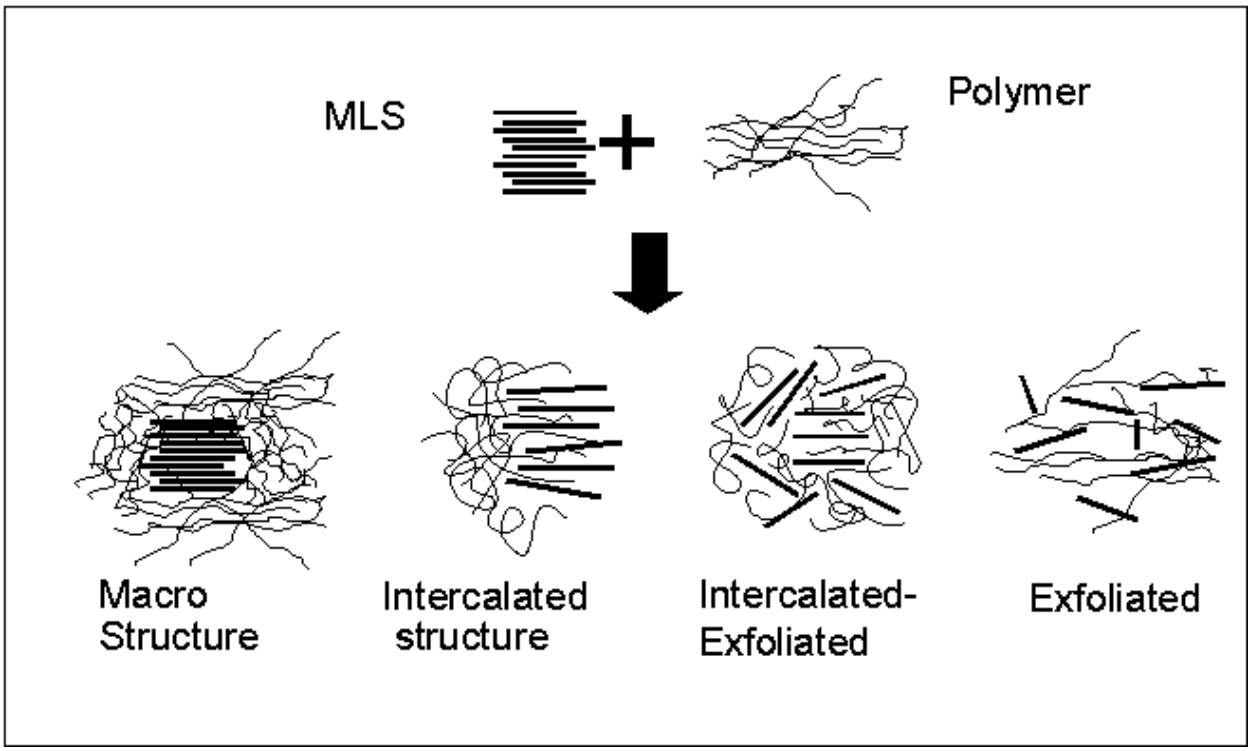

Figure 1: Various possible dispersions of montmorillonite layered silicate (MLS) within a polymer matrix nanocomposite.[15]

In order to optimize dispersion of nano-reinforcements within the matrix, the preparation of a polymer nanocomposite becomes a nontrivial endeavor. Four basic approaches have been explored in literature: in-situ intercalative polymerization, polymer melt intercalation, solution intercalation, and in-situ silicate formation. In-situ intercalative polymerization has been the dominant focus of most research, because it provides for the highest level of polymer / reinforcement interaction, and because it is a batch process that lends itself to common laboratory techniques. In this process,

monomer is first mixed with treated nano-reinforcement, and then polymerized. The highly mobile organic mers are therefore able to interact with, swell, and perhaps even exfoliate silicate nano-platelets in a low viscosity environment prior to polymerization. Successful intercalated and exfoliated nanocomposites generated with this method have been widely reported.[13,16,17] Along with higher degrees of intercalation, in-situ methods offer the flexibility of being compatible with both thermosetting and thermoplastic systems. Polymer melt intercalation is a general term used to describe a nanocomposite in which a thermoplastic matrix is polymerized in bulk prior to mixing with a nano-reinforcement. After polymerization, the polymer is melted and mixed with reinforcement via any combination of several methods including high shear, elevated temperatures, and plasticizing solvents. The primary advantage of melt intercalation is that it is compatible with high volume plastic manufacturing processes such as extrusion and injection molding. A second advantage is that it permits the use of highly controlled batches of polymer with very low molecular weight distributions. Melt intercalation is faced with the challenge of providing enough energy and molecular mobility to the polymer chains to enable them to interact efficiently enough with the nano-platelets to form intercalated dispersions; however, despite this difficulty, melt intercalated nanocomposites have been successfully prepared in both laboratory and commercial operations.[18,19,20] Solution intercalation is similar to melt intercalation, except that the polymer and nano-reinforcements are completely dissolved in an organic solvent. Nanocomposites precipitate from the solution as the solvent is evaporated. In-situ silicate

formation is a novel method wherein nano-silicate platelets are crystallized in-situ within an aqueous polymer gel.[21]

2.2. Montmorillonite Layered Silicate (MLS)

Montmorillonite layered silicate is the most common silicate material currently being used in the synthesis of polymer nano-composites. Named after the French town of Montmorillon, where it was first discovered, montmorillonite is the common name for hydrated sodium calcium aluminum silicate. It is a mineral of the smectite clay group, in the structural family of phyllosilicates. The term 'phyllosilicate' refers to the entire family of layered silicates that includes such common minerals as talcs, micas, and clays; its prefix phyllo- is derived from 'phyllon,' the Greek word for leaf. On the microscopic scale, phyllosilicates are composed of layers of crystalline platelets separated by small inter-laminar gaps called galleries. Each platelet is in turn made up of alternating layers of two primary substructures; sheets of tetrahedral silica fused to sheets of octahedral alumina or magnesia (figure 2). The reason for the great variety of materials and material properties found within the phyllosilicate family is that they may contain numerous different combinations of silica and metal oxide sheets (polymorphism), as well as different substitutionary elements present within the inter-laminar galleries and/or within the sheet lattices themselves (isomorphic substitution).

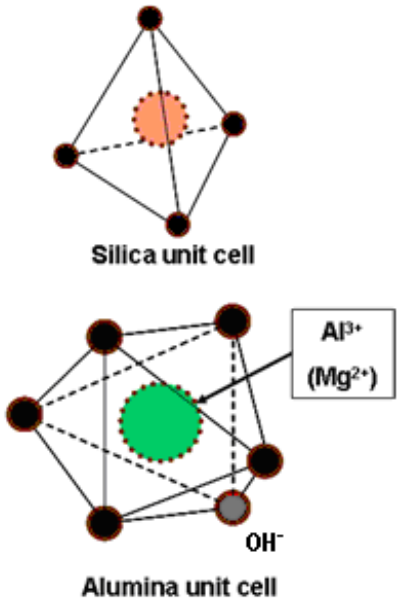

Figure 2: Unit cell structures found in montmorillonite layered silicate (MLS).

The most common arrangements of tetrahedral and octahedral layers in phyllosilicates are 1:1, 2:1, and 2:1:1. Smectite minerals, including montmorillonite, are clay materials with a two to one (2:1) phyllosilicate structure; in each platelet of a smectite, one octahedral sheet is sandwiched between two tetrahedral sheets. Bonding of the sheets to each other is facilitated by a charge imbalance in the silica tetrahedra caused by periodic vacant silicon sites. The imbalance permits apical oxygen atoms in the silica lattices to be shared with the octahedral sheet through isomorphic substitution of OH^- ions. The resultant sandwich structures are electrically balanced and approximately 1nm (10^{-9}m) thin, with basal O^{2-} atoms within the silica lattice exposed on both surfaces. The uncharged platelets are stacked loosely together, bound only by van der Wals forces. In nature, additional vacancies and/or ionic substitutions in either octahedral or tetrahedral unit cells can produce permanent negative charges in the assembled platelets. In smectites, the intensity of these charges ranges between 0.2 and 0.6 charges per unit cell,

attracting hydrated metal cations to inhabit the galleries between the platelets. Because the charge density is relatively small (in comparison with mica, for instance, which has 0.6-1.0 charges per unit cell), in most cases the hydrated cations do not become tightly bound to the platelet surfaces, and they may be exchanged with other cations outside of the galleries. Also, as the level of hydration around the platelets changes, the thickness of the hydrated layer around the gallery cations changes. Therefore, smectite galleries expand in hydrated conditions, and contract in dehydrated conditions. For this reason, smectites are often called 'swelling' clays.

Montmorillonite is a smectite with a dioctahedral silica/alumina sandwich structure. In the ideal, uncharged dioctahedral sheet, trivalent Al^{3+} occupies two out of every three available octahedral cells, leaving one vacant. In montmorillonite, however, some of the Al^{3+} sites in the octahedra are replaced by Mg^{2+} and/or other divalent cations (see figures 2, 3). These substitutions are the primary source of permanent charges within MLS. It should be noted that in a pristine environment, Mg^{2+} is the dominant substitutionary ion in MLS; however, in mixed soil samples, Fe^{2+} or other common metals constitute a considerable portion of the substitutionary ions in the octahedral lattices, depending on their local prevalence. MLS platelets typically range in diameter from 70nm to 1000nm, even though they are very thin (1nm). The ratio of major dimension to minor dimension is termed aspect ratio, and the aspect ratio of MLS is higher than that of virtually any other naturally occurring soil particle. Such a large aspect ratio provides a high specific surface area for adsorption of cationic species. To

put the amount of surface area in perspective, it has been estimated that one gram of MLS has enough surface area to cover 8 football fields!

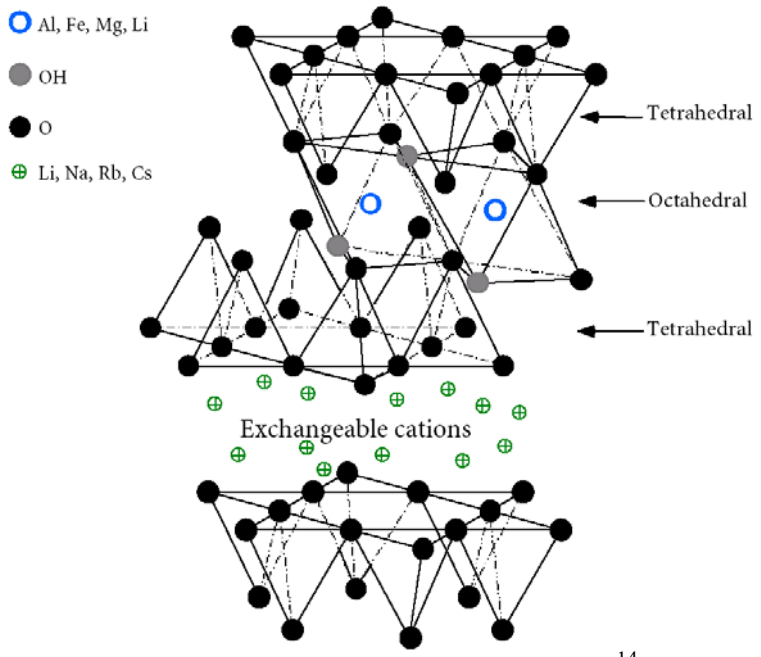

Figure 3: Crystaline layered microstructure of montmorillonite.[14]

The terms ‘montmorillonite’ and ‘smectite’ have occasionally been used interchangeably in industry, due to the fact that natural specimens of smectite never contain purely one mineral, but are composed of mixtures of MLS and other smectites with similar behavior, such as hectorite, saponite, or beidellite, not to mention small quantities of other phyllosilicate clays, such as illite or glauconite. Bentonite is an ore found in deposits of volcanic ash that is rich in MLS, and is also occasionally referred to interchangeably with montmorillonite; however, bentonite is not a mineral, but rather an agglomerate of swelling clays and other silicates. MLS is in fact the specific smectite with the most ideal swelling properties and the highest cation exchange capacity (CEC)

of the group; hence it has become the most popular and advertised of all the swelling clays. The reason that MLS out-performs other smectites is linked to its dioctahedral permanent charge, and the fact that because it has very little tetrahedral charge, it does not trap cations at the surface of its tetrahedral sheets. Nonetheless, commonly available MLS typically contains an unspecified concentration of other smectite minerals.

Montmorillonite is readily available due to its common occurrence in nature and its usefulness in a multitude of applications. Because of its high absorption of metal cations, MLS is effective for filtration, absorption, and containment of toxic heavy metals. It is frequently used to dam against toxic waste, and to purify water. In health care, it is used to absorb drugs for slow release into the body, and it is sometimes taken as a dietary supplement to help cleanse the body of latent toxins. Since most of the cations in its galleries are hydrated or hydrateable, MLS (and especially MLS with Na^{2+} gallery cations) is strongly hydrophilic by nature. For this reason, along with its high aspect ratio, it is the preferred thickening agent for aqueous solutions ranging from oil drilling mud to cosmetics! Montmorillonite is also used as a filler in plastics, and as a nanoscale reinforcement, as in the present work, but not in its naturally occurring form.

Because MLS is hydrophilic, it is naturally immiscible with organic polymer materials. In order for it to be useful as an additive to thermoplastics, it must be organically modified by the addition of organophilic surfactants. These surfactants are cationic, and migrate into the galleries where they are substituted in place of hydrated cations. The most common surfactants used with MLS are alkylammonium and alkylphosphonium salts. Figure 4 depicts the way in which these surfactants can reorient

themselves to facilitate the swelling of the MLS galleries and the intercalation of organic polymer species.

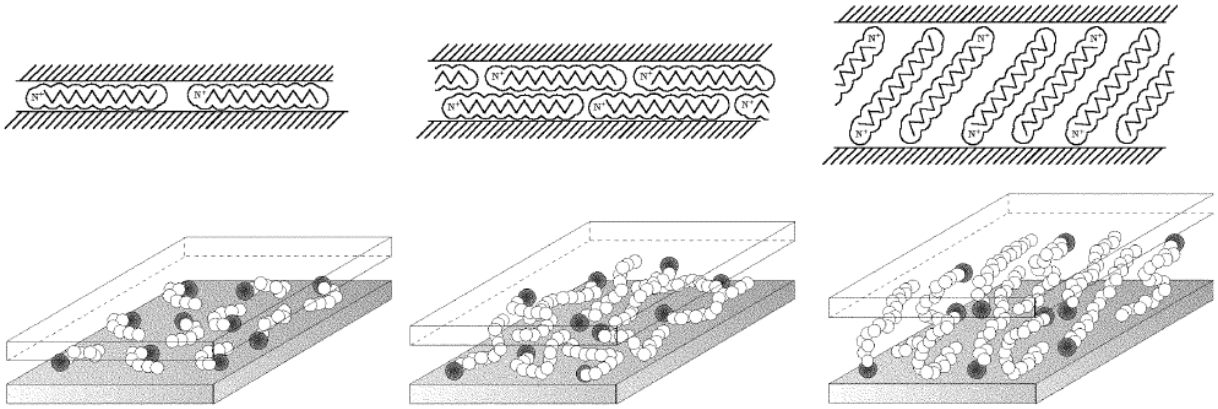

Figure 4: Intergallery swelling of montmorillonite organophilic surfactant (depicted with dark cationic "heads" and long aliphatic "tails").[14]

2.3. Structural Foams

The term "structural foam" has become commonly associated with high density injection molded parts incorporating an integral cellular core. In such applications, the advantages provided by the integral foam regions are primarily reduction of weight, reduction of material used per part, and improvement of shrink characteristics during cooling. In this work, the term "structural foam" is extended to include any low density polymer foam designed for structural applications. In this sense, molded parts, foam slabstock, and laminated sandwich core materials may all be examples of structural foams.

Structural foam technology has advanced rapidly over the past decade, yet the pace of materials research has been outstripped by a constantly increasing demand for stronger, lighter, and more highly engineered foams for product applications in

transportation, medicine, architecture, and consumer electronics. For example, in the aerospace industry, structural foams have been targeted to replace outdated technology in the design of wing structures, cabin interiors, control surfaces, and protective fairings. The studies of fatigue, fracture toughness, and environmental aging have all helped to encourage this transition as they have slowly exposed the limitations of traditional sheet metal technology and the potential for improvements and optimization of plastics based composite technology in the arena of structural design. The first structural foams were developed shortly before the onset of WWII, and the need for materials to substitute costly metal components during that era spurred the foam development through the 1950s. Unfortunately, not enough information regarding polymer aging was available at the time, and consequential failures of some misapplied foam materials may be partially responsible for the slow growth of structural foam technology between the 1960s and 1980s. Today, however, the beneficial properties of structural foams, such as their immunity to corrosion, resistance to moisture absorption, thermal and electrical insulation, radar transparency, and ease of production all contribute to their ever increasing popularity.

Currently, the most popular resins used in the manufacture of structural foams include polyurethane (PU), polystyrene (PS), polypropylene (PP), polycarbonate (PC), polyvinyl chloride (PVC), acrylonitrile-butadiene-styrene (ABS), styrene-acrylonitrile (SAN), and polyetherimide (PEI). Structural foams are generally considered to be isotropic in nature, and mechanical properties of structural foams are closely related to those of their bulk polymer precursors through relative density (foamed density /

unfoamed density).[22] Structural foams used in sandwich panels have been shown to exhibit stiffness that varies linearly with density at low relative densities.[23] Other factors that influence foam properties include the size, shape, and consistency of the foam cells. Grenestedt's recent and very thorough analyses of foam structure/property relationships are helpful in demonstrating the scope of these influences.[23,24,25] His studies show that variations and randomness in cell wall structures have a dramatic negative impact on bending mode deformations such as foam buckling in compression. Shear properties, which are dependant on stretching mode deformations, are effected to a much lesser extent. Resistance to face buckling of foam cored structures is related to cell size by the relationship:

$$\sigma_f \approx \left(\frac{t_f}{r}\right)^2 \qquad \text{(Equation 1)}$$

where r is the cell radius.[26] Clearly, small cell sizes are preferred for maximum buckling resistance. In summary, microcellular foams, with isotropic behavior and homogeneous cell size distribution, fit the profile for optimized mechanical properties.

Furthermore, nanocomposite structural foams promise to combine the best of two worlds: the research of Okamoto et al. indicates that flow induced alignment of nanocomposite materials during foaming may lead to preferentially reinforced foams with mechanical properties in excess of those predicted by scaling methods and relative density.[27] Additional work conducted by Daming et al. has indicated that the foam forming process may also act as a dispersion mechanism to break up coagulations of

additives at foam nucleation sites and improve nanocomposite dispersion within the foam.[6]

2.4. Supercritical CO2

Supercritical fluid (SCF) is a high temperature, high pressure, physical state of matter that shares characteristics with both liquids and gasses. Like gas, SCF exhibits high diffusivity, low viscosity, and no surface tension, yet, SCF may also be compressed to liquid-like densities and solubilities. SCF can transition to either liquid or gas phase without exhibiting phase separation.[9] The most commonly used SCF is supercritical carbon dioxide ($scCO_2$) because of its abundant supply, inert behavior, and ease of processing. Over the past decade, $scCO_2$ has gained acceptance as an effective solvent for the processing of polymers. Its unique properties now support an ever-growing number of new processing technologies. In the production of thermoplastic foams, the unique properties of $scCO_2$ make it especially well suited for use as both solvent and blowing agent. [7,12,28,29,30,31,32,33,34,35,36] Although many general chemistry texts fail to mention the existence of the supercritical state, geologists now realize that supercritical mixtures of water and silicates in the earth's mantle play a large role in the movement of techtonic plates and the formation of volcanic magma.[37] In fact, $scCO_2$ is also naturally occurring in the earth's crust and can be mined and piped long distances for industrial processes.

The discovery of SCF was originally made by French scientist Cagniard de la Tour in 1822. By 1869, $scCO_2$ had been prepared and preliminarily investigated; shortly thereafter, in 1879, Hannay and Hogarth made the landmark observation of the significance of supercritical ether as a superior solvent. Unfortunately, despite their

promising results, almost a century was to pass before SCFs were put to significant use in industry. By the 1950s, SCF processes had been developed for the extraction of such things as caffeine and plant oils, as well as for the fractionation of crude oil; however, it was not until the energy crisis of the 1970s that many of these processes were put to use on a large scale.

Today, $scCO_2$ is found in an ever-growing number of different industrial and laboratory applications. Most of these applications may be grouped into one of the following categories: extraction, fractionation, organic synthesis/reaction, cleaning/purification, doping/impregnation, materials analysis, foam blowing, and general solvating. Its use in the extraction and refining of crude oil has led to the construction of thousands of miles of pipeline to transport $scCO_2$ to refineries and remote sites in the northern territories of Canada and Alaska. At its plant in Houston, TX, Maxwell House uses $scCO_2$ in reactors 7 stories high to produce decaffeinated coffee in a semi-continuous process (figure 5).

The primary impetus behind the integration of $scCO_2$ in the plastics industry has been increased concern over the environmental dangers of chlorofluorocarbons (CFCs) and volatile organic compounds (VOCs) that has brought tightened environmental restrictions on the use of such materials. $ScCO_2$ is an environmentally benign alternative for those materials, and it also has capabilities that extend far beyond those of traditional solvents. As a compressible fluid, $scCO_2$ density (and thus solubility) may be "tuned" to suit different process needs. Also, as mentioned before, no phase separation exists between supercritical CO_2 and its liquid or vapor phases. Because of this phenomenon,

$scCO_2$ solvent may be depressurized into a gas and removed from fragile solutes without the presence of potentially damaging surface tension. For this reason $scCO_2$ is becoming the preferred solvent for cleaning and drying micro-electronic devices.

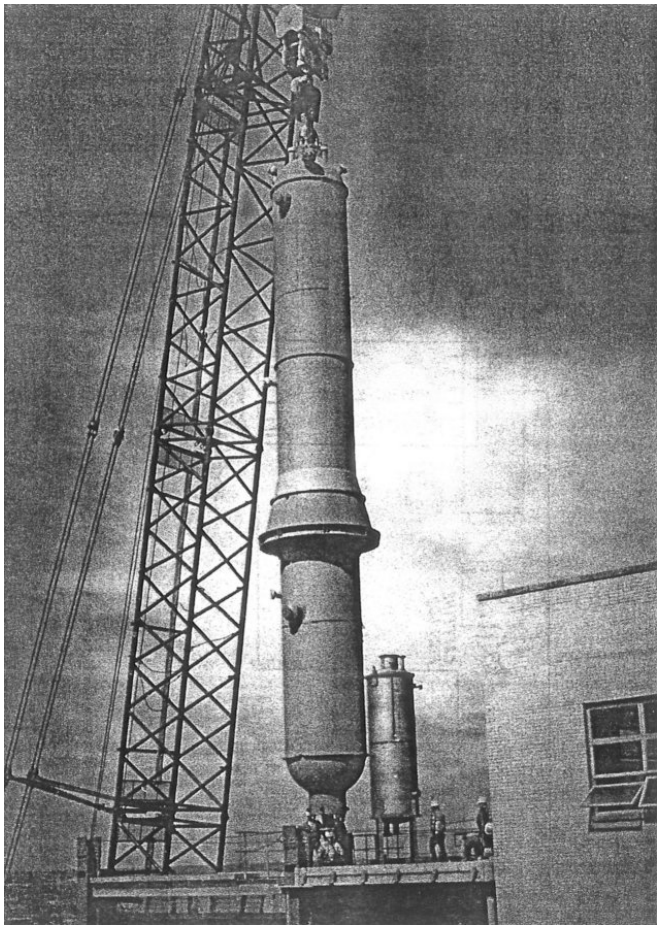

Figure 5: Photograph of a Maxwell House SCF reactor being lowered into plant. [38]

When any pure substance is heated and pressurized beyond its critical point, it can no longer exist in equilibrium as a liquid and a gas. Figure 6 is a phase diagram for carbon dioxide showing the supercritical region along with solid, liquid, and gas. As can be seen, the critical point is located at the maximus of the boiling curve. Also evident in the figure is the fact that when a fluid is in the supercritical region it can be neither

compressed into a liquid nor heated into a gas, regardless of how much pressure or heat is applied.

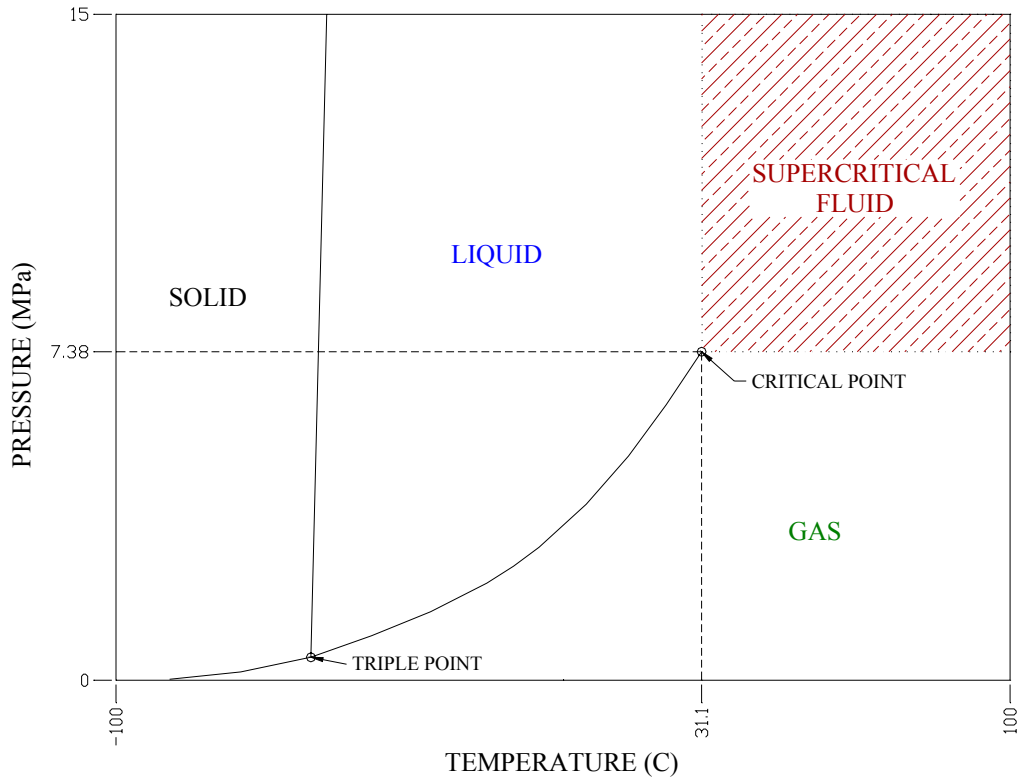

Figure 6: Phase diagram of carbon dioxide.

The critical point refers to the conditions at which the densities of coexisting equilibrium phases of liquid and gas intersect. At ambient temperature (and within the density range of .24 - .71 g/ml), compressed CO_2 exists in equilibrium as a two phase system of liquid and gas. The vapor pressure of the compressed gas phase at this temperature (24.85°C) is constant at 6.41 MPa, and the vapor density is constant at 0.24 g/ml. If more CO_2 is added to the system, it takes the form of a liquid, and as long as both liquid and gas phases are present, the density of the CO_2 system may be changed (by adding or removing liquid CO_2) without affecting the net pressure. As the temperature of this isochoric (constant volume) system is increased, however, the density and pressure of

the gas phase also increases (according to the ideal gas law), while the density of the liquid phase decreases due to thermal expansion.[39] If the temperature continues to increase, eventually the difference in density between the two phases disappears; for CO_2, that point, the critical point, is at 31˚C, 7.38 MPa (1074 psi), and .468 g/ml. Figure 7 shows the relationship between the density, temperature, and phase of CO_2 in the region of the critical point.

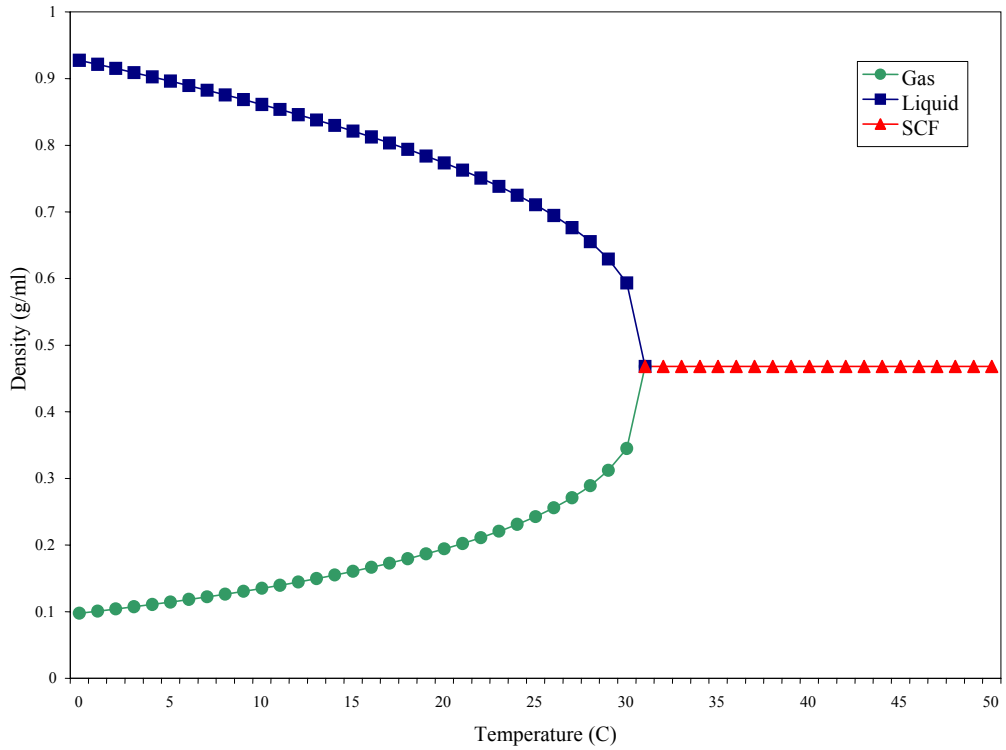

Figure 7: Density of isochoric liquid and gas CO_2 mixture.[40]

In the subcritical region, pressure and density of CO_2 are decoupled because of the phase separation previously described. In the supercritical state, however, pressure can be used to control density, and vice-versa. Figure 8 shows that above the critical

point, higher densities of $scCO_2$ exhibit much steeper pressure/temperature slopes, while in the subcritical region the different densities share the same slope.

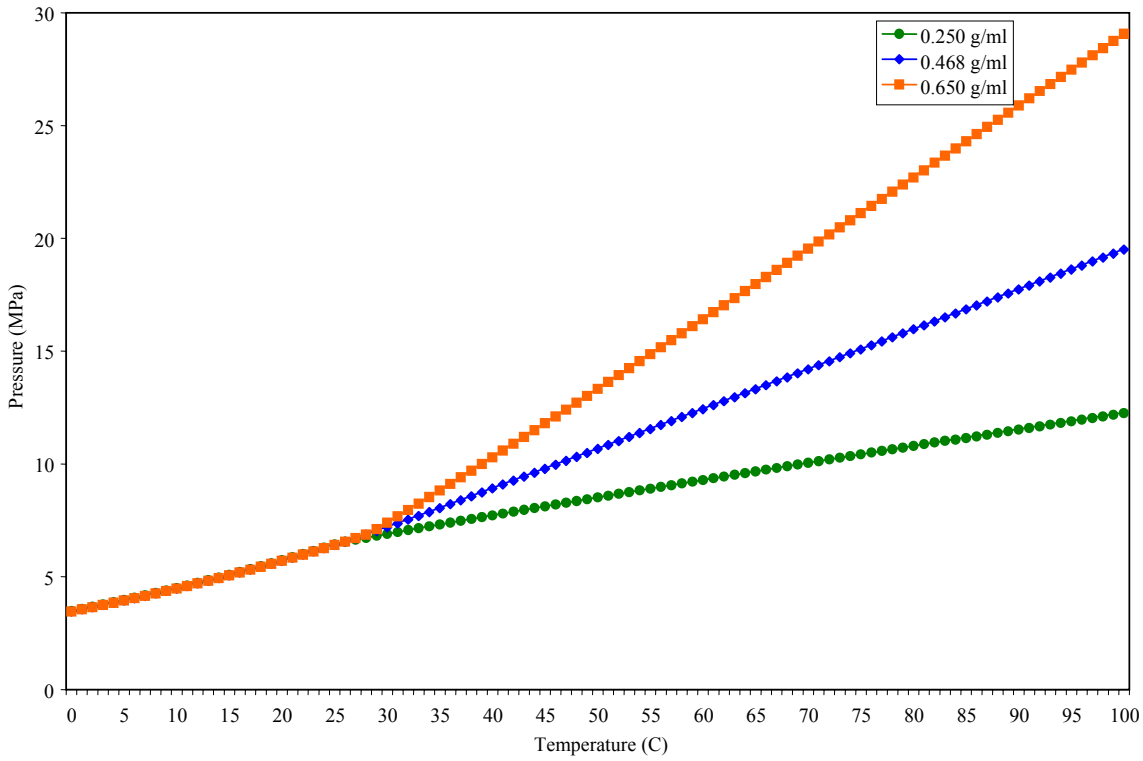

Figure 8: Isochoric pressure/temperature slopes of $scCO_2$ at various fixed densities.[40]

While each substance has a unique critical point, many require such high pressures and temperatures that they are impractical for industrial use. CO_2, on the other hand, has a very accessible critical point (31˚C, 7.38 MPa). Table 1 lists some properties of $scCO_2$ in comparison with liquid and gaseous CO_2. Table 1 lists the critical points of some other common supercritical fluids.

Fluid	T_c (°C)	P_c (MPa)
Ethylene	9.3	5.04
Trifluoromethane	26.2	4.86
Chlrortrifluoromethane	28.9	3.87
Carbon Dioxide	31.1	7.38
Ethane	32.3	4.88
Propylene	91.8	4.60
Propane	96.7	4.25
Ammonia	132.4	11.35
n-Pentane	196.5	3.37
Trichlorofluoromethane	198.1	4.41
Cyclohexane	280.4	4.07
Toluene	318.7	4.10
Water	374.2	22.12

Table 1: Critical temperatures and pressures of various fluids.

2.5. Interaction with CO_2 with Nanocomposite

2.5.1. Solubility

The measurement of solubility in high pressure compressible systems is a nontrivial issue, and one that is important to review in light of broad variations in published data.[41] Available techniques may be divided into two basic categories: static, and dynamic. Static methods have been predominant in analysis of polymer-SCF systems, largely because of their simplicity, but also because they often permit measurement of several different properties in each experiment, which is attractive for researchers investigating the broad spectrum of solvent-solute interactions such as diffusion rates, swelling, and phase transition. The most common static methods employed in sorption measurement are in-situ gravimetric, ex-situ gravimetric, volumetric, and phase separation (alternately called the “view cell” method). Dynamic methods require more elaborate equipment, and typically more sample material, but are

useful in the measurement of solubility in semi-continuous or continuous processes such as extraction or extrusion. For laboratories with equipment and instrumentation for such processes, dynamic methods may be preferred. Dynamic methods used for measuring solubility include the dynamic view cell method and various gas flow methods.

In-situ gravimetric measurements of polymer-SCF solubility have been used to extract precise data from samples of polymer swollen in an SCF environment. The works of Bonner and Prausnitz,[42] Wissinger and Paulaitis,[43] Zhang,[41] and Sato et al.,[44] among others, have made the gravimetric method the most popular method used in studying SCF systems. The technique is simple and inexpensive, requiring at its minimum that only a spring, sample pan, view cell, and cathetometer be added to laboratory pressure vessel apparatus in order to measure sorption. Experiments are conducted by first placing a dried polymer sample in a pan, which is then suspended from a calibrated spring inside the high pressure view cell. As pressurized SCF is introduced to the purged, sealed view cell, cathetometer measurements of spring extension are used to calculate the quantity of SCF absorbed in the polymer. Under normal conditions, the polymer is more dense than the surrounding supercritical fluid, and as it absorbs SCF into its free volume it becomes even denser. The equation for calculating solubility based on spring extension is presented by Zhang as:

$$\Delta m = k\left(x - x_0\right) + \rho_g\left(V_p + V_t\right) \qquad \text{(Equation 2)}$$

Where Δm is the mass of CO_2 absorbed, k is the spring constant, and ρ_g is the density of the SCF.[41] The term $(x\text{-}x_0)$ is the spring extension from initial conditions, and the term (V_p+V_t) is the total volume of swollen polymer plus pan and spring volumes. This latter

volume term is a buoyancy parameter; by taking the swollen polymer volume into account, it compensates for sorption not detected by the spring scale because of polymer swelling. Unfortunately, although cathetometer measurements of spring extension may be very accurate, the accuracies of solubility calculations based on equation 11 are limited by the accuracy of polymer swelling measurements. At best, volumetric calculations based on linear measurements magnify inaccuracies by a cube function; at worst, they are completely invalid based on secondary distortions of the polymer sample caused by plasticization, friction with the sample pan, and/or curling of the sample edges. Variations in these measurements are responsible for the largest disparities between published solubility data of PS/CO_2 systems. For example, Wissinger and Paulaitis calculated inordinately large buoyancy parameters based on deformations of a suspended sample (not in a pan), leading them to the unique conclusion that CO_2 shows an abrupt solubility increase in PS near glass transition.[43] Conversely, Zhang based his calculations on measurements of a flat sample lying on a glass surface; friction between the glass and sample caused his sorption estimates to be considerable lower than those of other researchers.[41] Sato et al. used a modified gravimetric method involving the use of a magnetic suspension balance (MSB). Because their MSB chamber did not have a view cell to measure swelling, they compensated for buoyancy by substituting the following for equation 2:

$$\Delta m = \left(m - m_0\right) + \rho_g \left[V_p \left(1 + S_w\right) + V_b\right] \qquad \text{(Equation 3)}$$

where S_w is a the theoretical degree of swelling, defined as:

$$S_w = \frac{(1+S)\upsilon}{\upsilon_0} \qquad \text{(Equation 4)}$$

In this equation, S is the solubility (D*m*/mass of polymer) and u is the specific volume of the polymer based on the Sanchez-Lacombe equation of state.[44] Sato et al. have demonstrated agreement between their results and previous published data; nonetheless, their technique has some drawbacks in that it is not purely empirical and it requires the simultaneous solution of equations 3, 4.

Ex-Situ Gravimetric measurements are perhaps the simplest sorption experiments to perform from an instrumentation point of view. Promulgated by Berens et al. in 1988, the technique involves first saturating a polymer sample with SCF in a pressure vessel for sufficient time to achieve equilibrium conditions, followed by *rapidly* removing the sample to ambient conditions and measuring weight loss over time.[45] Equilibrium solubility is then obtained by plotting desorption data and using a fit curve to extrapolate backwards from the time of the first recorded measurement to the time pressure was initially released. This method, like the in-situ gravimetric method, has been widely reported in polymer/SCF literature (Berens et al. 1992;[45] Shieh 1996;[46] Arora, Lesser, and McCarthy 1998;[11,36] Nikitin et al. 2002[47]). Figure 9 shows schematically the steps involved in the ex-situ gravimetric sorption experiment.

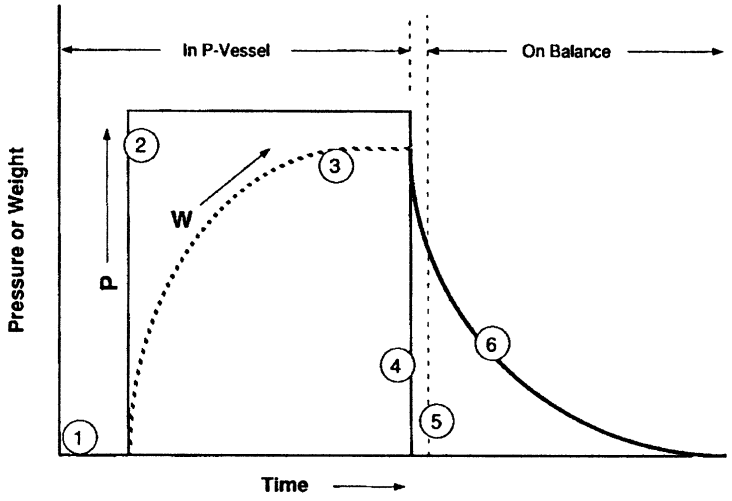

Figure 9: Schematic of sorption cycle for ex-situ gravimetric sorption measurements, taken from Berens et al.[45] Numbered steps are: (1) sample is loaded in pressure vessel; (2) solvent gas is introduced into vessel and rapidly pressurized to desired SCF condition; (3) the dotted line shows mass transfer of SCF into polymer over time until equilibrium solubility is achieved; (4) pressure rapidly decreases and desorption begins as pressure vessel is opened and sample is removed; (5) as quickly as possible the sample is placed on a balance scale and weight measurements commence; (6) the decreasing weight of the polymer is recorded as desorption continues to ambient equilibrium.

Arora et al. used the ex-situ method for study of PS/CO_2 mixtures, and found their results close to those of other published research. More importantly, they were able to use their measurements to successfully calculate diffusivity of scCO_2 in glassy polymers. Despite their successes in diffusion, however, the ex-situ method is plagued by several weaknesses that may prevent it from being a reliable source of equilibrium solubility measurements. One of these weaknesses is hinted at in Arora's work:

> "It should be noted that… …only the *absorption* kinetics and diffusivity can be accurately measured since CO_2 is leaving the sample by diffusing through the polystyrene and by creating pores, rendering the desorption a more complex system."[36]

When 10-20 MPa of pressure is rapidly vented from around an $scCO_2$ saturated polymer, the absorbed gas exerts enough force on its surrounding matrix to create pores, crazing, and other types of voids, especially in situations where the polymer host has been plasticized to any significant extent. These deformations occur in the first few seconds after pressure is released, before the sample can be removed from the chamber and weighed. Therefore, because the mechanisms of SCF egress from the polymer are different in the first few seconds than they are in the subsequent minutes, sorption data cannot be accurately extrapolated all the way back to the time of venting. Secondly, because pressure cannot be instantaneously released from the chamber (unless catastrophically) there is an pressure quench rate which has an important effect on the initial rate of desorption, and which also cannot be extrapolated from latter data. Due to these two effects, it is likely that solubilities predicted using ex-situ methods will be somewhat lower than the real values. More accurate data may be obtained by these methods if they are restricted to use at low pressures (where plasticization is less pronounced and internal hydrostatic forces created during pressure quench are reduced) and at low temperatures (where diffusion rates are slower). One other factor that may restrict the use of these methods are that only one equilibrium solubility data point is obtained for each complete cycle, leading to an extensive and laborious experimentation.

The volumetric (or pressure-decay) method is an in-situ technique that was first promoted for SCF-polymer solubility analysis by Koros and Paul in 1978.[48,49] Since that time it has been used, with minor modifications, for high pressure studies by Dey,[50] Sato et al.,[51] Krause et al.,[32] and Han. [52,53] The basic principal of the method is that a known

quantity of SCF is introduced into a chamber of known volume that contains a polymer sample of known volume. As the SCF is absorbed into the polymer sample, the pressure in the chamber "decays" (decreases), and the amount of pressure decrease can be used to calculate the amount of SCF absorbed by using the gas law:

$$n = \frac{PV}{ZRT} \qquad \text{(Equation 5)}$$

where Z is a constant (the compressibility factor) that is used to account for non-ideal behavior of the SCF. Koros and Paul's original equation to calculate the amount of solvent absorbed was:

$$n_{p\infty} = n_0 - \frac{(V_B - V_P)}{RT}\left\{\frac{[E_\infty - e_{0\infty}]}{z_\infty}\right\}K_B \qquad \text{(Equation 6)}$$

In this equation, n_0 is the initial number of moles of SCF compressed in the chamber, and the $(V_B - V_P)$ term signifies the volume of the chamber minus the volume of the sample. The second, bracketed term includes pressure readouts from the pressure transducers and a compressability factor; the last constant, K_B, is a calibration constant for the pressure transducers.[49] As can be seen, there is no consideration given to the volumetric effects of polymer swelling. In fact, this method would appear to neglect swelling altogether; however, Sato et al. added a term for swelling estimates based on the Sanchez-Lacombe EOS. The compensation they used was the same that they later applied to gravimetric measurements.[44,51] Other variations to the volumetric method may include the addition of extra pressure vessels in the experiment to act as reservoirs for temperature normalization and/or additional pressure configurations. In comparison with the in-situ

gravimetric method, the volumetric method has few advantages, and is much more problematic. Even the slightest inaccuracies in volume pressure measurements have a profound impact on results, and tiny leaks in the system also yield significant error. One way to decrease the delicate nature of the experiment is to increase sample size, but in many cases that is not an option.

A fourth static method for determination of solubility is the view cell technique, described by McHugh et al.[54] Professors Beckman and Enick have also used a similar method in various research programs.[55,56] In the view cell technique, a polymer sample and a known amount of solvent gas are loaded in a high pressure, variable volume cylinder as shown in figure 10. The volume of the test cell is controlled by sliding a piston within the cylinder. At one end of the cylinder, a sight glass permits viewing of the sample and solvent phases in situ. During the experiment, process temperature is first raised to above the critical point, and then the cell volume is slowly reduced. Eventually the gas enters its SCF phase; volume is then decreased further, at a slow enough rate to accommodate SCF diffusion into the polymer, until the compressed solvent becomes completely dissolved in the polymer sample and only one phase is observed (in the case of $scCO_2$/PS, this phase is a transparent, swollen polymer mixture). Once the phase separation disappears, volume is increased until the point the solution becomes "cloudy" (also called critical opalescence) and phase separation commences. That point is recorded as the "cloud point," and it can be used to calculate solubility if the amounts of gas and polymer originally introduced into the cell are known. An important advantage of the view cell method is that it permits measurement of solubility without requiring

consideration of swelling. The method can also be used to determine solution viscosities by measuring the time it takes for a small weight to fall through the saturated phase from one end to the other.[38,57] Disadvantages of the method stem from the fact that the sides of the floating piston must be very well sealed against the sides of the cylinder to prevent SCF from leaking out during the experiment. One decided limitation of the method is that it requires sufficient plasticization of the sample that it conform to the cell volume when fully saturated with SCF. Therefore the view cell method cannot be used for studies of polymers below their depressed T_g point.

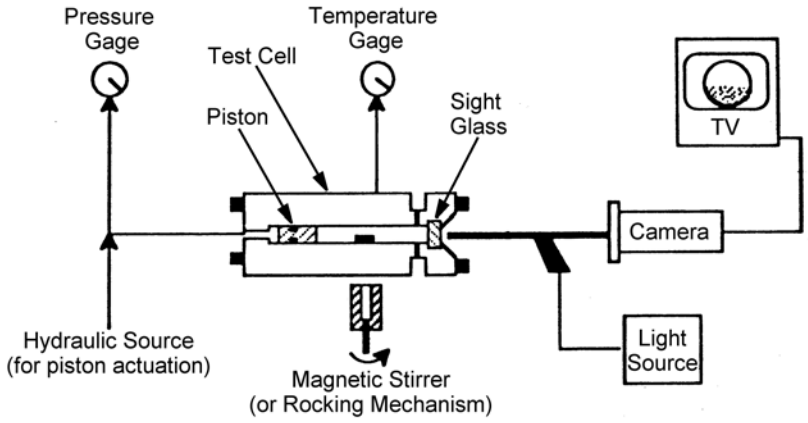

Figure 10: Schematic of static view cell type solubility experiment setup.[38]

A dynamic solubility experiment is one that is accomplished using continuous or semicontinuous processes by which data may be retrieved for a broad spectrum of process conditions using a single setup. Of such experiments, the two most commonly applied to polymer-gas solubility studies are the dynamic view cell method and the flow method. In the first, polymer is continuously compressed through an extruder in the presence of gas or SCF solvent, while in the second method solvent is continuously passed through system in the presence of pelletized polymer sample.

The dynamic view cell method has been used by Zhang, Xanthos, and Dey to explore solubility of $scCO_2$ in extruded PS and other thermoplastics.[58,59] Their method is similar to the static view cell method in that they first effectively increase pressure until they can visually detect the disappearance of phase separation, followed by a slow reduction of pressure to the point of critical opalescence. In the dynamic system, however, pressure is produced by a single screw extruder upstream of the sight glass, and is controlled through a metering valve downstream of the sight glass. Solubility is calculated by careful metering of CO_2 and polymer introduced to the extruder. Although the technique provides a practical method to optimize solvent absorption for extrusion processes, it is less precise than the static methods previously described, and it requires large quantities of extrudable sample. In addition, the process is limited to conditions above the T_g of the polymer/SCF mixture.

One of the earliest methods used in the measurement of SCF solubility was the dynamic flow method, published by Prausnitz and Benson.[60] Numerous variations of the flow method have since been developed, and have been employed by many research groups, including Van Leer and Paulaitis,[61] Johnston and Eckert,[62] Krukonis and Kurnik,[63] and Wu et al.[64] Details of the flow method setup are shown in figure 11. As can be seen, it involves a rather elaborate apparatus by which SCF is first metered, compressed, and conditioned before it is passed through a packed column of sample material in the extraction tank. Some sample is absorbed in the SCF, and is subsequently removed by low pressure precipitation in a U-tube. The U-tube is on a scale, which is used to continually monitor the amount of sample being absorbed and deposited by the

solvent flow. Careful comparison of the amount of precipitate versus the amount of solvent flow is used to calculate solubility. A series of experiments run at different flow rates can be used to insure equilibrium conditions. While the flow method is a robust technique for measuring solubility of a solid or liquid phase in SCF, it cannot be used to measure the opposite effect, namely solubility of SCF in the denser phase. Because of the large size of polymer molecules and their very low solubility in most inert solvents, the flow method is not practical for measuring polymer/SCF solubility. Nonetheless, this technique is important to the study of polymer processing with $scCO_2$ because CO_2 is often used as a solvent for smaller molecular species (e.g. monomers, dyes) in applications such as extraction, polymerization, and impregnation. [9,38,65]

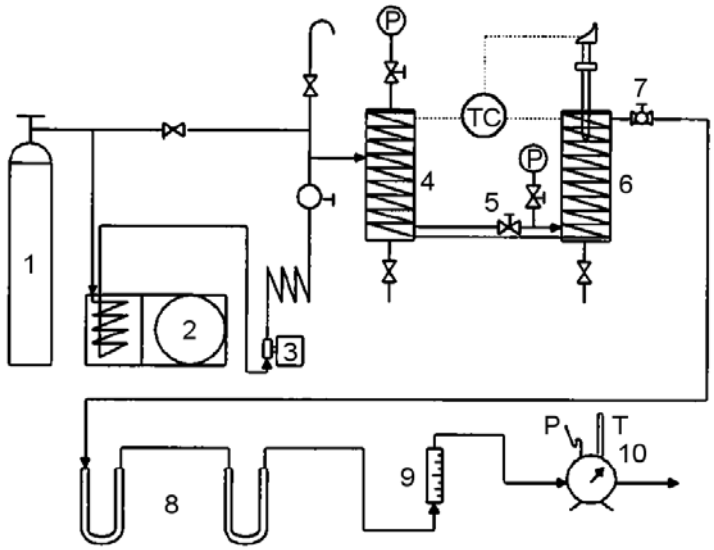

Figure 11: Schematic of dynamic flow method for measuring solubility in SCF.[64]
(1) CO_2 cylinder; (2) chiller; (3) HPLC pump, (4) surge tank; (5) regulating valve; (6) extraction tank; (7) heated metering valve; (8) U-tube collector; (9) flow meter; (10) wet test meter.

Because the measurement of polymer/SCF solubility at high pressures and temperatures is so rigorous, and the results so sensitive to proper instrumentation and meticulous procedure, it is always preferable to minimize the number of experiments conducted. One way to make fewer measurements a viable option is to fit the data with curves based on well established equations of state (EOS). Henry's Law has been used to approximate the solubilities of $scCO_2$ in polymers at moderate temperatures and pressures, where

$$C = \frac{p}{K'_C} \qquad \text{(Equation 7)}$$

In this case, the concentration (C) of gas absorbed is proportional to the partial pressure (p), where K'_C is Henry's Law constant with regard to concentration. At very high pressures, however, specific chemical and mechanical interactions preclude the accuracy of Henry's Law - especially in the temperature range surrounding and below polymer glass transition.

In order to account for the multiple contributions to SCF solubility in polymers, several authors have suggested a "dual-mode" model.[66,67,68] In the dual mode model, solubility behavior is considered as a combination of Henry's Law (linear with respect to pressure) and a Langmuir isotherm (lessened contribution as pressure increases). The Langmuir isotherm compensates for sorption of SCF into surface pores and excess free volume within the polymer by the relationship:

$$C \approx \frac{C'_H bP}{1 + bP} \qquad \text{(Equation 8)}$$

C_H' is the Langmuir capacity parameter, signifying the total excess free volume of the polymer; while *b* is the Langmuir affinity constant, which indicates the relative efficiency of Langmuir adsorption in the system. Although several variations of the dual-mode model exist, the simplest and most representative is the straight forward addition of equations 7 and 8:

$$C = \frac{P}{K'_C} + \frac{C'_H bP}{1 + bP} \qquad \text{(Equation 9)}$$

The Langmuir term works well to describe phenomena related to monolayers of solvent adsorbed onto surfaces and pore walls of rigid, semi porous solids; even in materials where the presence of porosity cannot be verified, the dual-mode model provides a statistical solution that can be closely fitted to empirical data. While the Langmuir term assumes a finite number of specific sorption sites in a frozen solute (glassy behavior), the Henry's Law term assumes unlimited swelling with increased pressure (eventual plasticization). Therefore, the dual-mode model is well suited to describe many glassy polymers in the region below and approaching plasticization by an SCF solvent. Unfortunately, although it does account for polymer swelling, this model does not take into account the dynamic effects of polymer compressibility at high pressures, and it does not describe the behavior of polymers/SCF systems in which solvent/solute interactions are small and swelling in insignificant. At pressures below 3 MPa, the dual sorption model has been successfully fit to data from some polymer/gas systems, including that of PC/CO_2 shown in figure 12. This figure gives a good representation of the shape of the dual-mode isotherm, which at first increases rapidly due to Langmuir adsorption, and

then approaches a linear asymptote analogous to Henry's Law behavior. Various extended versions of the dual-mode model have been proposed (Bondar et al.)[69] in which the use of multiple, pressure dependent, asymptotic parameters permits more versatile fitting to empirical data.

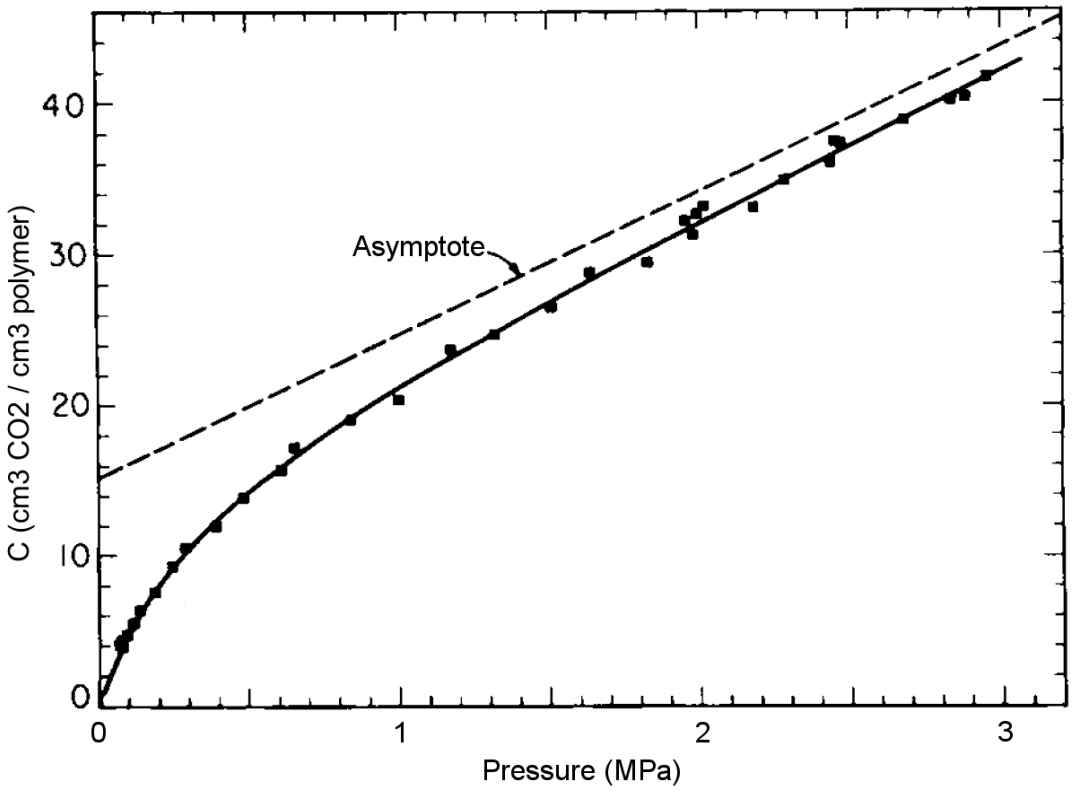

Figure 12: Dual-Mode model fitted to solubility data of CO_2 in polycarbonate at 35°C.[48]

In order to find a more comprehensive model to predict and fit solubility isotherms of SCF in polymeric materials at high pressures, It is useful to consider the lattice model of polymer solubility, advanced independently by Flory and Huggins during the 1940s and '50s.[70,71] Instead of assuming a static arrangement of pores and sorption

sites as in the dual-mode model, the Flory-Huggins model approximated sorption behavior by considering the influences of molecular mobility within a simplified two dimensional lattice, as shown in figure 13.

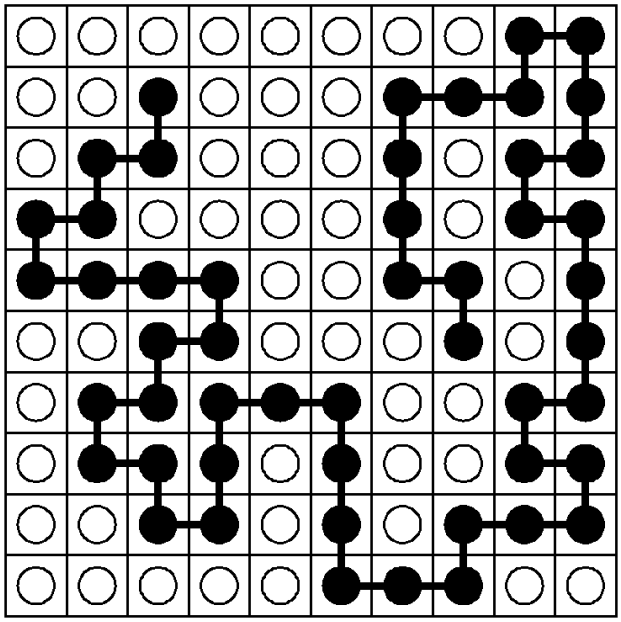

Figure 13: Lattice-Fluid model of polymer solubility.

In this model, each lattice site represents a unit of volume, and each circle represents either a solvent molecule (white circle) or a segment of a macromolecule (black circle). A polymer phase is represented by long series of segments (mers) linked together by thick lines. In order to facilitate straightforward calculations over a wide range of pressures, the Flory Huggins model assumes that the lattice is incompressible (i.e. the number of sites in the system remains constant, even at high pressures). Within this context, solubility relies in a large part on the entropy of mixing, which may be most simply presented by the Boltzman Equation:

$$\Delta S_m = k \ln W \qquad \text{(Equation 10)}$$

where *W* represents the number of possible arrangements of the molecules in a hypothetical lattice.[72] Because the mers of the large polymer molecules are permanently joined, the number of different ways that they can be arranged is greatly reduced. With the assistance of Stirling's approximation for large factorials, the entropy of mixing for polymer solutions may be derived as:

$$\Delta S_m = -R\left[n_1 \ln \phi_1 + \frac{n_2}{P_2} \ln \phi_2 \right] \qquad \text{(Equation 11)}$$

where n_1, Φ_1, n_2, and Φ_2 are the molar quantities and volume fractions of solvent and polymer molecules, respectively, and P_2 is the degree of polymerization.[73] In addition to the entropy of mixing, the Flory-Huggins model takes into account enthalpic interactions by including an interaction parameter χ, which has also been referred to as the "heat of mixing." It may be defined as:

$$\chi = \frac{(z-2)}{kT}\left[\Gamma_{ij} - \frac{1}{2}\left(\Gamma_{ii} + \Gamma_{jj}\right) \right] \qquad \text{(Equation 12)}$$

This equation is reminiscent of our earlier equation 5, and includes a coordination number (z) that is reduced by two, because each interacting polymer segment (excepting the ends) is limited by the fact that it has been previously bonded to two neighboring segments.[74] Utilizing equations 3 and 5, the Flory-Huggins interaction parameter can be related to the component solubility parameters by:

$$\chi = \beta + \frac{V_1}{RT}\left(\delta_1 - \delta_2\right)^2 \qquad \text{(Equation 13)}$$

where V_1 is the molar volume of solvent and β is a constant of entropic origin.[75]

Finally, using terms combined comprehensively to describe the entropy and enthalpy of mixing, along with fugacity of the solvent phase,[76] the Flory-Huggins model for polymer solubility may be expressed as:

$$\ln\left(\frac{p}{p_0}\right) = \ln(1-\upsilon_p) + \upsilon_p + \chi\upsilon_p^{\,2} \qquad \text{(Equation 14)}$$

in which p is solvent pressure, p_0 is solvent vapor pressure, υ_p is volume fraction of polymer.[77] The isothermic curves resulting from this equation are concave upwards, as exemplified in figure 14.

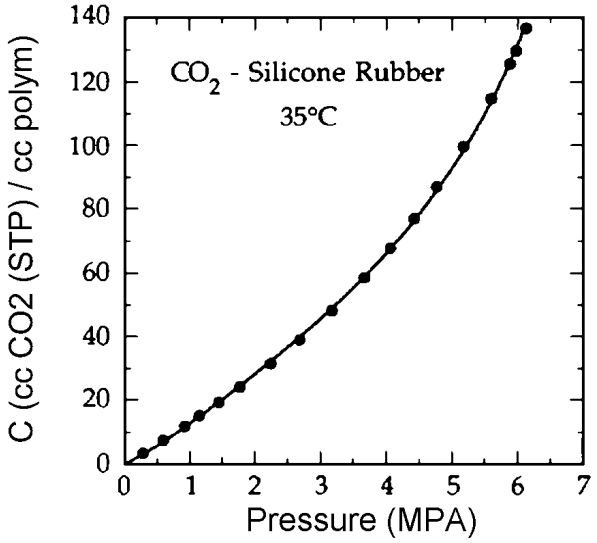

Figure 14: Sorption isotherm of $scCO_2$ in silicone rubber, showing Flory-Huggins behavior.[78]

Based on the shape of the Flory-Huggins isotherm, a simplification of the model has also been published.[79]

$$C = k_D p \exp(\sigma C) \qquad \text{(Equation 15)}$$

In this equation, C is the solvent concentration, p is pressure, k_d is the Henry's law parameter, and s is some constant related to the interaction parameter χ. This simplified formula has been used to successfully fit the Flory-Huggins model to the behavior of CO_2 in poly (ethylene-co-vinyl acetate), as shown in figure 15.[80]

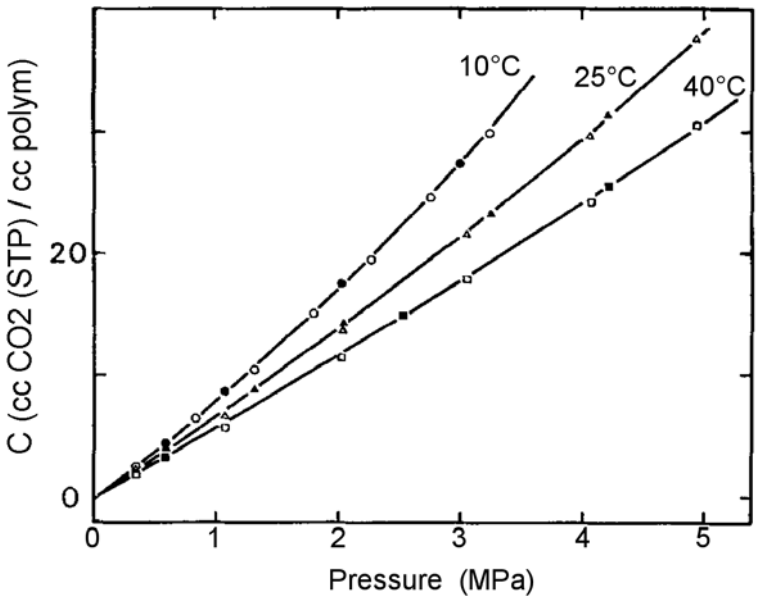

Figure 15: Sorption isotherm of $scCO^2$ in PEVAc, showing Flory-Huggins behavior.[80]

The Flory-Huggins model has been used very successfully to describe SCF solubility in rubbery polymers above glass transition temperature. In its original form, however, it cannot be used to predict or fit the behavior of glassy polymer systems, especially below T_g, because it does not take into account free volume or polymer compressibility (the restriction of free volume and molecular mobility at high pressures). For this reason, several extended versions of the lattice model have since been developed that improve its applicability to glassy polymers. Among those most often cited are the works of

Prigogine[81], Sanchez and Lacombe[82], Vrentas and Vrentas[83], Panayiotou and Vera[84], Conforti et al.[85], and Wissinger and Pauliatis[43]. In each of these works, emphasis was given to at least one of the following objectives: improved empirical fit, fewer required parameters, and/or more predictive functionality. In the case of supercritical fluid solvents, the most popular of the resultant models has been the Sanchez-Lacombe equation of state (S-L EOS).

The Sanchez-Lacombe EOS compensates for the contributions of both free volume and lattice compressibility by incorporating a parameter for the "reduced density" of the polymer: [86]

$$\tilde{\rho} = \frac{\rho}{\rho^*} = \frac{V^*}{V} = \frac{N(rv^*)}{V} \qquad \text{(Equation 16)}$$

where r^* is the idealized density and V^* is the idealized volume of the polymer based on the number of molecules (N), the number of mers per molecule (r), and the close-packed volume of each mer (v^*). Because actual densities are bounded by their close-packed values, $\tilde{\rho}$ takes the form of a fraction < 1. Recalling the lattice model of figure X, the effects of reduced density can be visualized by leaving an appropriate number of lattice sites empty, allowing them to provide "free volume" for increased molecular mobility and solvent sorption. This concept is similar in some ways to the Langmuir adsorption theory found in the dual-mode model, except that in Sanchez and Lacombe's model, the amount of free volume is not fixed, but is variable depending on induced factors of swelling or compression. The added flexibility of the S-L model enables it to fit more closely to empirical data.

Continuing with their usage of "reduced" parameters, Sanchez and Lacombe arrived at the following expression of their EOS:[82,86]

$$\tilde{\rho}^2 + \tilde{P} + \tilde{T}\left[\ln(1-\tilde{\rho}) + \left(1-\frac{1}{r}\right)\tilde{\rho}\right] = 0 \qquad \text{(Equation 17)}$$

The reduced pressure ($\tilde{P}$) and temperature ($\tilde{T}$) are related to interaction energy by the equations:

$$\tilde{P} = \frac{P}{P^*} = P\frac{v^*}{\varepsilon^*} \qquad \text{(Equation 18)}$$

$$\tilde{T} = \frac{T}{T^*} = T\frac{R}{\varepsilon^*} \qquad \text{(Equation 19)}$$

where e* is the mer-mer interaction energy.

For the case of calculating uptake of a high pressure gas in a bulk polymer, Sanchez provided the following solution for V_g (cm^3 gas per gram polymer), which can also be used for SCF polymer systems:[87]

$$V_g = \rho_2^{-1}\exp\left\{\tilde{\rho}_2\frac{M_1}{\rho_1^*}\left[\frac{P_1^*}{RT}-\chi\right]-r_1\left[1+(1-\tilde{\rho}_2)\frac{\ln(1-\tilde{\rho}_2)}{\tilde{\rho}_2}\right]\right\} \qquad \text{(Equation 20)}$$

This time χ is the Sanchez-Lacombe interaction parameter; parameter subscripts indicate which values are used, solvent (1) or polymer (2). The resultant isotherms for $scCO_2$ solubility in glassy polymers exhibit behavior that usually begins with a quasi-linear or upwards curving portion at low pressures, followed by a downward, convex curve at higher pressures, as illustrated in figure 16.

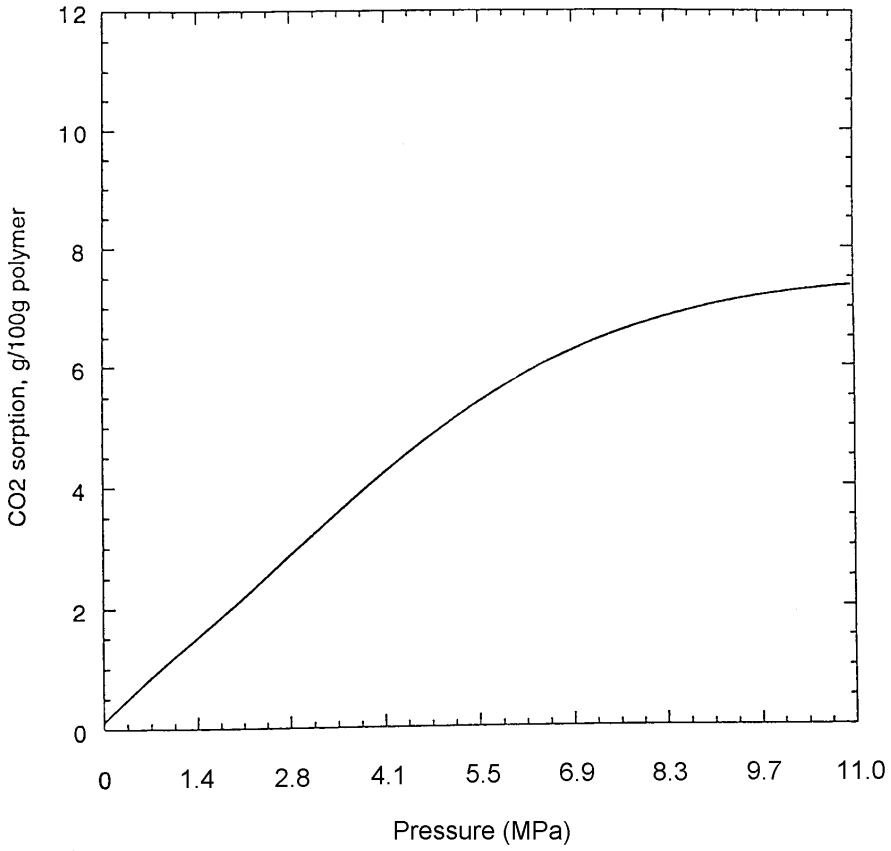

Figure 16: Sorption isotherm of $scCO_2$ in PS, showing Sanchez-Lacombe behavior.[41]

While the S-L EOS has met wide acceptance for empirical modeling of SCF/polymer solubilities, like other polymer equations of state, it promises only limited predictive ability. This limitation is made apparent in the wide variation of parameters used to fit similar materials in different circumstances. Table 2 provides some typical published values for various solvents and polymers, including some which have been reported differently by different authors. It should not be construed that these differing values are wrong; however, it should be noted that they were each estimated empirically by curve fitting data acquired under different experimental conditions. Sanchez and Lacombe

recognized this themselves, and encouraged researchers to include applicable pressure and temperature ranges with published parameters.

Species	P^* (MPa)	T^* (K)	ρ^* (g/cc)	r_1	Reference
Solvents					
CO_2	418	316	1.369	5.11	[88]
	464	328	1.426		[89]
	575	302	1.510	6.60	[90]
	660	283	1.62	7.6	[91]
	720	280	1.618	8.4	[92]
N_2	172	134	0.902	4.80	[88]
Methane	225	206	0.468	4.50	[88]
Acetone	533	484	0.917	8.40	[87]
Toluene	402	543	0.966	8.50	[87]
Cyclohexane	321	543	0.918	6.52	[88]
	383	497	0.902	8.65	[87]
Polymers					
PS	358	735	1.105		[90], [93]
PMMA	505	696	1.269		[94]
PVA	505	627	1.265		[95]
	508	590	1.283		[96]
PE (linear)	426	649	0.904		[94]
PVC	530	729	1.461		[87]
PDMS	292	498	1.081		[88]
	302	476	1.104		[89]
PEMS	302	552	1.126		[97]

Table 2: Sanchez-Lacombe EOS parameter values for common solvents and polymers.

2.5.2. Depression of Glass Transition (T_g)

There are three basic approaches currently used to measure T_g at high pressures: mechanical, thermal, and physical. Mechanical approaches include the creep compliance method and the ultrasonic method. The creep compliance method has been perhaps the most commonly used because it involves the least complicated equipment to achieve the most definitive measurements.[98] In this method, a strip of material is suspended vertically

in a pressure vessel, and a small weight is attached to it. As pressure is increased in the vessel, the rate of creep compliance is measures visually through a window in the vessel using a cathetometer. T_g is identified by a sudden increase in creep compliance. Although the measurements involved are relatively simple, and the observed change at T_g is typically quite large, accurate calculation using this method is nontrivial. Compensations must be made for dilation and buoyancy of the sample due to swelling, and experiments must be conducted at a pace slower than solvent diffusion through the sample.

The ultrasonic method, used by Wang et al., correlates changes in the speed of high frequency sound to changes in the Young's modulus of a material.[99] By taking pulse-echo ultrasound measurements of a polymer/SCF system within a pressure vessel, and overlaying them with reference spectra, polymer compliance is indicated by shifts of characteristic peaks in the data. T_g is identified as a sudden change in the Young's modulus. In their work, Wang et al. used creep compliance results to calibrate and corroborate their ultrasonic results, since modulus and T_g are both frequency dependant properties.

Thermal measurements of T_g center around the use of high pressure differential scanning calorimetry (DSC). The DSC method of T_g detection requires a more elaborate setup, such as described by Chiou et al.,[100] or Banerjee and Lipscomb.[101] In the later case, a microcalorimeter is equipped with high pressure cells and used in scanning mode to approximate the functionality of a DSC. As a pressurized polymer/solvent sample is heated to glass transition within the calorimeter, the T_g is identified by a sudden change in the heat capacity (C_p) of the sample as compared to that of a reference. Results using

this method can be very accurate, and have been found to be in good agreement with published values. Nonetheless, care must be taken (as in other methods) to use sufficiently small samples and slow heating rates in order to avoid data lag due to diffusion. Also, it may be argued that in many cases the change in C_p is less pronounced and less definitive than the results found via the creep compliance method.

Physical methods of T_g measurement, including gravimetric and dilatory methods, are often used in conjunction with sorption experiments because they require similar equipment. In the gravimetric method, T_g is detected by a change in the rate of polymer weight gain during solvent absorption. Similarly, the dilatory method uses changes in the rate of polymer swelling to indicate T_g. Neither method is often used in detailed studies of glass transition, because the discontinuities of slope relied upon are often very subtle and broad, leading to imprecise results.[98]

2.5.3. Diffusion

Many of the methods used to determine diffusion of CO_2 in polymers are identical to those static methods used to measure solubility, namely in-situ gravimetric, ex-situ gravimetric, and volumetric. In all of these methods, diffusion is measured directly as saturation over time. In gravimetric methods, the rate of weight increase or decrease of a sample is directly related to diffusion rate of solvent into or out of the sample. Challenges to diffusion measurement are likewise similar to the challenges that face measurements of solubility, especially the effect of swelling, and in the case of ex-situ methods, any nonlinear diffusion during pressure quench. The effect of swelling in diffusion measurements is known as buoyancy, because it describes mass uptake of solvent into the

polymer that is not detectable by gravimetric methods in-situ. Ex-situ methods are not affected by buoyancy, but as previously discussed, in supercritical systems, most of the SCF nucleates and escapes from the polymer between the time that the pressure vessel is opened and the time that the sample can be removed for weighing. In this study, it will be shown that foam is formed and expanded in an SCF supersaturated polymer within the first few seconds of depressurization, precluding any ex-situ measurement of diffusion.

Of central interest to the development of a foam production process is the time required for blowing agent diffusion and distribution within the host matrix. The traditional and well accepted model for this diffusion is the concentration dependent Fickian model. Arora, Lesser, and McCarthy documented the CO_2 absorption kinetics of pure PS at high pressures and showed that mass uptake varies linearly with the square root of time, indicating Fickian behavior.[36] At 25.3 MPa and 80°C, they were able to achieve equilibrium CO_2 saturation in a 1.6mm thick sample in 2-3 hours. For Fickian diffusion into a plane sheet, Crank derived the solution[102]:

$$\frac{M_t}{M_\infty} = 1 - \sum_{n=0}^{\infty}\left[\frac{8}{(2n+1)^2\pi^2}\exp\left\{\frac{-D(2n+1)^2\pi^2 t}{4l^2}\right\}\right] \qquad \text{(Equation 21)}$$

M_t/M_∞ is the fraction of equilibrium mass uptake at time t, D is the diffusivity, and l is the thickness of the sheet.

While the Fickian model has been successfully applied to many polymer/solvent relationships, some noted exceptions exist. Polymer films, glassy polymers, and polymers undergoing phase transformation during saturation exhibit anomalous diffusion behavior known as “Case II” diffusion.[103] Case II diffusion may be due to a combination of

factors, but is primarily attributed to first order relaxation of viscoelastic stresses within the polymer.[104] In the case of SCF simultaneously plasticizing and diffusing through a polymer, Kazarian and Vincent have shown that diffusion rates can be highly sensitive to the degree of plasticization undergone by the polymer during saturation.[65,103] The end result is that Case II diffusion provides a model for the explanation of accelerated, non-concentration dependent contributions to overall diffusion. A combination of Fickian and Case II models have been proposed by Vincent[103]:

$$\frac{M_t}{M_\infty} = (1-\alpha)F\{D\} + \alpha\{1-\exp(-kt)\} \qquad \text{(Equation 22)}$$

where *F{D}* is the Fickian diffusion described in equation 21, α is the fraction of diffusion due to Case II behavior, and *k* is some time constant of Case II diffusion related to diffusion rate over thickness such that:

$$k = \frac{v}{l} \qquad \text{(Equation 23)}$$

Several researchers have taken advantage of the accelerating effects of Case II diffusion in SCF / polymer systems; one example of its application is the addition of disperse dyes to plastic films.[65,105,106]

A graphical comparison of Fickian diffusion and Fickian / Case II diffusion is given in figure 17.

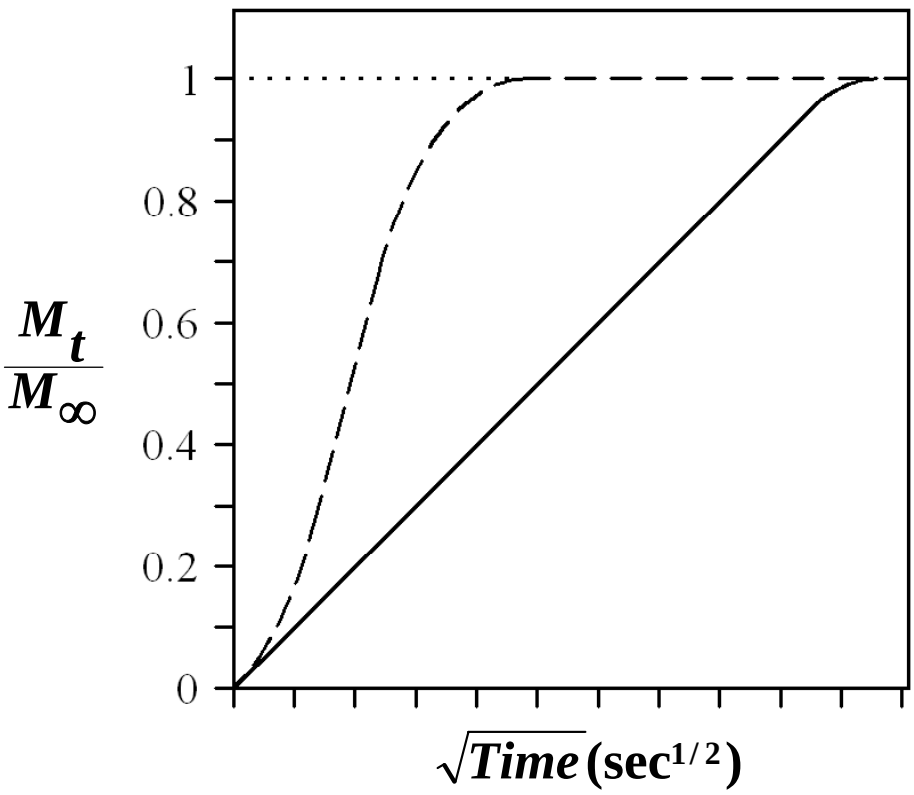

Figure 17: Diffusion rate of solvents in swollen, plasticized polymers.
Fickian [——] versus mixed Fickian / Case II [-----] diffusion.

2.6. Nucleation and Growth of Foam Cells

Several models have been proposed to help describe the dynamics of foam expansion.[107,108,109] Because polymer foam expansion involves the simultaneous nucleation, growth, and freezing of cells in a highly non-Newtonian fluid, no accurate and comprehensive models have been yet derived to describe it. Instead, traditional models generally address isolated and simplified aspects of the process (e.g. homogenous nucleation, or single bubble growth). Joshi et al. have suggested an integrated approach to account for simultaneous nucleation and growth in a viscoelastic material.[110] Their model is especially applicable to this study because it involves the use of $ScCO_2$ as a blowing

agent. In their model, nucleation and growth occur within a given radius (i.e. cell) of a supersaturated volume of melt, the "influence volume." In figure 18, the influence volume is the gray shaded region.

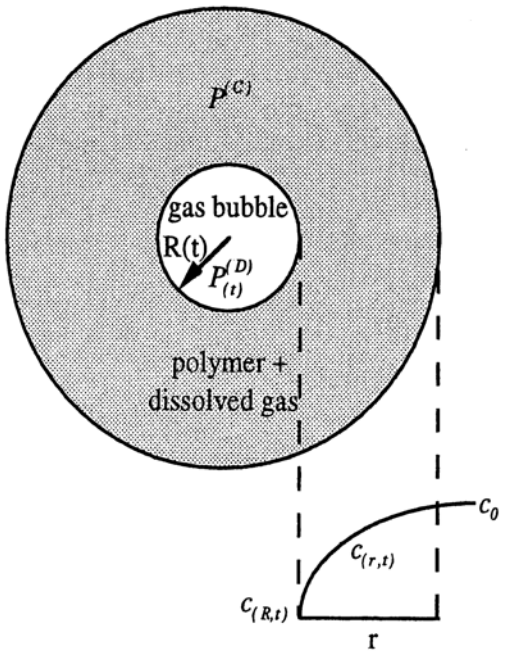

Figure 18: Model for single bubble nucleation and growth.[110]
$c_{(R,t)}$ = gas concentration at surface of bubble
$c_{(0)}$ = gas concentration at t=0
$R_t + r$ = radius of influence volume

While the absorption of CO_2 by PS has in many instances been described as Fickian, the net desorption of CO_2 through PS above T_g is of non-Fickian due to the presence and interaction of the many nucleated cells and their associated influence volumes. Because of this added complexity, Goel and Beckman have proposed a modified, concentration dependant model for desorption of CO_2 in polymers.[8] Their model, taking into account the dynamics of the foaming process, predicts and characterizes the "skinning effect" seen on many foams. During depressurization and

foam generation, absorbed CO_2 molecules near the polymer surface are able to rapidly diffuse out of the solid, rather than nucleate to grow foam cells; the increased rate of desorption by these molecules causes a "skin" to form on the foam exterior. The "skin" of the foam is a non-porous polymer layer followed by a gradient of small cells near the surface to large cells towards the center of the foam block. When predictable and controllable, the skin effect is desirable for certain applications, such as net molding of structural foam parts.

In order for nucleation and growth to occur within a bulk of supersaturated polymer, nucleation must be thermodynamically favorable based on the pressure gradient and the surface tension of the material. Goel and Beckman also modeled nucleation and growth of foam cells using classical theory and arrived at the following equation for homogenous nucleation rates[7]:

$$N_h^0 = C_0 f_0 \exp\left(\frac{-\Delta G_h}{kT}\right) \qquad \text{(Equation 24)}$$

where N_h^0 is the initial nucleation rate, C_0 is gas concentration, f_0 is gas frequency factor, k is the Boltzmann's constant, and ΔG_h is the energy of nucleation such that:

$$\Delta G_h = \frac{16\pi\gamma^3}{3\Delta P^2} \qquad \text{(Equation 25)}$$

ΔP is the magnitude of the pressure gradient caused by the pressure quench process of foaming, and γ is the surface energy of the polymer/SCF interface.

Nucleation of foam cells may be either homogeneous or heterogeneous. Homogeneous nucleation, defined by Goel and Beckman's theory, has been shown as a dominant mechanism in CO_2 saturated polymers only at high pressures, roughly 27MPa

and above.[7] Heterogeneous nucleation can occur at much lower nucleation energies, however, and can be stimulated by the addition of fine fillers into the polymer matrix. For many years prior to the discovery of nanocomposites, small fillers such as MLS were being mixed into foam precursors for use as foam nucleation enhancers. The reduced surface tension at the interfaces between the different phases of a nanocomposite may act as a catalyst for heterogeneous foam nucleation by providing numerous sites for cell formation.[12,111,112] Figure 19 illustrates heterogeneous nucleation at intercalated MLS platelets within a nanocomposite sample.

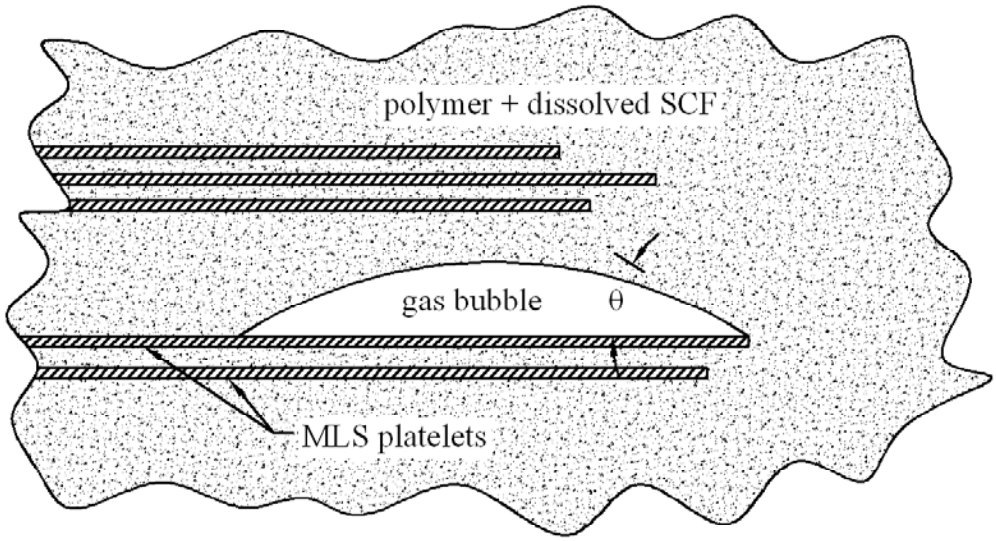

Figure 19: Schematic of heterogeneous bubble nucleation.

The concept of heterogeneous nucleation implies that areas rich in MLS will also be areas of increased bubble nucleation. While this idea presents a processing challenge (i.e. MLS must be evenly dispersed for foam density and cell size to be consistent) it also introduces two potential material benefits. Daming et al. have shown that bubble nucleation at agglomerated clusters of MLS actually has the effect of exfoliating and

dispersing the agglomerates. Furthermore, the work of Okamoto et al. has shown that bubble growth at MLS rich regions can induce alignment of the reinforcing platelets around the cell walls. The research of both groups points to the potential for nanocomposite foams to have specific properties higher than those of their parent nanocomposite materials.

3. SYNTHESIS AND CHARACTERIZATION OF PS-MLS NANOCOMPOSITE

3.1. Materials

Styrene monomer was obtained as neat resin from Aldrich Chemical Co., Milwaukee, WI. The initiator used for polymerization was 0.5wt% reagent grade benzoyl peroxide. The montmorillonite layered silicate (MLS) used was Cloisite® 20A, from Southern Clay (Southern Clay Products, Inc., Gonzales, TX).

3.2. Preparation of Nanocomposite

Polystyrene (PS) nanocomposites were prepared via in-situ intercalative bulk polymerization. Various concentration mixtures of MLS/styrene were used, including 0%, 1.0%, and 3.0% MLS by weight. In the first stage of synthesis, styrene monomer, initiator, and MLS were combined by stepwise mixing using a Caframo® BDC1850 mechanical stirrer (Caframo Corp., Wiarton, ON). The mixture was then polymerized through bulk free radical polymerization on a hot plate at 45°C for 72 hrs. A final cure cycle in a convection oven was performed at 65°C for 48hrs. After polymerization, the PS nanocomposite blocks were compression molded at 135°C to form 1.1mm thick laminates.

3.3. Laminate Properties

Processing Considerations

Polystyrene can be synthesized using any of numerous methods of chain (addition) polymerization, and the use of different methods can yield different properties. For instance, metallocene catalysis is a process used to polymerize syndiotactic

polystyrene, a poly-crystalline morphology of PS with high molecular weight and low polydispersity. Although such novel methods are available and yield superior, tailored polymers, they only account for a very small portion of commercial PS production. Most commercially manufactured PS is atactic polystyrene, and is produced by free radical polymerization. In this process, free radicals of peroxide initiator (e.g. benzoyl peroxide) are reacted with styrene monomers to begin a chain reaction of styrene monomers joining randomly from end to end. Atactic polystyrene is characterized by amorphous structure and a generally broad molecular weight distribution.

There are four common methods of free radical polymerization: bulk, suspension, emulsion, and solution. Each of these methods involves a different economy of manufacture, and yields product suited for different applications. Because the free radical polymerization is an exothermic reaction, the later three methods have an advantage in that polymerization takes place dispersed within a bath of fluid whose temperature can be readily controlled. Unfortunately, these methods also require additional equipment, processing steps, and environmental precautions that make them difficult to justify economically. For that reason, bulk polymerization accounts for the majority of polystyrene manufactured globally today.[113]

The two primary challenges to bulk free radical polymerization are temperature control and molecular mobility. Lack of precise control over both heating and cooling of the monomer mixture during synthesis will lead to auto acceleration of the process, which at minimum will result in a lower molecular weight polymer and may in fact cause thermal deterioration of properties. In this study, a simple hotplate was used to control the

temperature of the polymerizing sample. Because the hotplate did not provide the option for cooling, and was not able to automatically compensate for temperature fluctuations within the sample, it is very likely that some auto acceleration of polymerization took place during synthesis of the samples.

In addition to the importance of temperature control, molecular mobility is important to the bulk polymerization process. As polymerization progresses, the reactive mixture naturally increases in viscosity. Good mixing is essential to insure a low molecular weight distribution. In our samples, mixing was attempted first by using a magnetic stirrer in the bottom of the sample container, but this technique did not provide adequate shear force to continue mixing at higher viscosities. The solution was to use a mechanical stirrer with a forked paddle to mix the sample until gelation. The mechanical stirrer also was beneficial to insure good mixing of the nanocomposite reinforcements within the monomer; however, the technique was not without complications. Because styrene readily evaporates in air, it was essential to maintain a good seal over the sample container during polymerization; with the mechanical stirrer in use, gasketing was required to seal around the rotating shaft. As an extra precaution against inaccurate nanocomposite concentrations, samples were weighed before and after polymerization to determine the mass of evaporated monomer.

Thermal Properties

Measurements were made using differential scanning calorimetry (DSC) to determine the glass transition temperature of the polymer laminate. Results are given numerically in table 3, and depicted in figure 20, below. The T_g was calculated as the mid

point of the endothermic slope of phase transformation. In agreement with published data, the T_g of the pure PS was found to lie between 97˚ and 100˚C.

Addition of 1% by weight MLS to the polystyrene lowered the T_g of the nanocomposite by roughly 15˚C. This result appeared somewhat counterintuitive, given the fact that MLS acts as a thermally stable reinforcing agent within the polymer matrix. In this case, however, the presence of small amounts of nanoscale reinforcement served to disrupt the normal interactions and entanglements of polymer chains in the PS without making a significant donation from the thermal characteristics of the MLS itself. Such behavior supports the model of an exfoliated composite system, in which reinforcing platelets are widely dispersed and polymer/platelet interaction is high.

At higher concentrations of montmorillonite, however, such as 3% MLS, the T_g of the laminate rose again to a value on par with the pure PS, indicating that there exists a minima beyond which the properties of the additive become physically apparent in the properties of the composite as a whole. It is also probable that at higher concentrations the silicate distribution is more highly intercalated than exfoliated; the intercalated MLS may congregate more discretely, limiting interactions with the bulk polymer structure.

Material	D Cp (J/g*°C)	T_{g0}† (°C)	T_g (°C)	Endo. Peak (°C)	Peak Area (J/g*°C*min)
PS	0.27	95	97	102	0.07
1% MLS	0.17	81	83	90	0.09
3% MLS	0.28	95	98	104	0.02
† T_{g0} refers to point of endothermic onset of phase transformation					

Table 3: Thermal properties of PS+MLS nanocomposite laminates.

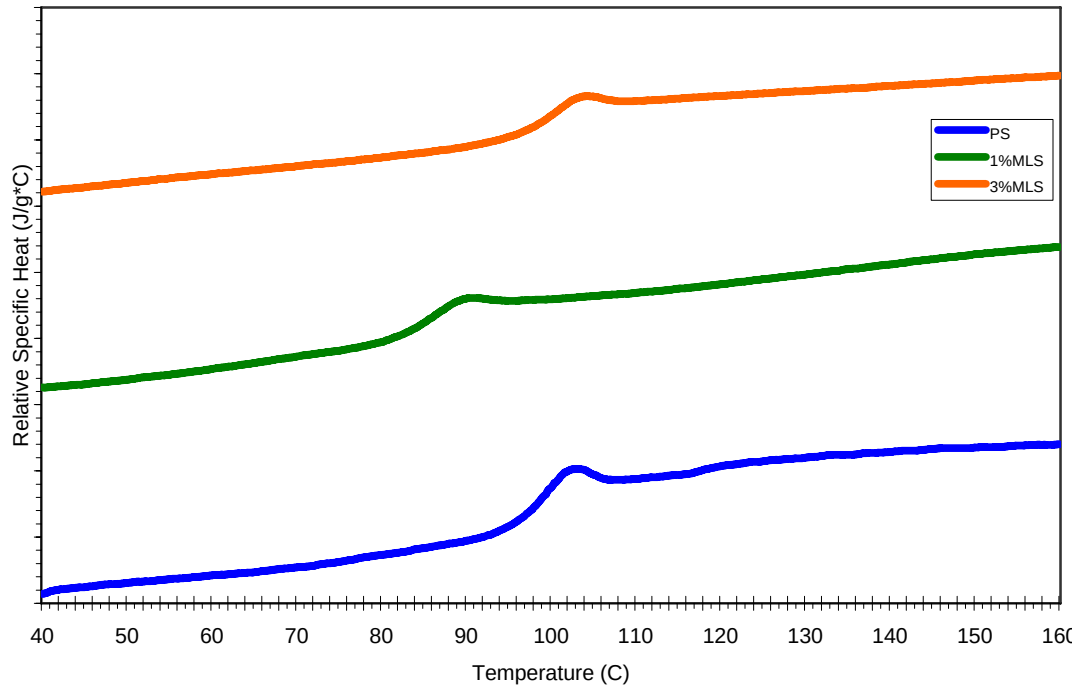

Figure 20: Specific heat – temperature profiles showing depressed T_g of PS+1%MLS sample.

XRD Characterization

In order to verify our observations regarding the presence of exfoliation and intercalation within the nanocomposites, we used X-ray diffraction (XRD) to measure the inter-gallery spacing between the silicate layers in the laminates. The X-ray spectrum of each sample was compared to that of a pure MLS reference and examined for evidence of diffraction peak broadening, intensification, and/or shifting. In both the 1% and 3% MLS composites, the [001] peak appeared both intense and narrow, implying that the layers of silicate in the samples had retained their order and had not experienced extensive exfoliation. The peaks did appear shifted downward on the spectrum, however, which confirmed that the d-spacing, corresponding to the size of the galleries between the MLS layers, had increased due to intercalation (table 4, figure 21). Thus the X-ray data showed

that while intercalation is the dominant form of polymer-MLS interaction, the effects of exfoliation appear to be very limited within both the 1% and 3% nanocomposite.

Sample Composition	[001]		
	FWMH (degrees)	2-Theta (degrees)	d spacing (nm)
MLS	1.65	3.2	2.8
PS+3%MLS (unfoamed)	0.65	2.9	3.0
PS+1%MLS (unfoamed)	0.55	2.9	3.0
PS+1%MLS (foamed)	0.50	2.6	3.4

Table 4. X-ray diffraction data showing increase in gallery d-spacing due to intercalation.

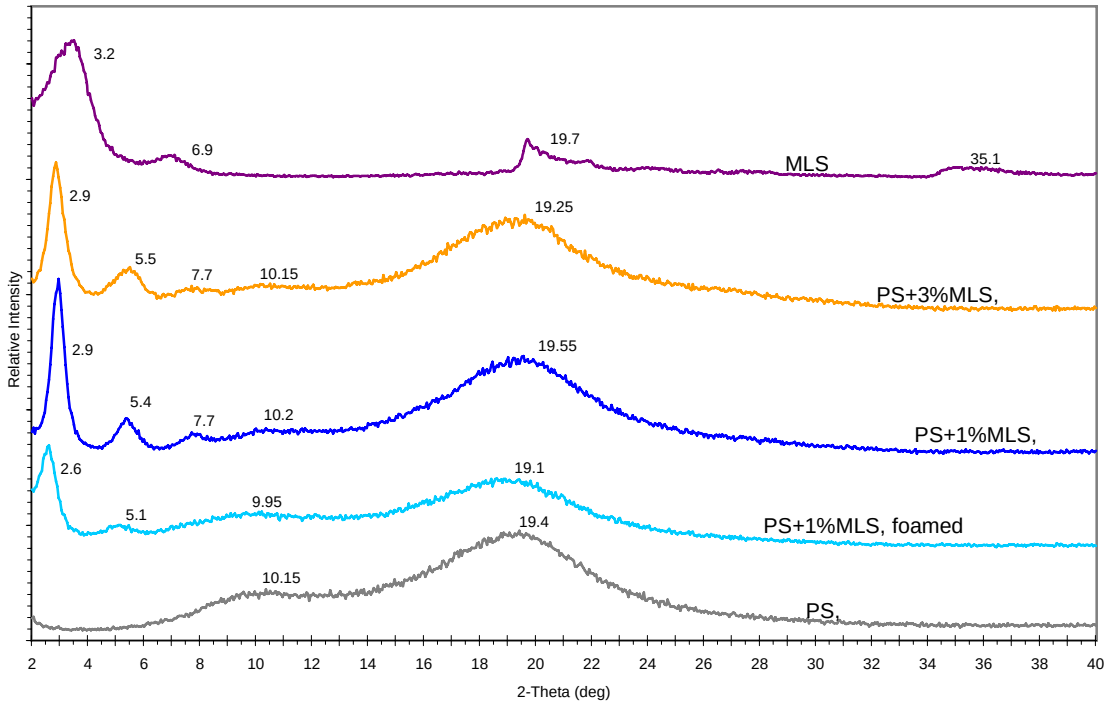

Figure 21: XRD spectra of PS+MLS nanocomposites.

Mechanical Properties

The PS laminate specimens were also mechanically characterized in flexure using a three point bend testing method. The ultimate flexural strength of the samples was approximately 12 MPa, which is lower than that of many commercially available polystyrene resins, while the flexural modulus was measured at 3.3 GPa, which is stiffer

than many of the same cured resins. Thus our laboratory synthesized polymer appeared somewhat brittle.

As expected, the addition of MLS to the polystyrene increased its mechanical properties. In fact, the addition of only 1% silicate yielded an increase of 75% in the flexural strength of the polymer. The flexural modulus of the same material, however, actually decreased 10%; this decrease in stiffness can be attributed to the same cause responsible for lowering the T_g of that 1% composite mixture. Accordingly, both the stiffness and the strength were found to be significantly higher in the 3% nanocomposite than in the pure polystyrene (table 5, figure 22).

Sample Composition	Modulus (GPa)	Ultimate Stress (MPa)
PS	3.3	12
PS+1% MLS	3.0	21
PS+3% MLS	4.2	26

Table 5: Mechanical properties of PS+MLS nanocomposite laminates (3PB test).

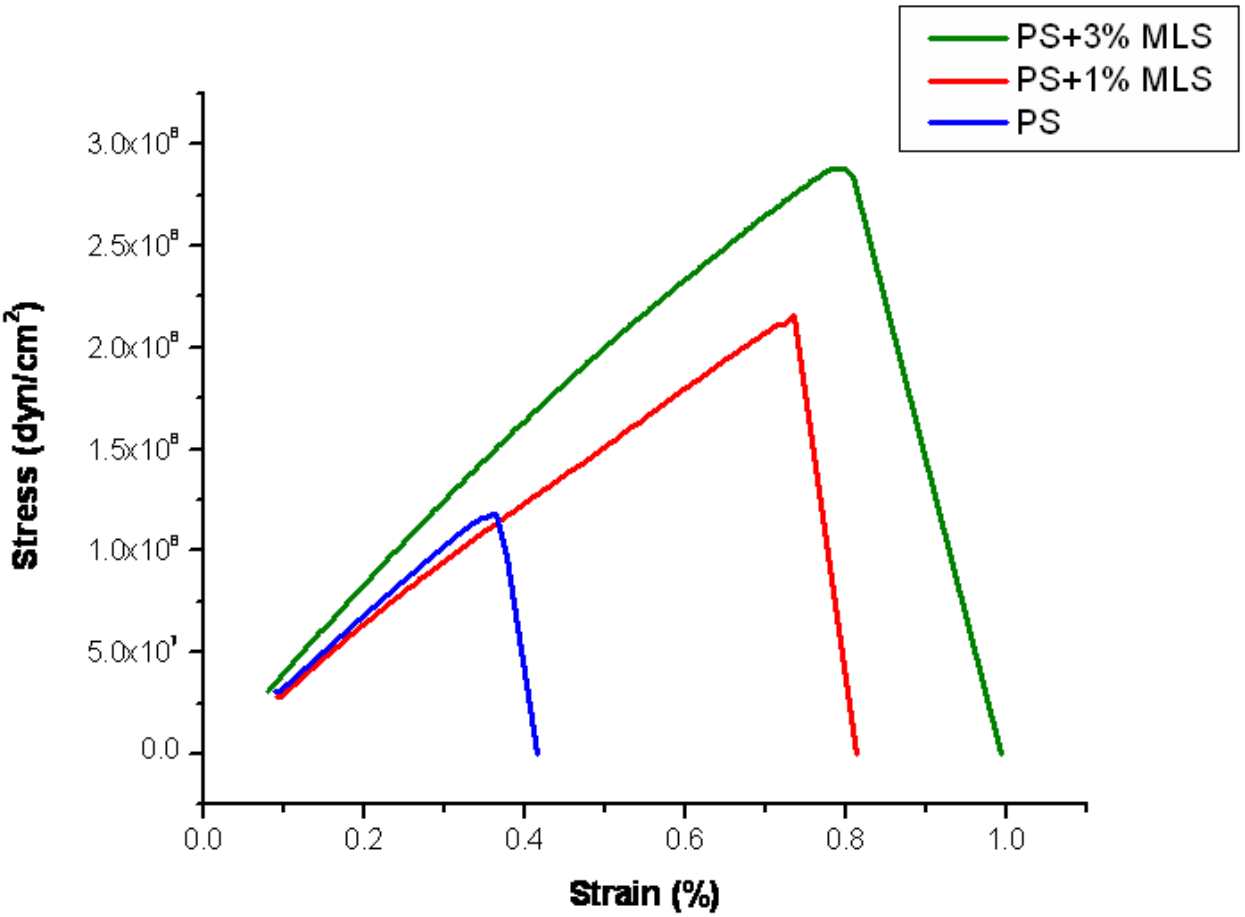

Figure 22: Mechanical properties of PS+MLS nanocomposite laminates (3PB test).

4. SYNTHESIS AND CHARACTERIZATION OF FOAMED NANOCOMPOSITE

4.1. Foaming Process

Supercritical foaming was performed in a Polaron® critical point drier (Model E3100, Quorum Technologies, Newhaven, UK, www.quorumtech.com; see figure 23). For each experiment, a 40mm disk was cut from one of the nanocomposite laminates. The disk was rested on a wire grate and placed inside the drier's reactor chamber. The chamber was cooled to 10°C, and pressurized with liquid CO_2 to approximately 5-6 MPa. The temperature was then raised at 1°C/minute to the process temperature. During this time, the pressure in the chamber increased according to the Ideal Gas Law, and was regulated using a vent valve to maintain process pressure. Process temperatures used were 60°, 75°, and 85°C (table 6). Process pressures, except as noted, were 9.5-10.5 MPa. After reaching desired temperature and pressure, the sample was allowed to soak for a set time, and then was rapidly vented to atmosphere, or quenched, in < 5 seconds. The sample was then cooled at a rate of 1°C/minute to room temperature before removing from the reactor.

		MLS Concentration		
		0%	1%	3%
Foam Process Temperature	60 C	X	X	
	75 C	X	X	X
	85 C		X	X

Table 6: Matrix of experimental foam batches generated.

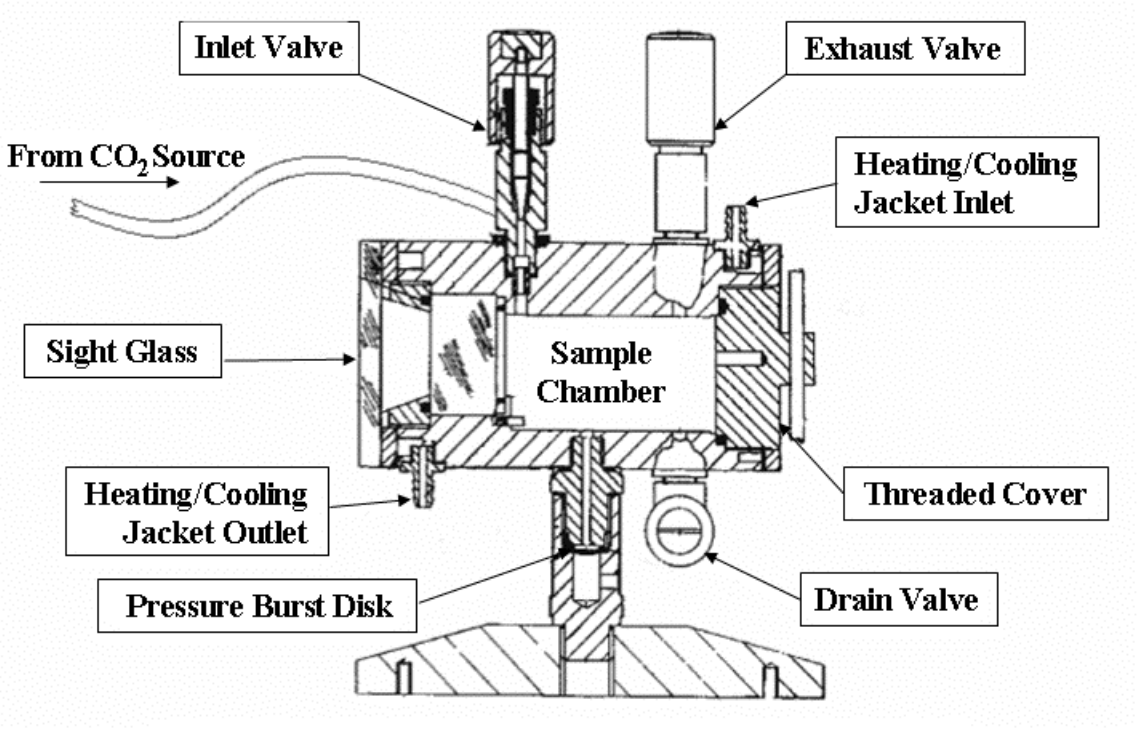

Figure 23: Supercritical reactor used to generate foam samples.

4.2. Fabrication of a $ScCO_2$ Reactor with Improved Capability

During the process of experimentation in this study, it became evident that a larger scale supercritical CO_2 ($scCO_2$) reactor would be necessary to foam samples large enough to demonstrate commercial viability or the process. With that in mind, we designed and built a reactor setup capable of processing samples up to 20.3cm in diameter by 30.5cm long. Figure 24 shows a preliminary illustration of the reactor setup.

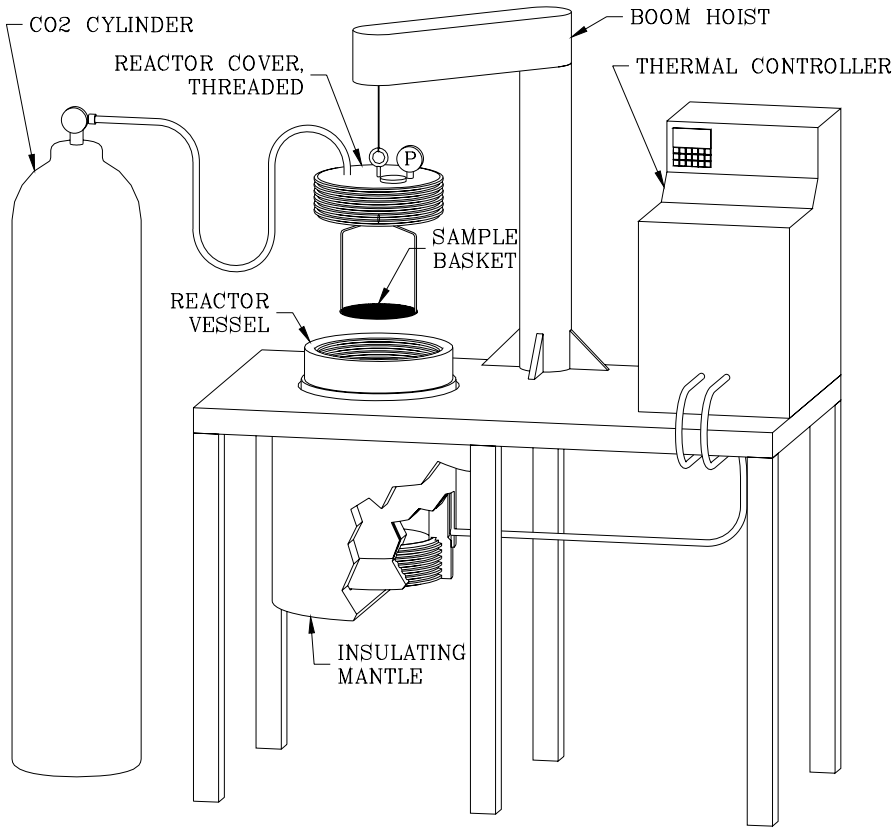

Figure 24: Preliminary sketch of scaled-up scCO2 reactor.

The reactor was designed to be mounted vertically in a benchtop, with an acme threaded lids on each end for simplicity of accessing and servicing the pressure vessel. Dovetail o-ring grooves are provided on each lid for a face seal with the body when tightened. The design of the vessel body includes a welded jacket for circulation of heat transfer fluid from a thermal control unit (TCU). CO_2 is supplied simply from a cylinder or pump to a manifold on the upper lid.

During fabrication, the reactor setup was modified slightly to incorporate all components onto a mobile cart for convenient transport to and from the laboratory. The final product is shown in figures 25, 26, and 27.

Figure 25: Scaled-Up scCO2 reactor, front view.

Figure 26: Scaled-Up scCO2 reactor, left side view.

Figure 27: Scaled-Up scCO2 reactor, right side view.

As can be seen in the photographs, the cart is equipped with a small crane for lifting the lid assembly (which by itself weighs 30kg). The TCU and reactor are capable of heating and cooling from ambient temperature to 315°C, and the vessel's operating pressure range extends to 21 MPa.

4.3. Solvent / Polymer Interactions

In order to understand and optimize the use of $scCO_2$ for the formation of nanocomposite polymer foam, it is important to understand the molecular interactions that occur between the $scCO_2$ and the nanocomposite. Supercritical carbon dioxide acts as a benign solvent in glassy thermoplastic polymers such as polystyrene. Absorption of $scCO_2$ by those materials results in polymer swelling and plasticization. Additionally, in the process of foam generation, reduction of pressure and the subsequent desorption of

CO_2 results in void nucleation and growth. The extents of all these effects are governed by the fundamental parameters of solubility and diffusion.

4.3.1. Solubility

For any solvent-solute system, solubility is influenced by the contributions of three types of molecular level interactions: physical, mechanical, and chemical.

Physical interactions are based on weak forces (van der Waals forces) between molecules, including dipole-dipole and quadrupole interactions, dispersion forces, and hydrogen bonds. Carbon Dioxide cannot experience hydrogen bonding and does not have a dipole moment, due to its symmetrical linear bond configuration, shown in figure 28. CO_2 does, however, exhibit a large quadrupole moment (Q). [38]

$$\Gamma_{ij} \approx -C_3 \frac{Q_i^2 Q_j^2}{r^{10} kT} \qquad \text{(Equation 26)}$$

Equation 1 shows the simplified intermolecular force (Γ_{ij}) due to quadrupole moment (Q_1, Q_2). C_3 represents a constant. As can be seen, the strength of quadrupole contribution is limited by the fact that it is inversely proportional to the tenth power of the intermolecular distance *r*; dipole contributions, on the other hand, are inversely proportional to r^6. The relative insignificance of the quadrupole forces in CO_2 are evidenced by the fact that CO_2 is a gas at ambient conditions, and has a relatively low critical point.

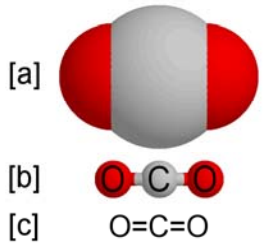

Figure 28: Molecular structure of CO_2 represented schematically using: [a] van der Waals radii, [b] ball and stick model, [c] Couper structure.

Polarized solvents tend to be more effective at lower temperatures where polar attractions between solvent-solute molecules are the most effective. At high solvent temperatures close to the critical point, however, dipole influence is much diminished, as evidenced by the appearance of gas-like properties. Because supercritical conditions are inherently inhospitable for dipole interactions, there is little incentive for the use of polar solvents as SCF (supercritical fluid) solvents. They may, however, be effective as cosolvents with SCF, as will be discussed later in this chapter.

In the case of $scCO_2$ and polystyrene (PS) nanocomposite, because neither material is dipolar, the physical intermolecular forces at work are predominantly dispersion forces. Dispersion forces, caused by momentary dipoles and induced intermolecular vibrations, are governed by the simplified equation:

$$\Gamma_{ij} \approx -C_1 \frac{\alpha_i \alpha_j}{r^6} \qquad \text{(Equation 27)}$$

where α_i and α_j are molecular polarizabilities, r is the intermolecular distance, and C_1 is a constant.

Calculations of miscibility based on physical interactions compare the strengths between solvent-solvent, solute-solute, and solvent-solute molecular pairs.

$$E = z\left[\Gamma_{ij} - \frac{1}{2}\left(\Gamma_{ii} + \Gamma_{jj}\right)\right] \qquad \text{(Equation 28)}$$

In order for solvent-solute interactions (Γ_{ij}) to be favorable, the interchange energy of mixing (E) must be positive (where Γ_{ii} and Γ_{jj} represent like-like interactions).[114] Z represents the coordination number, or number of possible ways for interactions to occur. In a highly polarized solvent, solvent-solvent interactions may become dominant and limit miscibility; likewise if a solvent is nonpolar, solute-solute interactions may dominate. Optimum physical miscibility is obtained when the intermolecular forces of the solvent and solute are balanced. In order to quantify intermolecular dispersion forces in a form useful for miscibility calculations, Hildebrand and Scott introduced a term called the solubility parameter (δ).[115] Using solubility parameters, they calculated heat of mixing (DH) as:

$$\Delta H = \phi_1\phi_2\left(\delta_1 - \delta_2\right)^2 \qquad \text{(Equation 29)}$$

Where Φ1 and Φ2 are volume fractions of solvent and solute, and δ_1 and δ_2 are their respective solubility parameters. In this equation, solubility increases as DH approaches zero.[41] Thus, in order to optimize physical solubility of scCO2 in a polymer, it is important that the two materials have similar solubility parameters. One rule of thumb for this relationship is $\left(\delta_1 - \delta_2\right) \leq 1$.[38]

While the original definition of the solubility parameter was quite simple:

$$\delta = \sqrt{\Delta E / V} \qquad \text{(Equation 30)}$$

(where ΔE is the energy of vaporization in a vacuum),[115] it was only applicable to low molecular weight compounds for which ΔE could be measured using a practicable method. For high molecular weight materials (e.g. polymers), solubility may be measured indirectly by measuring swelling due to solvents of known solubility. This method, however, has yielded imprecise and inconsistent results.[116] Coleman et al. present an approach (originally attributed to P.A. Small in 1953) that estimates polymer solubility parameters based on molar attraction constants. Their calculations use the relationship:

$$\delta = \Sigma F_{ij} V \qquad \text{(Equation 31)}$$

where F is a molar attraction constant. [116,117] Table 7 shows representative calculations and measurements of polymer solubility parameters taken from their work.

Polymer	δ Experimental (cal cm^{-3})$^{1/2}$	δ Calculated (cal cm^{-3})$^{1/2}$
Polypropylene	8.2-9.2	7.4
Polyethylene	7.7-8.4	8.0
Poly(methyl methacrylate)	9.1-12.8	9.0
Polystyrene	8.5-9.3	9.5
Poly(vinyl chloride)	9.4-10.8	9.9
Poly(ethylene terephthalate)	9.7-10.7	11.5
Polyacrylonitrile	12.5-15.4	13.8

Table 7: Solubility parameters of some common polymers.[116]

Just as polymer solubility parameters are difficult to obtain due to their high molecular weights, SCF solubility parameters are problematic due to the inability to vaporize the supercritical phase. Based on the fact that the energy of vaporization used in equation 5 is analogous to the "cohesive energy" of the material, Johnston and Peck presented the following definition for the SCF solubility parameter[118]:

$$\delta = \sqrt{\frac{u^{ig} - u}{v}} = \sqrt{\frac{h^{ig} - RT - h - Pv}{v}} \qquad \text{(Equation 32)}$$

where v is molar volume, u^{ig} is the internal energy of an ideal gas, and u is the internal energy of the SCF. In this case, the more that the fluid behaves as an ideal gas, the closer the solubility parameter approaches to zero. Giddings et al. previously proposed a more simple expression based on the density dependence of solubility:

$$\delta = 1.25 P_c^{1/2} \left(\rho_r / \rho_{r,1} \right) \qquad \text{(Equation 33)}$$

where P_c is the critical pressure (in atmospheres), ρ_r is the reduced density, and $\rho_{r,1}$ is the reduced density at boiling (given a value of approximately 2.66).[119] The work of Giddings is often cited in texts regarding supercritical CO_2, and is reviewed in detail by McHugh and Krukonis.[38]

Both equations 32 and 33 show that the solubility of supercritical fluids is variable, dependent on density. To further elaborate upon this point, figures 29 and 30 show variable densities and variable solubility parameters of CO_2 in the critical region. Note the similarity of the two figures.

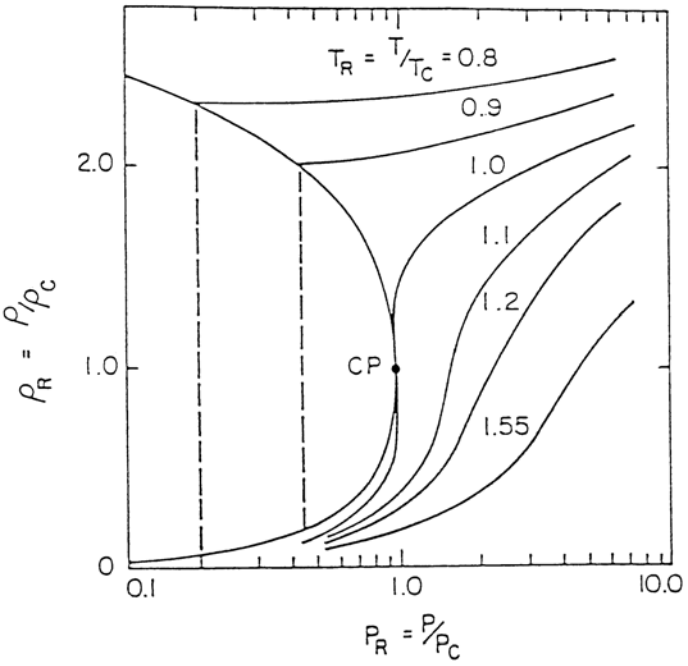

Figure 29: Reduced density of CO_2 as a function of reduced pressure at different isotherms.[41]

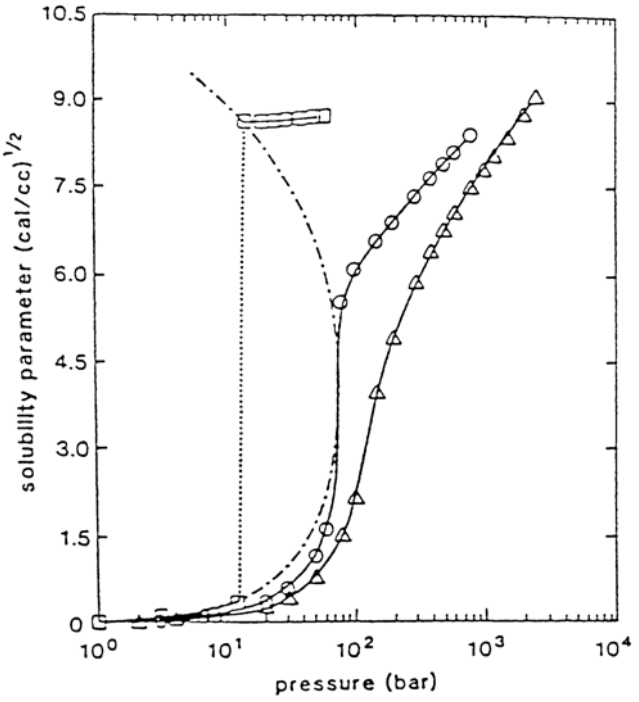

Figure 30: Solubility parameter of CO_2 as a function of pressure at different isotherms.[41,118]

A comparison of the solubility parameters of $scCO_2$ and polystyrene should provide some indication of the miscibility of the two compounds. According to equation 7, the solubility parameter of gaseous CO_2 is essentially zero, whereas the solubility parameter of PS is approximately 9.5 (table 7). Following equation 8, it would be necessary to pressurize $scCO_2$ to a reduced density (ρ_r) of approximately 2.12 (almost 1g/ml) in order to achieve the favorable relationship $(\delta_1 - \delta_2) \leq 1$. Such a high density would require 50 MPa of pressure at 40°C, and almost 90 MPa at 80°C. These pressures are far beyond the reach of most industrial polymer manufacturing processes, not to mention the SCF vessels in our laboratory, which are designed for operation below 12 MPa. Nonetheless, several recent studies have shown that $scCO_2$ is partially soluble in PS, up to 13% by weight at pressures below 20 MPa.[120,52,121]

The reason that CO_2 solubility in PS is not predicted by solubility parameters alone is that, as mentioned before, physical models of SCF/polymer miscibility do not fully describe systems with other specific chemical interactions. In fact, Hildebrand warned that the use of solubility parameters should not even be extended to cases involving dipolar solvents.[38] Therefore, it is important to add to our analysis of solubility an understanding of the contributions of specific chemical interactions in $scCO_2$/polymer systems.

Specific chemical interactions that facilitate solubility may include hydrogen bonds, acid-base relationships, or other electron donor-acceptor interactions. In the case of $scCO_2$, Kazarian et al. have investigated the possibility of Lewis acid-base relationships between CO_2 and carbonyl groups of various polymer molecules.[122] The

concept of CO_2 acid-base relationships was first proposed by Hildebrand, Prausnitz, and Scott in 1970 as an explanation for the solubility of CO_2 in polymers with grossly different solubility parameters, and specifically aromatic polymers.[123] According to their theory, CO_2 could behave as an electron acceptor (Lewis acid) in the presence of various electron donor species in polymers. Figure 31 shows schematically how a CO_2 molecule could align itself with an electron donor carbonyl group in either a 'T' and 'Bent T' configuration, respectively.

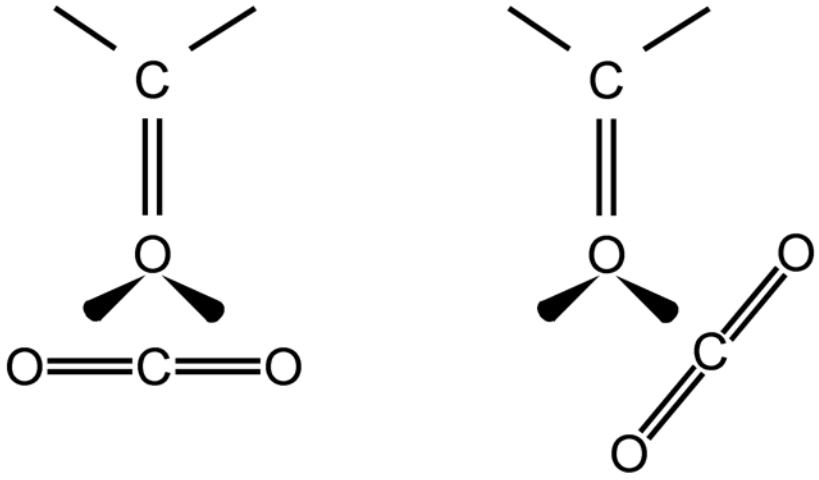

Figure 31: Lewis acid-base configurations between CO_2 and polymer carbonyl groups.[103]

Because of the strong quadrupolar arrangement of the atoms in the CO_2 molecule, any interaction in which CO_2 acts as a Lewis acid must involve a simultaneous attraction of the carbon atom and repulsion of the two oxygen atoms on either side. This results in a bending strain on the molecule. As can be seen in the above figure, for interactions with carbonyl groups this bending attraction can be due to two possible configurations. Kazarian et al. hypothesized that if such an interaction was taking place, it should affect the characteristic bending mode of CO_2 molecular vibration. In order to detect molecular

stretching modes, M. Vincent (working with Eckert and Kazarian) measured the IR spectrum of CO_2 dissolved in various polymer systems.[103] Using FT-IR and ATR-IR spectroscopy, he was able to confirm that in the presence of basic polymers, the bending mode (v_2) of CO_2 was both shifted and split into two distinct bands, each representing one of the two possible configurations of CO2 / carbonyl group interaction. Other stretching modes, such as asymmetric stretching (v3) were unaffected. Polymers with measurable basicity, such as polymethyl-methacrylate (PMMA), polyvinyl-methyl-ketone (PVMK), polyvinyl-acetate (PVAc), polyamide (PA), polyethylene-teraphthalate (PET), and polyvinyl-fluoride (PVF), all induced splitting in the CO2 bending peaks; however, polymers without strong electron donor sites, including PE and PS, were not found to exhibit a split v2 peak in their FT-IR spectra. Therefore, it was discovered that although Lewis acid-base interactions do have a strong influence on $scCO_2$ solubility in many polymers, they do not predict improved solubility of CO_2 in PS.

Vincent's IR spectra did, however, point to a different type of interaction between CO_2 and PS. His plots showed that in polystyrene, the v_2 peak of CO_2 is broadened; this indicates distortion of the bending mode by some other electrostatic interaction between the electron receptive carbon atom of CO_2 and the PS molecule.

At the same time that Vincent and Kazarian were analyzing supercritical fluids with IR spectrometry, Miyoshi et al. were trying to use NMR spectroscopy to explore solubility of $scCO_2$ in polystyrene.[124] In order to accomplish their experiments, they first had to develop a novel high pressure chamber made of Pyrex that could contain their polymer samples in the presence of SCF (they used both CO_2 and Xe). The method they

developed, described as HPMAS (high pressure MAS), was a high pressure adaptation of ^{13}C CPMAS NMR (carbon-13, cross polarization, magic angle spinning nuclear magnetic resonance).[125] Their results, in agreement with Vincent's IR work, evidenced specific electrostatic forces between the PS chains and the CO_2. In the NMR spectra this was revealed as a decrease of sideband intensities, which are linked to anisotropy of carbon atoms in the phenyl ring of polystyrene. They proposed that the interaction observed was in fact a CO_2 induced shift of the phenyl ring. Such an interaction is similar to Lewis acid-base relationships in as much as they are both enabled by the CO_2 quadrupole field; however the Phenyl ring / CO_2 interactions are much weaker and without fixed conformations. In order to understand the difference between the two, it may be helpful to compare CO_2/PS solubility with CO_2/PMMA solubility. Both polymers have similar solubility parameters (~9.5) and both have glass transition temperatures (T_g) well above the critical point of CO_2 (100°C, 130°C respectively). PMMA contains basic carbonyl groups, and it has been shown that CO_2 solubility in PMMA is in excess of 30% by mass at temperatures and pressures close to the critical point of CO_2.[46]

Shieh and Liu have attempted to quantify the varying effects of specific chemical effects on solubility by using power laws:

$$C = kP^n \qquad \text{(Equation 34)}$$

where C is sorption concentration, k is a constant related to heat of sorption, P is pressure, and the exponent n is the "sorption intensity" which accounts for specific interactions between solvent and solute. They reported that using their method, PMMA exhibited a sorption intensity 1-2 times higher than that of PS (in $scCO_2$).[46]

In addition to physical and chemical influences on solubility, mechanical contributions must also be considered. Mass transfer of solvent into the solute requires the bulk material to accommodate whatever volume of solvent is absorbed. In the case of CO_2 absorption by a polymer, the added volume is partially accounted for by polymer swelling. Solubility may be enhanced, however, by the presence of excess free volume between loosely packed chains of polymer molecules, as well as by decreased stiffness of the polymer chains. The former effect has been found to be more influential at low concentrations and pressures, whereas the latter is more predominant if the polymer becomes highly plasticized.

As pressure is added to a polymer/CO_2 system, two opposing influences occur. The first is that, as discussed previously, the density and solubility parameter of the CO_2 increases, along with the likelihood of favorable solvent-solute interaction. The second is that the density of the bulk polymer also increases, which decreases the molecular mobility of polymer chains as well as the free volume between chains.[125] At low pressures, vapor solubility is higher in low density polymers. As pressure increases, the slope of vapor solubility is dependant on the balance between the two opposing influences (increased solvent-solute interaction vs. decreased polymer mobility). Initially, this balance of forces may be approximated by a constant according to Henry's law. Sato et al. have demonstrated this experimentally in the binary system of PS/CO_2.[44] Figure 32 depicts the results of their work. As can be seen, their experimental data tracks linearly, as solubility increases in direct proportion to pressure. Also evident is the fact that as temperature is increased, the slope of solubility vs. pressure decreases. Increasing

temperature at a given pressure effectively decreases the density of CO_2 in the system, thereby simultaneously decreasing both the partial pressure of the CO_2 (p) and increasing K'_C. The latter effect may be explained by Le Chatelier's principle; because the dissolution of gases in solids is generally entropic (tending towards disorder) and exothermic (releasing heat energy in the process), the addition of heat to the system (by increasing temperature) will normally cause a shift in the equilibrium towards lower solubility.[126] K'_C may be expressed as work per mole, and reflects the energy required for dissolution; therefore it is inversely proportional to solubility.

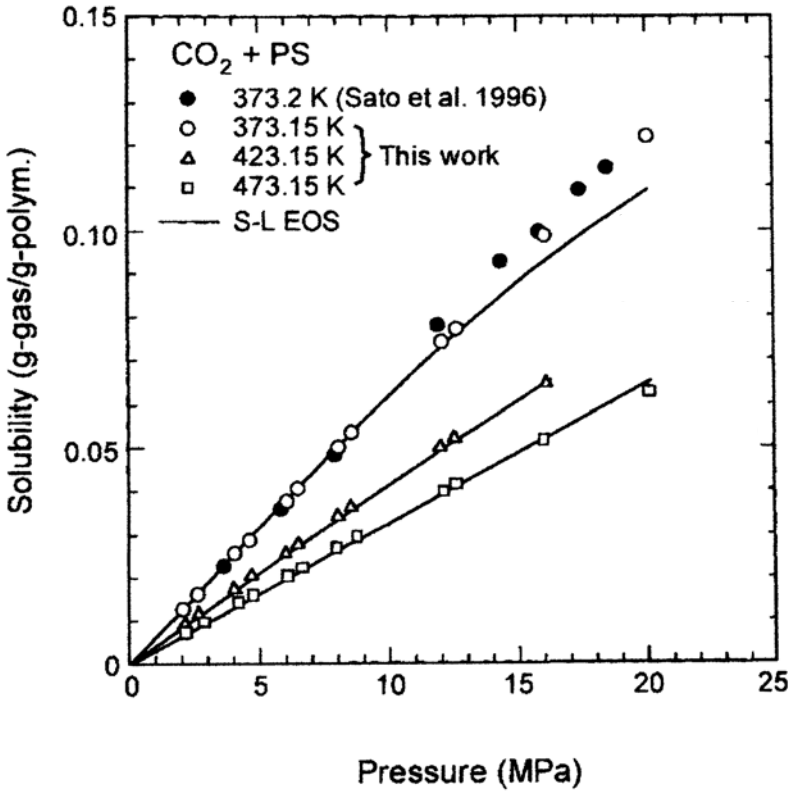

Figure 32: Solubilities of CO_2 in polystyrene melts between 100°C and 200°C.44

In all cases, however, above a certain characteristic value, the solubility of a compressed gas in a polymer ceases to be a linear function. Zhang has reported that in the

case of PS/CO_2 systems at 35°C, Henry's law may be used for pressures up to 3 MPa.[41] Beyond that limit, the solubility curve approaches a limit. This limit has been found to lie around 13% CO_2 by mass.[121,44] (Zhang has estimated the limit at a lower value close to 8%).[41] Zhang, as well as Nikitin et al. have implied that the solubility limit is related to the swelling limit for polymers in the glassy phase.[41,47] For polymers plasticized or heated to the rubbery or liquid phases, the solubility limit may be a related to non-ideal compressibility of the SCF.

Han et al. have effectively modeled the solubility of PS/CO_2 and have found that at 20°C a solubility limit is approached at 6 MPa, below the critical point.[127] Figure 33 presents a 3D rendering of their model.

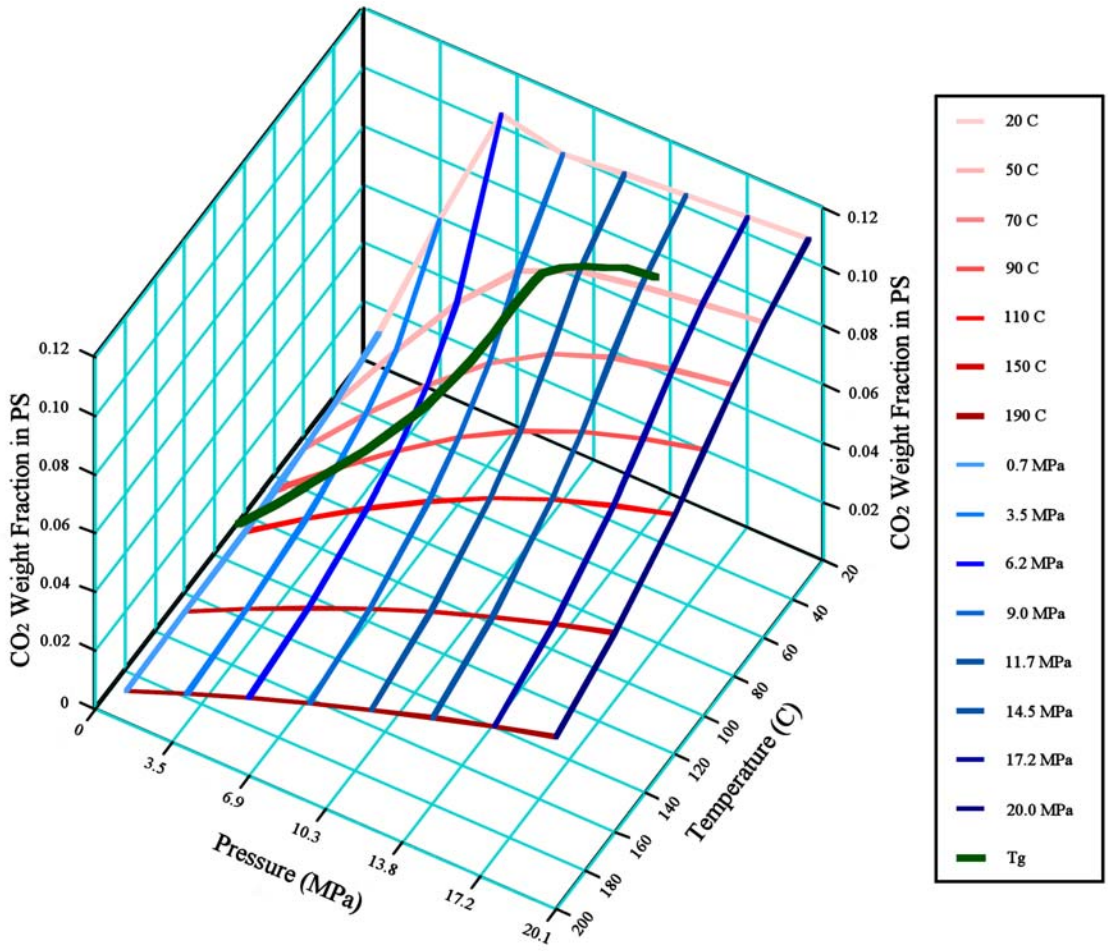

Figure 33: Equilibrium content of CO_2 in PS at various temperatures and pressures.127

Mechanical effects on solubility also may play a special role in the processing of composites. Chen et al. have shown that absorbed gasses can reside at the interfaces between bulk polymers and reinforcing fillers.[128] Figure 34 is a sketch showing the theoretical existence of micropores, void-like imperfections inherent in the mixing of filled polymers.

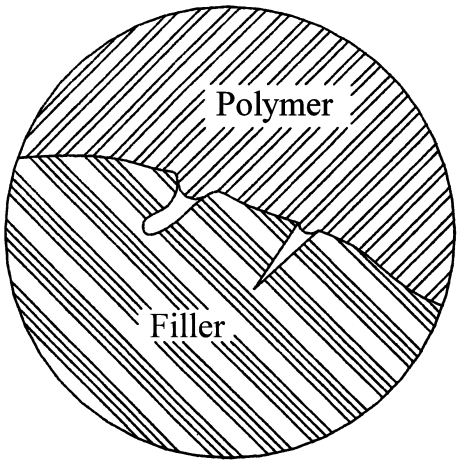

Figure 34: Micropores at polymer/filler interface of nanocomposite.128

In the process of compounding polymers with common fillers such as talc or $CaCO_3$, Chen's group found that it is very conceivable that polymer surface tension could create such micropores, and they theorized that their existence should result in higher gas absorption by filled polymers. Assuming that the fillers did not absorb any CO_2, they measured and normalized the gas absorption of filled and unfilled HDPE and PVC. In both cases it was confirmed that gas absorption was in fact related to the presence of fillers, although the relationship was not linear. In one typical example, the addition of 2% CaCO3 filler in PVC increased CO_2 sorption from 3.0% to 3.4%, while the addition of higher percentages of filler were accompanied by diminishing increases in sorption.

4.3.2. T_g Depression

As mentioned previously, one of the primary effects of polymer / SCF interactions is polymer plasticization, which is indicated by an observed depression (reduction) of the glass transition temperature (T_g) of glassy polymers.[129,130,131,120] The amount that a polymer's T_g is reduced depends on the level of polymer/SCF interaction

(i.e. the solubility), as well as on the pressure placed on the system. It is this phenomenon of depressed T_g that permits polystyrene to foam at temperatures far below its natural T_g of roughly 100°C. It has been shown that in the presence of supercritical CO_2, at pressures of 20 MPa (2900psi), the T_g of polystyrene is reduced to 35°-40°C.[99] Within the pressure range used in this study, the T_g was reduced to approximately 60°-70°C.

Glass transition in polymers has traditionally been modeled using one of two major theories: either the free volume theory or the entropy theory. The free volume theory, introduced by Fox and Flory, assumed that molecular mobility is primarily a function of free volume and temperature.[132,133] According their theory, increasing pressure on a polymer system results in densification and an increase in the glass transition temperature due to reduced free volume and molecular mobility. Such phenomena are observed in single component glassy polymers. Although many extended and modified versions of the free volume theory exist, the original concept leads to the conclusion that glass transition may be defined as the point where the opposing effects of temperature and pressure yield a critical specific volume (V_g). This V_g should remain a constant characteristic of the material; models based on this theory are often termed "iso-free volume" models. A critical issue encountered by these iso-free volume models is that experimental results show that as pressure is increased, glass transition does occur at lower and lower values of V_g.[134,135] A second (and perhaps ultimately more important) problem with free volume models lies in the fact that they do not take into account thermodynamic factors. Because free volume models are fundamentally kinetic instead of thermodynamic, they run aground on the hypothetical "Kauzmann paradox." The

Kauzmann paradox implies that if no thermodynamic basis for glass transition exists, it should be possible for a supercooled liquid, cooled at an infinitely slow rate, to achieve a state of entropy equal to or lower than that of its corresponding crystalline material.[136] Such a possibility would be in violation of the third law of thermodynamics, and should necessarily be addressed by any comprehensive theory of glass transition.[137]

In order to address weaknesses in the free volume theory, a thermodynamic model of glass transition was introduced by Gibbs and DiMarzio, who called it the entropy theory of glass transition (it is now famously known as the Gibbs-DiMarzio theory).[138] According to the entropy theory, conformational entropy decreases within polymer systems as intramolecular interactions stiffen the cooling macromolecular chains; the stiffened chains have exponentially fewer possible conformations since they require cooperative rearrangement of stiffened segments. In this manner Gibbs and DiMarzio were able to satisfy the Kauzmann paradox while simultaneously addressing the issue of the pressure dependence of T_g. In later work, they showed that the pressure dependence is finite, and that densification of glassy polymers (reduction of free volume, entropy) approaches an upper boundary as pressure is increased.[139]

Although thermodynamic models of glass transition are more widely applied today than are free volume models, it is generally recognized that a comprehensive theory should include elements of both.[140] One such theory is the popular Adam-Gibbs theory.[141] The Chow model is another oft cited theory of glass transition, one which is both predictive in nature and tractable for simple calculations.[129] Originally intended as an extension of the Gibbs-DiMarzio theory, the Chow model predicts T_g depression

based on monomer molecular weight (M_M), solvent solubility, and the specific heat of transition for the pure polymer (ΔC_{pp}):

$$\ln\left(\frac{T_g}{T_{g0}}\right) = \beta\left[(1-\theta)\ln(1-\theta) + \theta\ln(\theta)\right] \qquad \text{(Equation 35)}$$

where T_{g0} is the glass transition temperature of the dry polymer, T_g is that of the polymer/solvent system, and β and θ are dimensionless parameters equal to:

$$\beta = \frac{zR}{M_M \Delta C_{PP}} \qquad \text{(Equation 36)}$$

$$\theta = \frac{v_M(1-\varphi_P)}{zv_S\varphi_P} \qquad \text{(Equation 37)}$$

v_M and v_S are the monomer and solvent molecular volumes, respectively; z is the lattice coordination number (established previously as 2 for polymer systems). The Chow model has been applied successfully to so many polymer/scCO$_2$ combinations that it has become a benchmark by which many researchers correlate their empirical data. Like other theories based on the lattice model, it is primarily applicable in situations where solvent and monomer molecules are similar in size.

Regardless of whether a kinetic or thermodynamic approach is taken, plasticization by solvent absorption is an intuitive concept. The introduction of a low molecular weight species interstitially within a polymer lattice increases both the specific volume of the polymer and the configurational entropy of the system, both of which may be used to describe a depression of the T_g. Where results of different models vary is in their prediction of T_g trends at very high temperatures; one of the reasons for such differences is that different polymer/SCF systems behave differently at very high

pressures. Polystyrene, for instance, has been shown to exhibit a T_g minima in the presence of $scCO_2$ at around 20MPa and 36°C, reported by Wang et al. and shown in figure 35.[99] In order to explain the existence of the T_g minima, Wang used a kinetic approach to show the balance of two trends: continually decreasing free volume due to hydrostatic pressure, which eventually overcomes the limited plasticization effect of solvent solubility.

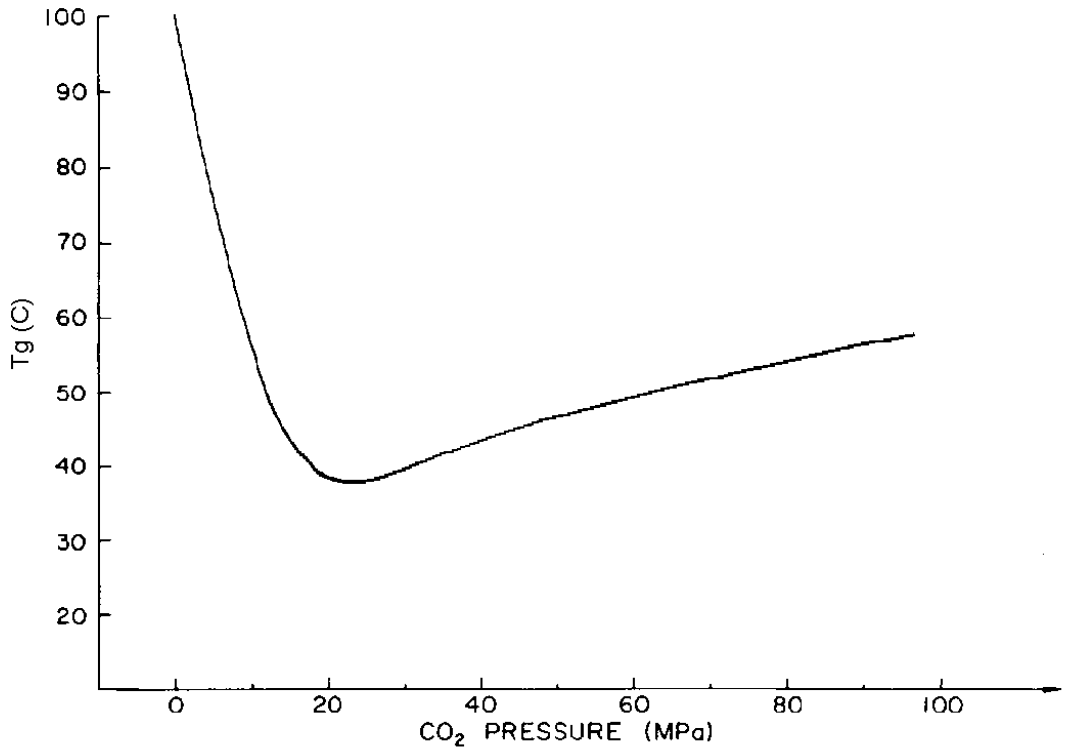

Figure 35: T_g of PS in the presence of $scCO_2$ at varying pressures. Adapted from Wang et al.[99]

PMMA, which is characterized by higher $scCO_2$ solubility than PS, does not exhibit a similar minima. In fact, Wissinger and Pauliatis reported that increasing pressure had little effect on the T_g of PMMA.[120] Condo and Johnston, who modeled its

glass transition over a wider range, found that the T_g of PMMA was in fact affected by pressure, but that beyond a pressure maxima of about 5.8 MPa the polymer and solvent became fully miscible and resulted in a liquid mixture at all observed temperatures.[98] Figure 36 illustrates the pressure maxima they found in the glass transition curve; the effect leads to a phenomenon called "retrograde vitrification," where within a range of pressures and temperatures (e.g. 3.5 MPa, 0°C), a low temperature liquid can actually be solidified by raising its temperature.

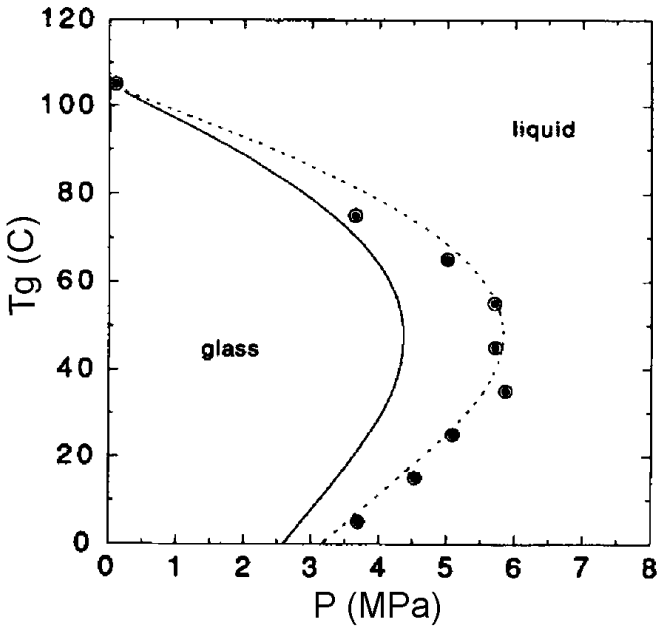

Figure 36: T_g of PMMA in the presence of $scCO_2$ at varying pressures; [——] predicted T_g, [- - -] observed.[98]

In both the cases of PS and PMMA, the factor that correlates best with T_g depression within the pressure ranges commonly encountered in SCF processing is the solubility of SCF within the polymer. Because $scCO_2$ is an efficient solvent in both these systems, T_g exhibits a nearly inverse linear relationship with mass absorption of solvent

at all but the highest pressures. This relationship between T_g and solubility has been frequently expressed by the approximation:

$$T_g \approx T_{g0} - k\omega_S \qquad \text{(Equation 38)}$$

where k is some constant and ω_S is the weight fraction of solvent in the polymer system.[129,142]

4.4. Foam Properties

4.4.1. Poly(Styrene) Foam

Process Temperature Effects

Our foaming experiments were successful in creating macrocellular, closed cell foams both in pure polystyrene and polystyrene / montmorillonite layered silicate (PS+MLS) laminates. For complete foaming of the 1.1mm thick pure PS laminates, we found that a minimum 1 hour soak was required for diffusion of supercritical CO_2 throughout the sample prior to pressure quench. This parameter is consistent with the findings of similar work, in which soak times for SCF foaming of small samples has been published at 3 hours to 24 hours for process temperatures of 80˚C and lower.[7,12,29] In our experiments, uniform polystyrene foams were obtained at temperatures at or above 60˚C, pressures at or above 9 MPa, and soak times at or above 4 hours. 60˚C was very near the effective glass transition temperature of the samples when they were saturated with SCF CO_2 in the reactor vessel. Because of this proximity to the T_g, variations in temperature had a large effect on the morphology of the foams. At temperatures below the effective T_g, foaming did not occur at all; instead, when the reactor pressure was released to generate foaming, expansion of the absorbed CO_2 in the laminate caused crazing and

cracking in the laminate. At the lowest successful foaming temperatures, cell size was smallest, often less than 10μm, cell shape was ellipsoidal, and cell walls were thick. When higher process temperatures were used, cells became larger, and interaction between cells caused the cell walls to become thin and flat; if the temperatures used were too high, these walls would rupture, creating voids and/or local areas of open-celled foam structure. The effects of soak temperature on foam development are due to more than one simultaneous influence. First, temperature has an inverse relationship to the viscosity of the PS, thereby enhancing both nucleation and growth of cells. As viscosity decreases, so does the critical radius of void nucleation; and this effect tends to increase cell density (cells/cm^3). At the same time, it also decreases the energy required for cell growth, which permits greater volumetric expansion of the foam. A second effect of temperature, however, lies in its relationship to diffusion rates. As temperature increases, so does the rate of desorption of the foaming agent from the bulk polymer, both into the growing foam cells as well as into the atmosphere surrounding the sample in the reactor chamber. This desorption leaves localized depleted regions in the foam where there is insufficient dissolved CO_2 to initiate void nucleation; thus decreasing the total density of cells while increasing the sizes of the extant cells. Depletion of CO_2 near the exposed surfaces of the foam also causes the skinning effect, in which cell size and density gradually decreases with distance from the surface, leaving a nonporous polymer "skin" over the outside of the sample. In figure 37 below, the skinning effect can be seen towards the bottom of the cross sectional micrograph.

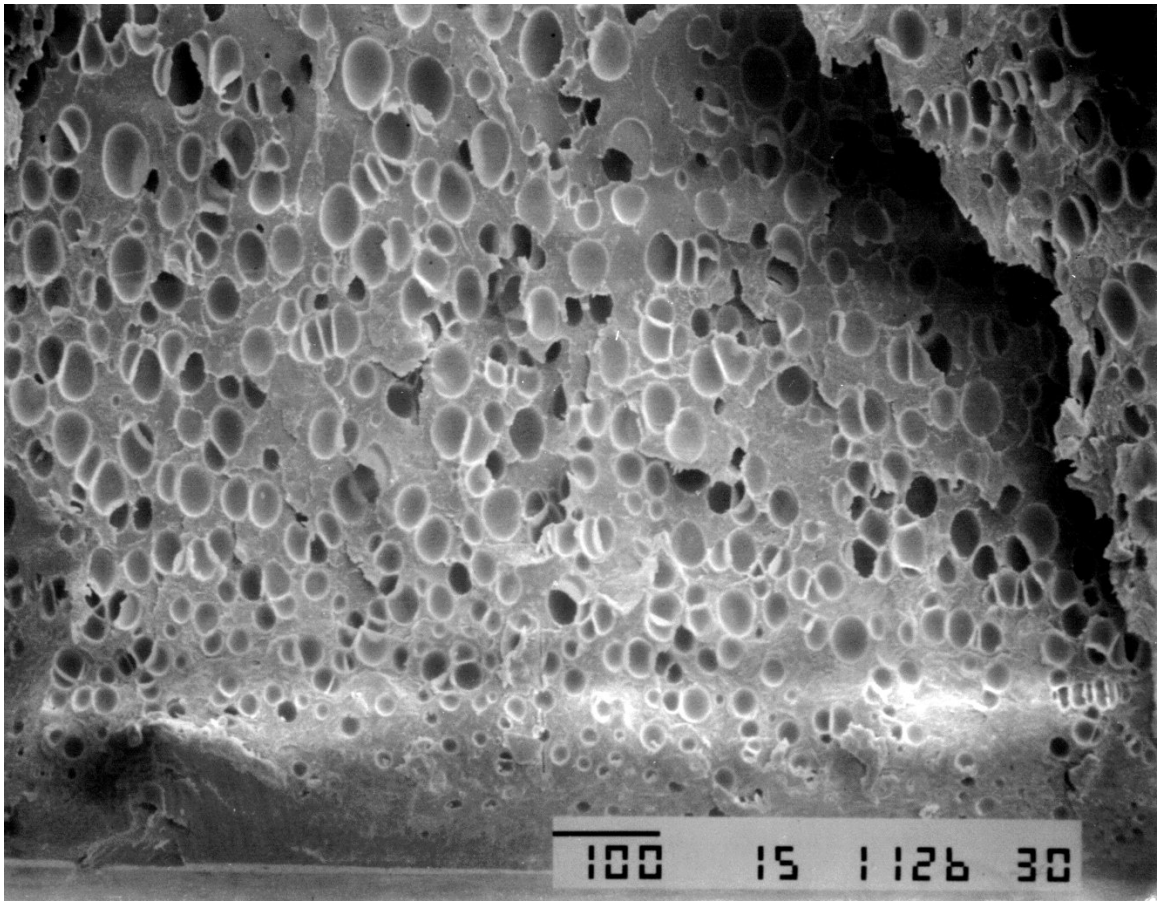

Figure 37: Micrograph of PS foam showing skinning effect at bottom edge.

The end result of the process temperature effect on the foam product was that cell density was initially seen to decrease as temperature increased, in agreement with previous findings.[7,10,36] At 85˚C, however, cell density showed a moderate increase. This may be attributed both to lowered critical radius of void nucleation, and to the limitation of cell geometry that occurs as a finite volume of CO_2 desorbs into them. Figure 38 shows the effect of processing temperature on foam morphology as observed by scanning electron microscopy (SEM).

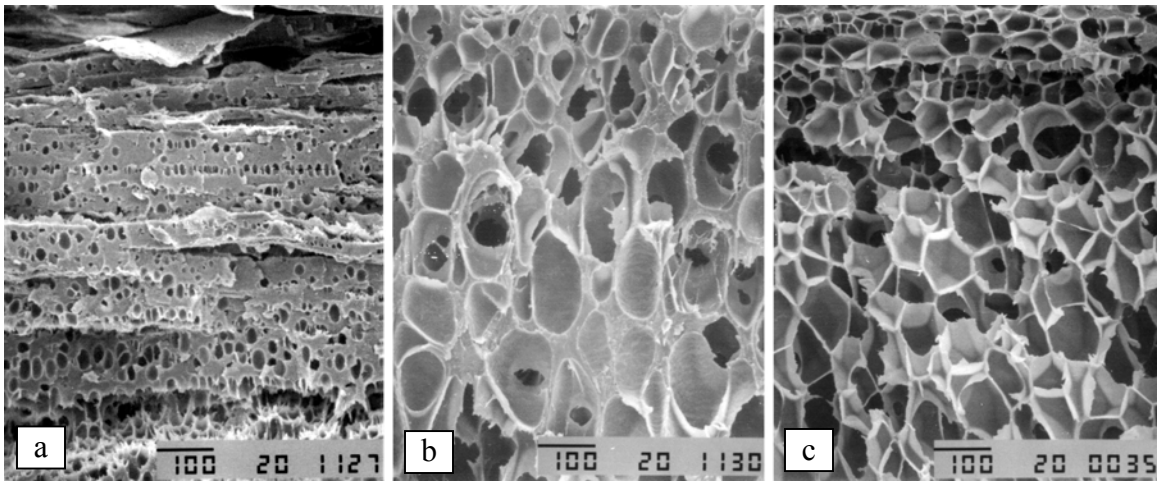

Figure 38: Micrographs of PS showing effect of temperature on foam structure. Processing at: [a] 60°C (Nf=2.4E7); [b] 75°C (Nf=7.6E5); [c] 85°C (Nf=3.0E6)

Process Pressure Effects

Pressure has been shown to have an effect on foam morphology in several key ways. First, increased pressure in the reactor during soak increases the total mass uptake of CO_2 by the sample, which in turn increases potential volumetric expansion of the foam product while decreasing the effective T_g of the sample. As stated previously, the T_g of the PS laminates in our experiments was decreased to around 60˚C at 10MPa; had we doubled our pressures to 20MPa, the T_g would have been lowered to approximately 40˚C. Another variable influenced by process pressure is the total pressure drop during quench. Because the pressure differential between the CO_2 inside the sample and the atmosphere outside the sample provides the energy for void nucleation and foam expansion, higher pressures obviously present the theoretical potential for increasing the total number of homogenous nucleation sites as well as the volume of the foam generated. In our experiments, however, the highest pressures attainable were around 12 MPa, and changes in soak pressure were not shown to have as significant an impact on cell morphology as

other factors. In order to fully experiment with the effects of higher pressure on foam morphology, one would have to perform experiments in the regime of 20-25MPa, where homogeneous nucleation is a dominant mechanism in foam growth; at those pressures and above, changes in process pressure have been shown to be the most critical parameter to cell density and size.[7] Below those pressures, heterogeneous nucleation is dominant, and changes in pressure do not have as substantial an effect on the population of nucleated cells. Of much greater impact to our experiments was the rate of pressure quench. If the pressure was released from the reactor too slowly, mass transfer of CO_2 within the sample prevented the generation of uniform foams. Immediately upon decrease of reactor pressure, supercritical CO_2 begins phase transformation into gaseous CO_2, which has a much higher diffusion rate even than SCF. As the gas desorbs into nucleated cells and out of the polymer, the T_g of the composite begins to rise. It is this effect that "freezes" the foam cells after expansion. By slowing the quench rate, more CO_2 is permitted to escape during the process; T_g increases and the viscosity rises. Simultaneously, there is less pressure differential in the material to drive void nucleation. The result is similar to that of lowering both processing temperature and pressure. Foams formed with slow quench rates exhibited thick, crust-like skins, shear zones in which expanding foam cells were ruptured as they moved across hardened polymer, and large irregularities in cell size (Figure 39). In order to create uniform foams, quench times were maintained below 5 seconds.

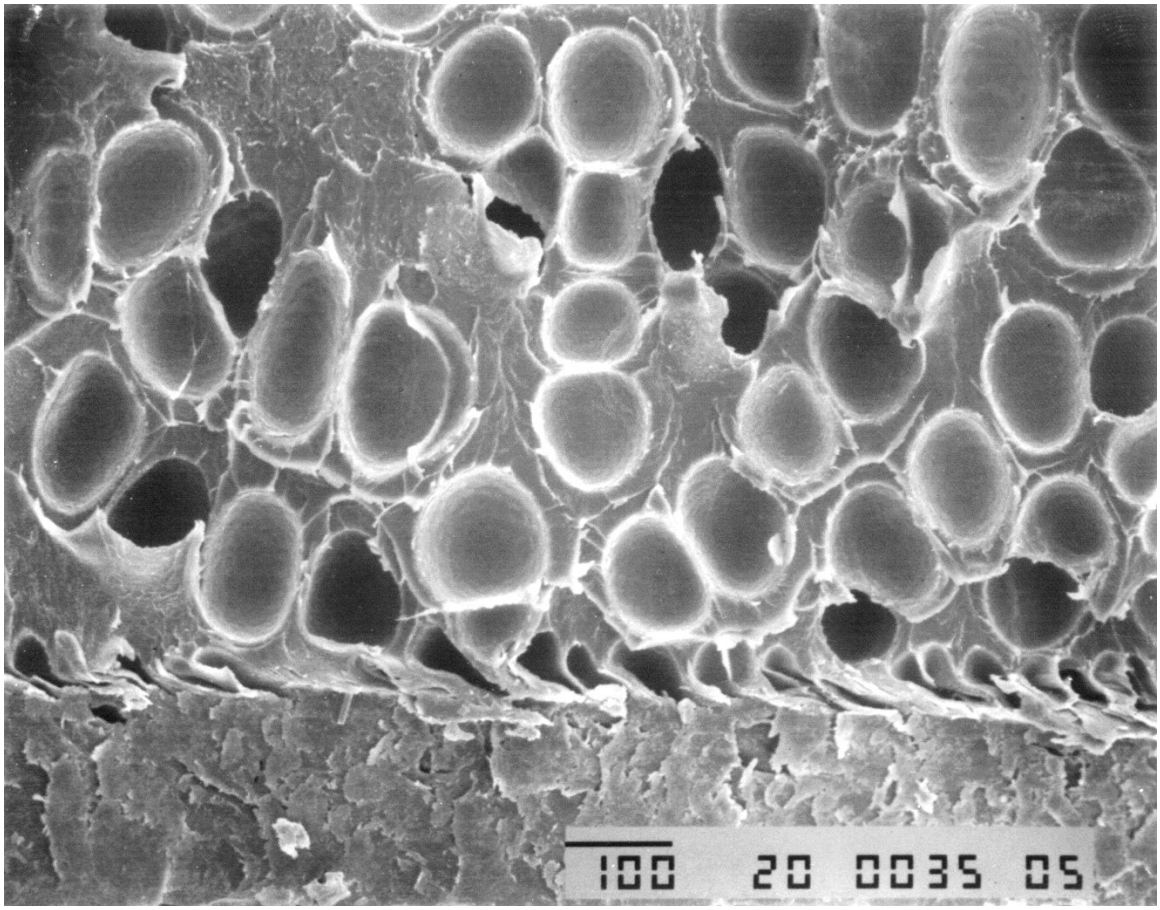

Figure 39: Micrograph showing negative effects of slow pressure quench rate.

Thermal Properties

The foaming process had no measurable effect on glass transition temperature of the polymer samples. In the differential scanning calorimetry (DSC) curves of the foamed samples, however, there an increased prominence of the endothermic peak at glass transition (table 8, figure 40). The presence of the larger peak implies that the foam blowing process increased the degree of non-equilibrium glassy state in the material.

Material	D Cp (J/g*°C)	T_{g0}† (°C)	T_g (°C)	Endo. Peak (°C)	Peak Area (J/g*°C*min)
PS	0.27	95	97	102	0.07
PS (foamed)	0.41	98	99	104	0.19
PS (annealed)‡	0.41	94	97	102	0.07
1% MLS	0.17	81	83	90	0.09
1% MLS (foamed)	0.40	81	82	89	0.14
1% MLS (annealed)‡	0.34	80	82	88	0.07
3% MLS	0.28	95	98	104	0.02
3% MLS (foamed)	0.40	94	95	100	0.10
3% MLS (annealed)‡	0.40	97	99	104	0.06
† T_{g0} refers to point of endothermic onset of phase transformation					
‡ Second heat for foamed samples after being annealed at 170°C for 30 minutes					

Table 8: Thermal properties of PS+MLS nanocomposite foams before and after processing.

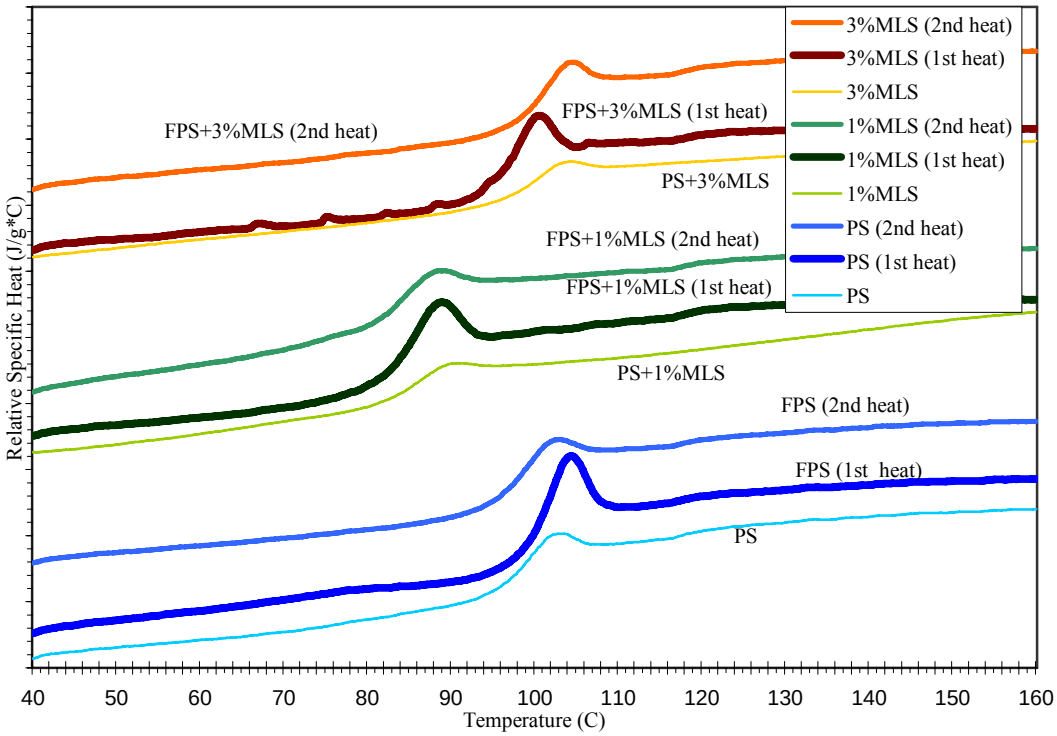

Figure 40: Specific heat – temperature profiles showing increased endothermic peaks of foamed samples FPS (first heat only).

During foaming, the highly strained material in the foam cell walls may have inherited some localized alignment of the polymer chains (Figure 41). After annealing in the melt state for 30 minutes at 170°C, however, the samples were cycled a second time in the DSC, and all of them had returned to their pre-foamed endothermic behavior.

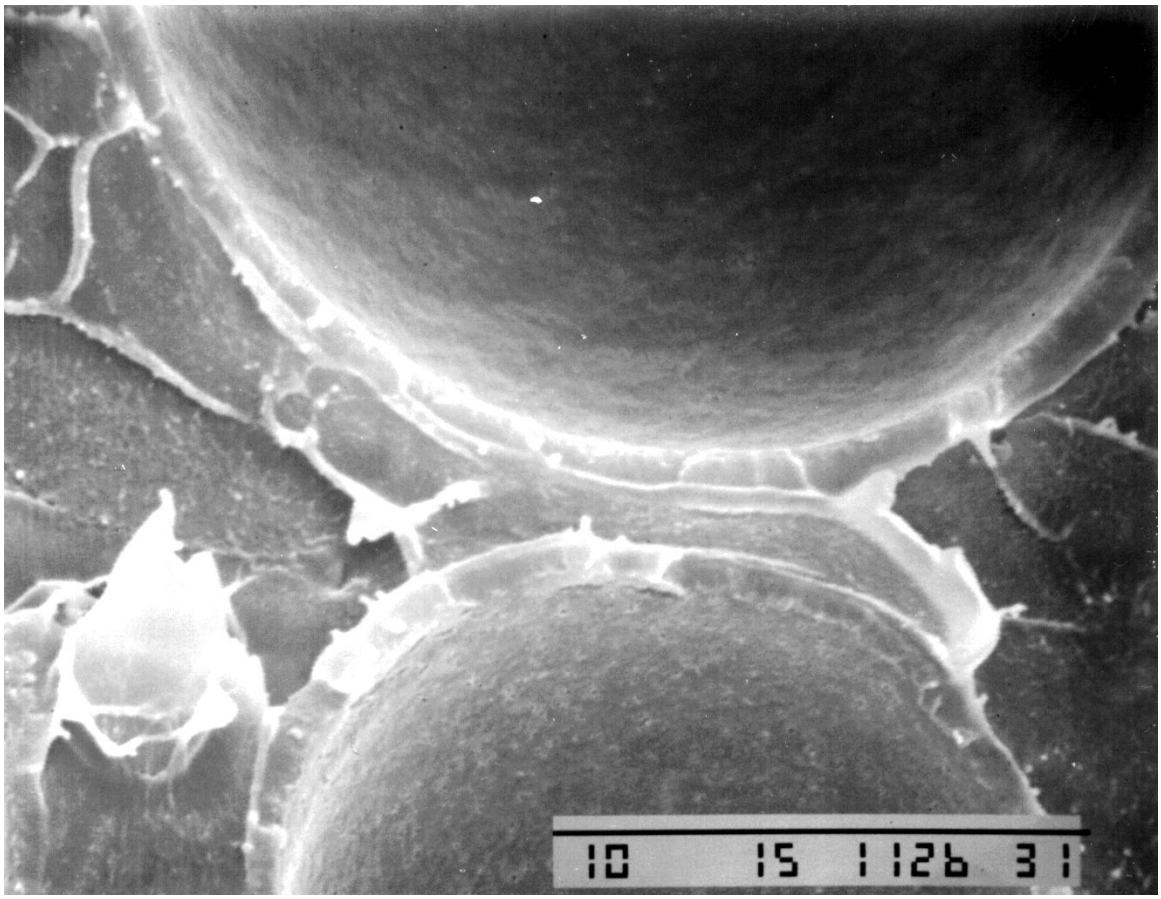

Figure 41: Micrograph of PS foam showing strain induced polymer alignment around cells.

Microscopy and Physical Measurements

Scanning electron microscopy was used to examine physical features of the foamed samples. Scaled micrographs were scanned and measured to determine foam density, cell size, etc. At low cell densities and sizes, where cell shapes were uniformly ellipsoidal and cell walls thick, the ratio of average cell width to height was measured at

approximately 1:1.5, with the longest dimension of each cell being in the through thickness direction of the laminate (Figure 42). The same ratio was consistent through all the samples, although more irregularity was found in those samples in which the cells had grown to the point of impinging on each other.

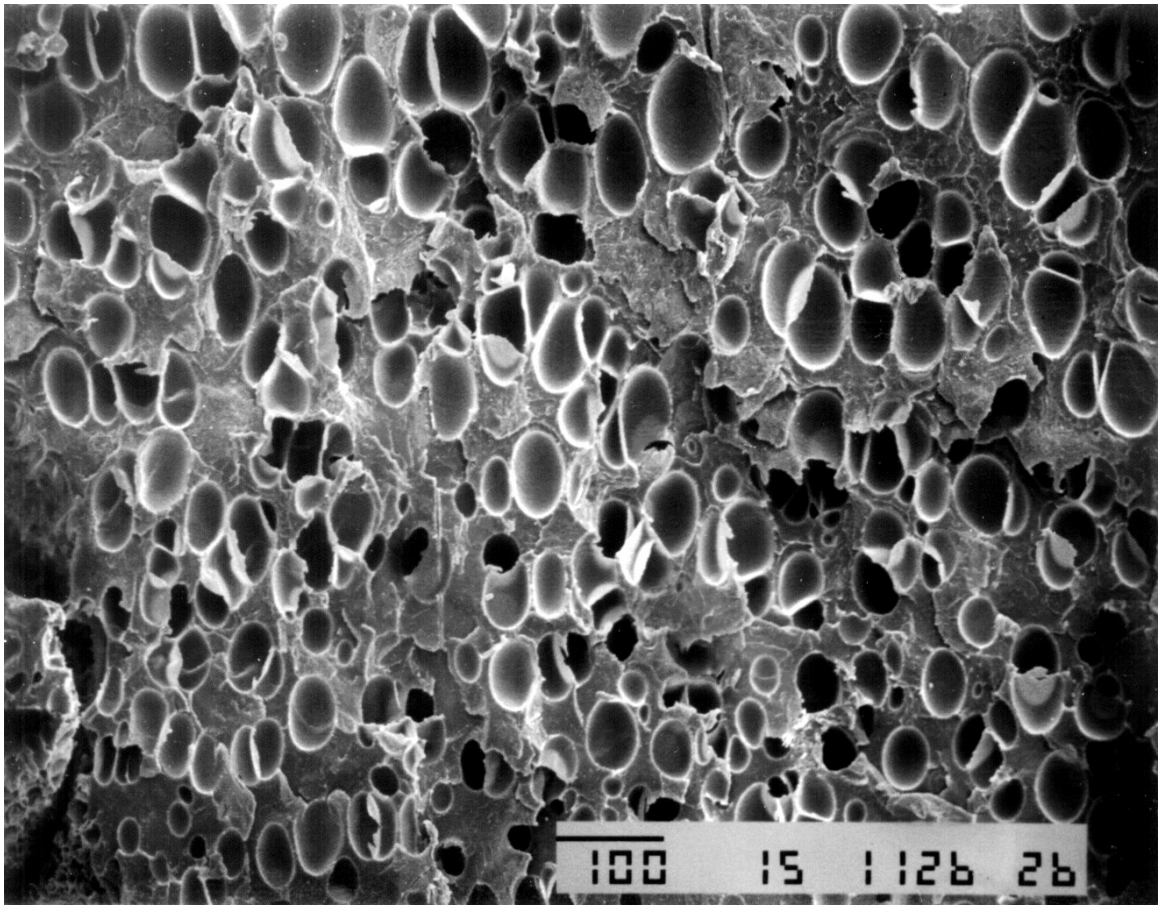

Figure 42: Micrograph of PS foam showing typical cell elongation in Z-axis.

Cell density was calculated in a method similar to that used by Kumar and Suh,[143] adjusted for asymmetrical cell growth. In this model, number of cells / cm^3, N_f, may be expressed as:

$$N_f = (nM^2/A)^{3/2} (r_c)^{1/2} \qquad \text{(Equation 39)}$$

where n is the number of cells seen in a micrograph, M is the magnification factor, A is the area of the micrograph, and r_c is the ratio of cell width over height. The addition of the last term was required due to the preferential elongation of foam cells in the through thickness direction that was observed.

The cell densities and sizes varied widely based on processing and material parameters; densities achieved spanned the range from 10^4 to 10^8 cells/cm^3. Cell size in the bulk foam also varied accordingly, with cell diameters most typically in the range of 10-100 microns. In regions near the surface of the foam, however, where the skinning effect was apparent, cell diameters gradually decreased to as low as 1 micron or less. In many micrographs, a distinct "eggshell" phenomenon was displayed, in which a smooth thin layer of material was made visible in the fracture surface surrounding each bubble of foam (see figure X). This "shell" appears to have been generated by the straining of the CO_2 depleted polymer around each cell during cell growth. The resultant layer evidently contains residual stresses, and its highly strained nature may contribute to the toughness and/or other mechanical properties of the foam as a whole. It may also be responsible for the enlarged endothermic peaks in the DSC curves, discussed earlier.

4.4.2. PS + MLS Nanocomposite Foam

Effect of MLS Concentration and Distribution

MLS concentration in the nanocomposite influenced foam morphology strongly, as might be expected. Higher concentrations of MLS created a higher density of nucleation sites for heterogeneous nucleation, thus increasing the cell density. Cell size is

shown to decrease as cell density increases, preserving the net volume expansion of the foam as a function of temperature, pressure, and CO_2 saturation (Figure 43).

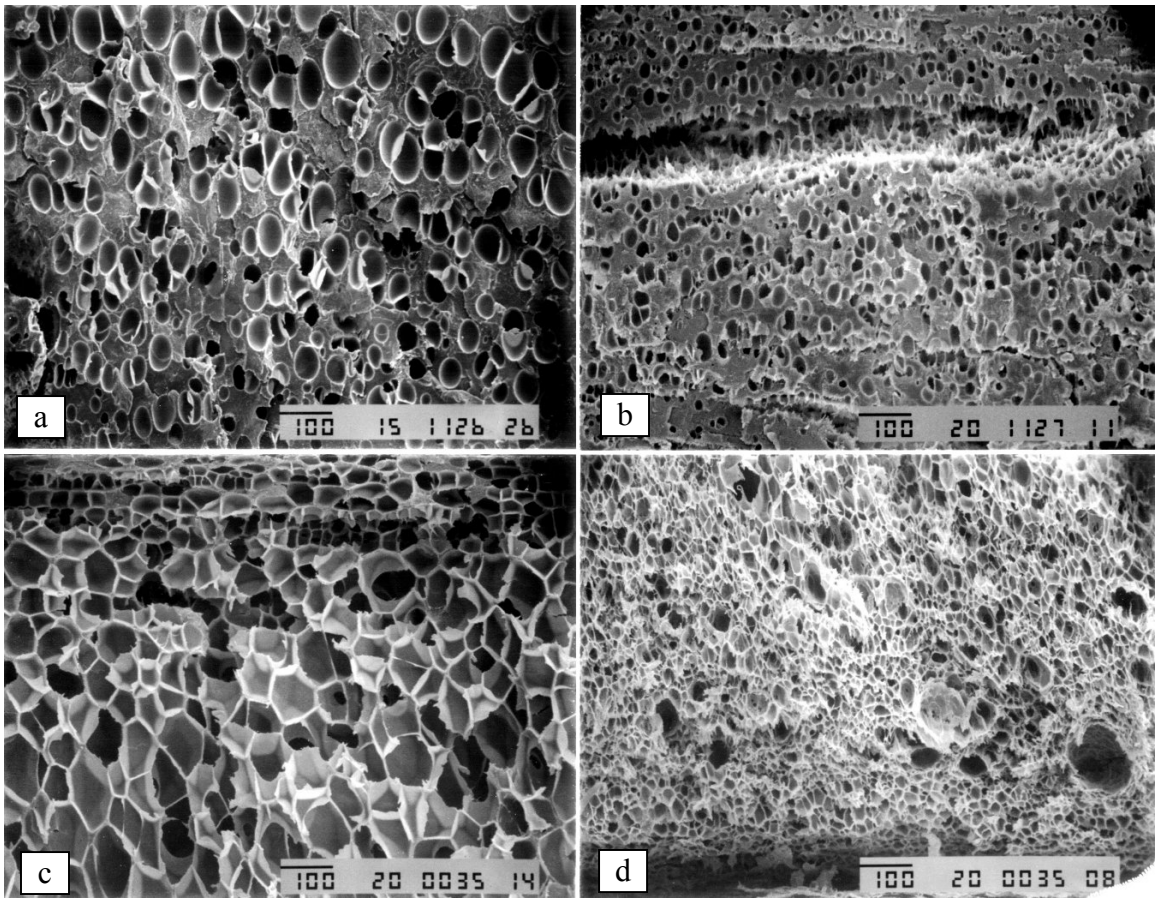

Figure 43: SEM micrographs showing increased cell density (Nf) with MLS concentration. (100X magnification).
[a] Pure PS, 60°C, [b] 1%MLS, 60°C, [c] 1%MLS, 85°C, [d] 3%MLS, 85°C.

The distribution of MLS in the polymer also had an effect on cell nucleation, especially at low temperatures / high viscosities. In the compression molding of the samples, a preferential orientation was introduced that aligned the silicate into layers parallel to the laminate major axis. As evidence of this and of heterogeneous nucleation, PS+MLS foams generated at low temperatures exhibited void nucleation solely within those segregated layers (Figure 44).

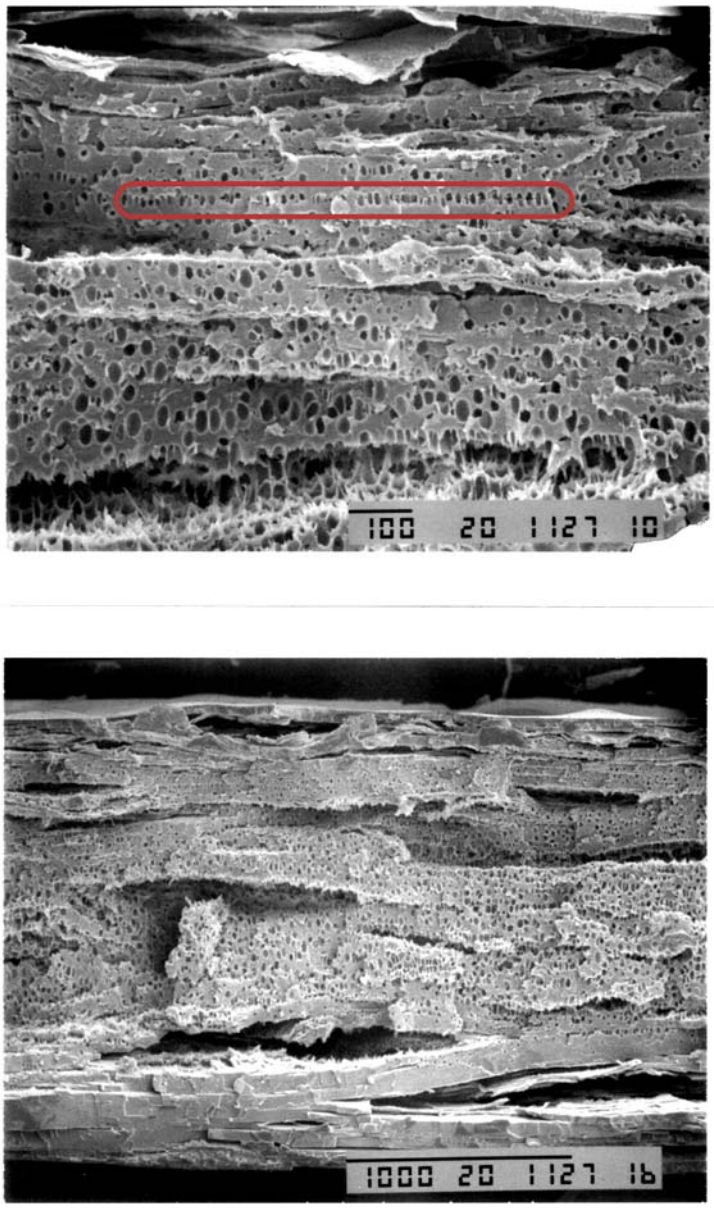

Figure 44: SEM micrographs showing pastry-like layered void formation corresponding to MLS rich planes.

Foam formation at higher temperatures was able to disturb those layers and cause the silicate to reorient around the cells, and the resultant foam materials showed preferential orientation of grain-like nanocomposite structures parallel to the cell walls (Figure 45).

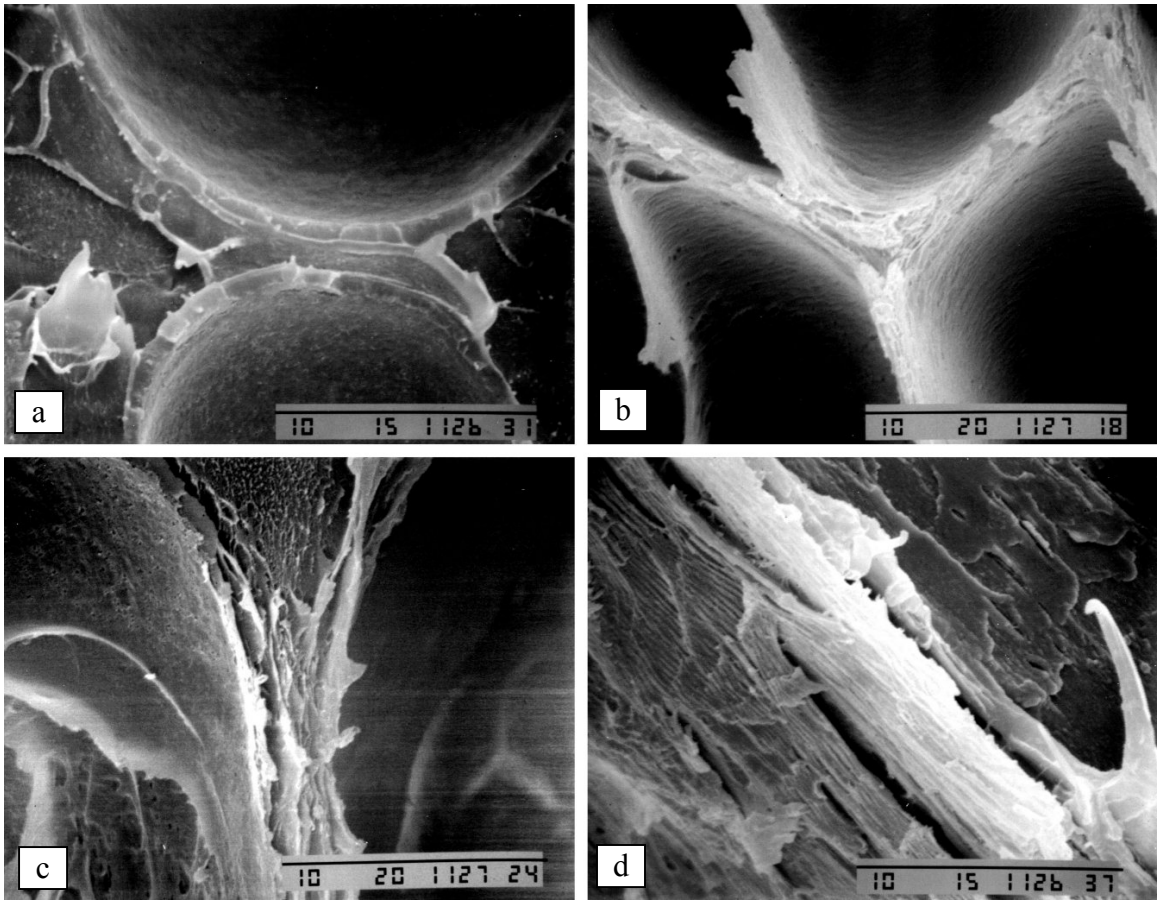

Figure 45: Micrographs showing aligned grain structure in cell walls of nanocomposite. (5000X magnification).
[a] Pure PS (egg shell effect), 60°C, [b] 1%MLS, 60°C, [c] 1%MLS, 85°C,
[d] 1%MLS, 75°C.

In general, the temperatures were required to generate uniform nanocomposite foams were higher than those required to generate pure PS foams, even though the T_g of the nanocomposite laminates was not higher (and in the case of the 1% composite it was lower) than that of the PS laminates. The reason that higher temperatures were required is that the presence of the silicate in the polymer both increased its viscosity above the glass transition and provided localized anisotropic deformation mechanisms (such as delamination) in place of normal cell nucleation and growth. As described above, low

process temperatures for the PS+MLS laminates resulted in segregated layers of bubbles. These bubbles often coalesced into large sheet-like pockets that delaminated the sample into a flaky, pastry-like material.

Another, unexpected result of the presence of clay in the sample was a highly accelerated absorption rate for the supercritical CO_2. Unlike the pure PS samples, which required hours of soak time in the supercritical CO_2 chamber (figure 46 depicts effects of incomplete diffusion), PS+MLS laminates created uniform foams after as little as only 5 minutes in the presence of the SCF. This implies that there is a secondary mechanism of mass transfer of CO_2 in the nanocomposite foams, one that is significantly faster than the linear diffusion model predicts. We suspect that diffusion at the polymer/MLS interfaces may be accelerated by the differences in CO_2 solvency of the two materials.

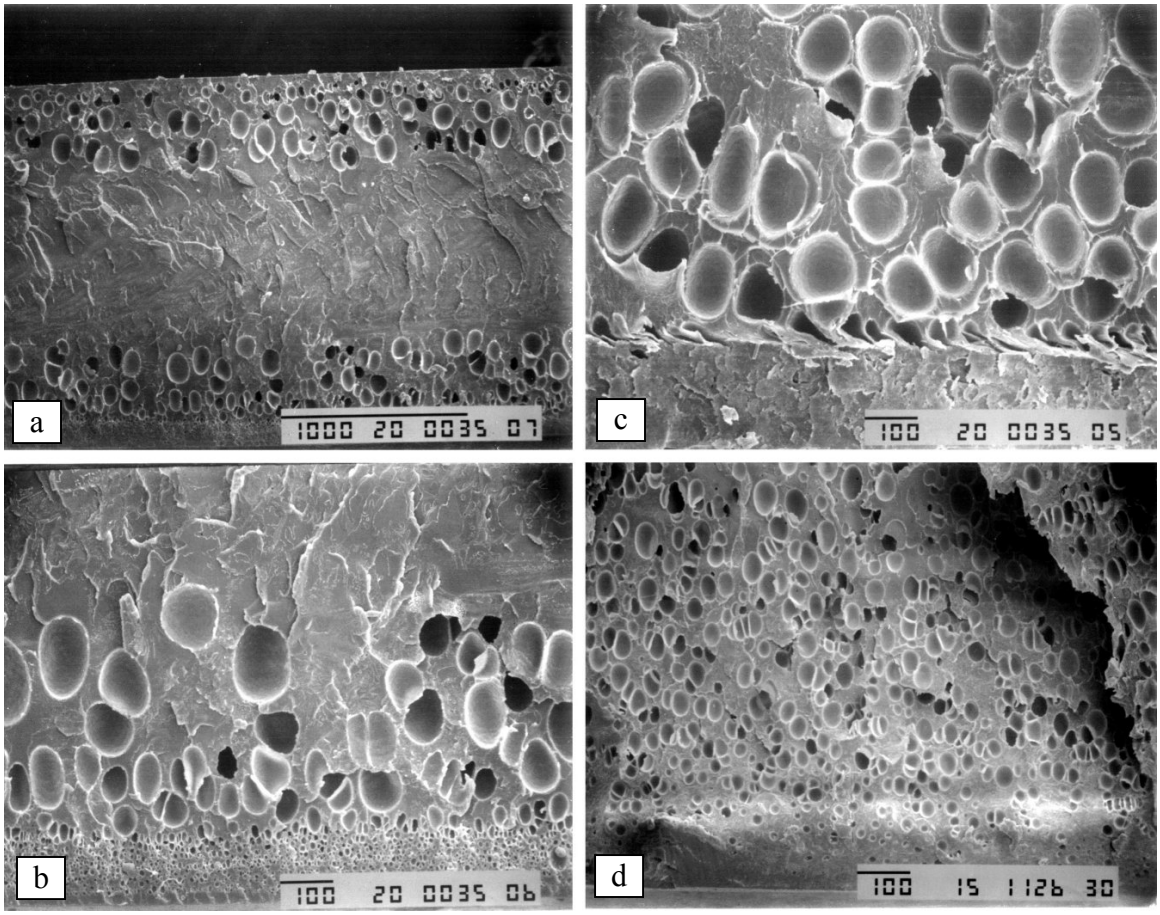

Figure 46: SEM micrographs showing affect of saturation time on CO2 diffusion through pure PS at 10MPa.
[a] 75°C, 15 min soak (35X) (incomplete diffusion) [b] detail of same (100X), [c] 75°C, 1 hr soak (100X), [d] 60°C, 5 hr soak (100X).

Thermal Properties

The thermal properties of the PS+MLS foams exhibited the same trends as the pure PS foams. T_g was unchanged, and an endothermic peak was clearly visible during the first glass transition in the DSC (see figure 40).

Microscopy

Scanning electron microscopy was also used to analyze the foamed samples of nanocomposite. In these samples the cell shapes, sizes, and densities fell within the same

range as those of the pure PS samples, with cell diameters and densities varying widely based of process conditions and MLS concentration.

The “eggshell” phenomenon previously discussed in relation to PS foam morphology could not be seen in the micrographs of the nanocomposite laminates, although it is likely that similar highly strained material exists around the cells of the nanocomposite foam. Instead, what is visible in the fracture surfaces of the PS+MLS samples is the presence of oriented MLS layers. At magnifications of 5000X and above, oriented layers of silicate can clearly be seen lying parallel to the circumference of each foam cell. These layers appear in a “wood-grain” pattern on the micrographs, and the spacing between the layers measures less than 200nm. The existence of these layers is evidence of the robust mechanical form and potential of nanocomposite foams in structural applications.

5. SUMMARY

5.1. Foam Preparation

The objective of this work was to develop and characterize a structural foam material of thermoplastic nanocomposite using a safe and environmentally benign technology. In accordance with this goal, nanocomposite foams were successfully generated from montmorillonite reinforced polystyrene using CO_2 as a blowing agent, and were characterized by differential scanning calorimetry, X-ray diffraction, scanning electron microscopy, and dynamic mechanical analysis.

In order to fabricate said foams, nanocomposite was first synthesized by in-situ polymerization of styrene in the presence of surfactant-treated montmorillonite. During this step, which involved bulk free-radical polymerization, temperature control and thorough mixing were very important to the quality of the resultant nanocomposite. After synthesis, nanocomposite samples were compression molded into 1 to 2 mm thick laminates. The compression molding had the effect of aligning the nanocomposite in layers parallel to transverse strain. These layers became evident later in some of the foamed samples, especially those foamed at low temperatures.

The foaming method used for this study was a constant temperature, variable pressure batch process in which predominately macrocellular foams were formed by first saturating nanocomposite laminates with supercritical CO_2 in a high pressure reactor, and then rapidly quenching pressure to allow the CO_2 to nucleate and grow foam cells. Saturation of the laminates took place via diffusion of supercritical fluid (SCF) through

the nanocomposite, so soak times were governed by diffusion rate and equilibrium solubility of the CO_2 within the nanocomposite. Solubility of CO_2 in the laminate was an essential variable in the foaming process because it effected the magnitude of plasticization (depression of glass transition temperature T_g) of the pre-foamed samples, as well as the quantity of gas available for cell growth. Because higher solvent density is directly related to solubility, optimization of the foaming process involved using high pressures and low temperatures. While maximum pressure was limited by the service pressure of the reactor used, the minimum temperature was limited by the T_g of the plasticized nanocomposite. In this study, the minimum temperatures useable varied between 60°C and 80°C, depending on the concentration of montmorillonite layered silicate (MLS) in the nanocomposite. In order to increase both pressure and temperature capabilities, as well as chamber size for future experiments, we designed and fabricated a new, 20.3cm ID supercritical CO_2 reactor capable of 21MPa and 315°C. The new equipment will be used for the continued development of nanocomposite foams.

Aside from solven density, the rate of pressure quench was also of critical importance to the generation of foam. Low reactor evacuation times, less than 5 seconds, were required in order to produce fine cell structures with consistent density distribution. Slower quench rates resulted in coarse cell structures, cracking, delamination, and a thick skinning effect at the sample surface.

One surprising and encouraging discovery of this work took place during foam preparation, when it was observed that CO_2 diffusion into the nanocomposite samples was vastly accelerated in comparison with diffusion into pure polystyrene samples. It is

theorized that the increased rate is due to some Case II diffusion contribution occurring at the polymer / MLS interface during plasticization and impregnation. This feature could greatly enhance the economic benefit of using nanocomposites in the generation of both commercial micro- and macrocellular foams.

5.2. Characterization

Differential scanning calorimetry (DSC) of nanocomposite and foam samples revealed that neither the addition of low concentrations of MLS nor the generation of foam cells had a significant effect on the glass transition temperature of the parent polystyrene. Samples with 1% MLS did exhibit slightly depressed T_g in comparison with the other samples. It has been theorized that the presence of a widely dispersed 2^{nd} phase of MLS within the polystyrene (PS) may locally disturb some short range order within the thermoplastic matrix.

X-ray diffraction of nanocomposite laminates was performed in order to detect the presence of intercalated or exfoliated distribution of MLS within the material. The results showed that 2-theta diffraction peaks were present in all the samples containing MLS, and that those peaks were all shifted downwards by approximately .3 degrees, indicating a high likelihood of intercalated microstructures for both the 1% and 3% MLS samples. Similarly, X-ray diffraction (XRD) of foam samples indicated yet more shifting of the MLS 2-theta peak, which implies that the foaming process may have provide an added benefit of dispersing and expanding intercalated nanoreinforcements.

dynamic mechanical analysis (DMA) was performed on the pre-foamed nanocomposite laminates in order to confirm the mechanical benefits of the

nanocomposite. As expected, the ultimate flexural strength of the samples increased dramatically with increasing concentration of MLS (e.g. The addition of 3% MLS by weight to pure polystyrene more than doubled the flexural strength of the material).

Scanning electron microscopy (SEM) characterization revealed that MLS concentration and dispersion within the sample laminates had a strong effect on cell density, shape, and size. The effects of changing process temperatures and pressure quench rates were also clearly identifiable on the micrographs. Most crucially, however, the SEM images showed evidence of preferential nanocomposite orientation around expanded cells, which promises to yield enhanced physical and mechanical properties to this new family of foams.

REFERENCE LIST

1 1997 Economic Census, Manufacturing Industry Series: Polystyrene Foam Product Manufacturing. U.S. Census Bureau (1999).

2 Forman, C., P-120X: Polymeric Foams, Business Communications Company Inc, Norwalk, CT (2001).

3 Nauta, W., J., Stabilization of Closed Cell, Low Density Polyethylene Foam. PhD Thesis, University of Twente, 2000.

4 UNEP IE, Sourcebook of Technologies for Protecting the Ozone Layer: Flexible and Rigid Foams: September 1996 Update. United Nations Environment Programme, Paris (1996).

5 Park, C., Park, O.O., Lim, J.G., Kim, H.J., Polymer, **42**, 7465, (2001)

6 Daming, W., Qingyun, M., Ying, L., Yumei, D., Weihong, C., Hong, X., Dongyun, R., J. Polym. Sci.: Part B: Polym. Phys., **41**, 1051 (2003).

7 Goel, S.K. and Beckman, E.J., Polym. Eng. Sci., **34** (14), 1137 (1994).

8 Goel, S.K. and Beckman, E.J., Polym. Eng. Sci., **34** (14), 1148 (1994).

9 Kazarian, S.G., Polym. Sci., Ser. C., **42** (1), 78 (2000).

10 Liang, M.-T. and Wang, C.-M., Ind. Eng. Chem. Res., **39** (12), 4622 (2000).

11 Arora, K., Lesser, A., McCarthy, T., Macromolecules, **32** (8), 2562 (1999).

12 Zeng, C., Han, X., Lee, L.J., Koelling, K., Tomasko, D., Conference Proceedings - ANTEC 2002, 1504 (2002).

13 Okada, A., Kawasumi, M., Usuki, A., Kojima, Y., Kurauchi, T., Kamigaito, O., Mater. Res. Soc. Proc., 171, 45 (1990).

14 Giannelis, E. P., Krishnamoorti, R., Manias, E., Adv. Polym. Sci., 138, 107 (1999).

15 Ranade, A.; D'Souza, N. A.; Gnade, B. Polymer, **43**, 3759 (2002).

16 Zeng, Q. H., Wang, D. Z., Yu, A. B., Lu, G. Q., Nanotechnology, 13, 549 (2002).

17 Okamoto, M., Morita, S., Taguchi, H., Kim, Y. H., Kotaka, T., Tateyama, H., Polymer, 41, 3887 (2000).

18 Vaia, R. A., Ishii, H., Giannelis, E. P., Chem. Mater., 5, 1964 (1993).

19 Hernandez-Luna, A., D'Souza, N.A., Conference Proceedings – ANTEC 2002, 1461 (2002).

20 Manias, E., Touny, A., Wu, L., Lu, B., Strawhecker, K., Gilman, J.W., Chung, T.C., Polym, Mat.: Sci. Eng., 82, 282 (2000).

21 Carrado, K. A., Xu, L. Q., Chem. Mater., 5, 1694 (1998).

22 Lin, H.-R., Polym. Testing, 16, 429 (1997).

23 Grenestedt, J. L., J. Mech. Phys. Solids, 46 (1), 29 (1998).

24 Grenestedt, J. L., Tanaka, K., Scripta Materialia, 40 (1), 71 (1999).

25 Grenestedt, J. L., Bassinet, F., Int. J. Mech. Sci., 42, 1327 (2000).

26 Zenkert, D., ed., The Handbook of Sandwich Construction. Chameleon Press, London (1997).

27 Okamoto, M., Nam, P. H., Maiti, P., Kotaka, T., Nakayama, T., Takada, M., Ohshima, M., Usuki, A., Hasegawa, N., Okamoto, H., Nano Lett., 1 (9), 503 (2001).

28 Han, X., Zeng, C., Lee, L.J., Koelling, K., Tomasko, D., Conference Proceedings - ANTEC 2002, 1915 (2002).

29 Fu, Y., Palo, D., Erkey, C., Weiss, R., Macromolecules, **30** (24), 7611 (1997).

30 Mizumoto, T., Sugimura, N., Moritani, M., Sato, Y., Masuoka, H., Macromolecules, **33** (18) 6757 (2000).

31 Martinache, J., Royer, J., Siripurapu, S., Hénon, F., Genzer, J., Khan, S., Carbonell, R., Ind. Eng. Chem. Res., **40** (23), 5570 (2001).

32 Krause, B., Mettinkhof, R., van der Vegt, N., Wessling, M., Macromolecules, **34**, (4), 874 (2001).

33 Lee, M., Tzoganakis, C., Park, C., Polym. Eng. Sci., **38** (7), 1112 (1998).

34 Lee, K.-N., Lee, H.-J., and Kim, J.-H., Polym. Int., **49**, 712 (2000).

35 Siripurapu, S., Gay, Y., Royer, J., DeSimone, J., Spontak, R., Khan, S., Polymer, **43**, 5511 (2002).

36 Arora, K., Lesser, A., McCarthy, T., Macromolecules, **31** (14), 4614 (1998).

37 Bureau, H., Keppler, H., Earth and Planetary Sci. Let. **165** (2), 187 (1999).

38 McHugh, M.A., Krukonis, V.J., Supercritical Fluid Extraction, Butterworth-Heinemann, Boston (1994).

39 Span, R.; Wagner, W., J. Phys. Chem. Ref. Data, **25** (6), 1509 (1996)

40 Thermophysical Properties Of Fluid Systems, NIST Chemistry WebBook, U.S. Secretary of Commerce, 2003. <http://webbook.nist.gov/chemistry/fluid/>

41 Zhang, Y., Molecular Interactions Between Supercritical Fluid and Polymers. PhD Thesis, University of Toledo, (1997).

42 Bonner, D.C., Prausnitz, J.M.; J. Polym. Sci. Polym. Phys. Ed., **12**, 51 (1974).

43 Wissinger, R.G., Paulaitis, M.E., Ind. Eng. Chem. Res., **30**, 842 (1991).

44 Sato, Y., Takikawa, T., Takishima, S., Masuoka, H., J. Supercritical Fluids, **19**, 187 (2001).

45 Berens, A.R., Huvard, G.S., Korsmeyer, R.W., Kunig, F.W., J. Appl. Polym. Sci., **46**, 231 (1992).

46 Shieh, Y.-T., Liu, K.-H., J Polym. Res., **9**, 107 (2002).

47 Nikitin, L.N., Gallyamov, M.O., Vinokur, R.A., Nikolaec, A.Y., Said-Galiyev, E.E., Khokhlov, A.R., Jespersen, H.T., Schlaumburg, K., J. Supercrit. Fluids, **26**, 263 (2003).

48 Koros, W.J., Paul, D.R., Rocha, A.A., J. Polym. Sci.: Polym. Phys. Ed., **14**, 687 (1976).

49 Koros, W.J., Paul, D.R., J. Polym. Sci.: Polym. Phys. Ed., **14**, 1903 (1976).

50 Dey, S.K., Adv. in Polym. Tech., **10** (4), 327 (1990).

51 Sato, Y., Yurugi, M., Fujiwara, K., Takishima, S., Masuoka, H., Fluid Phase Equilibria, **125**, 129 (1996).

52 Han, X., Baxter, A., Koelling, K., Tomasko, D., Lee, L.J., Conference Proceedings - ANTEC 2002, 1910 (2002).

53 Han, X., Continuous Production of Microcellular Foams. PhD Thesis, Ohio State University, 2003.

54 McHugh, M.A., Seckner, A.J., Yogan, T.J., Ind. Eng. Chem. Fundam., **23**, 493 (1984).

55 Hoefling, T, Stofesky, D., Reid, M., Beckman, E., Enick, R.M., J. Supercrit. Fluids, **5** (4), 237 (1992).

56 Mesiano, A.J., Enick, R.M., Beckman, E.J., Russell, A.J., Fluid Phase Equilibria, **178**, 169 (2001).

57 Sen, Y.L., Kiran, E., J. Supercritical Fluids, **3**, 91 (1990).

58 Zhang, Q., Xanthos, M., Dey, S.K., J. Cellular Plastics, **37** (6), 517 (2001).

59 Dey, S.K., Zhang, Q., Faridi, N., Xanthos, M., Conference Proceedings - ANTEC 1997, **43**, 1998 (1997).

60 Prausnitz, J.M., Benson, P.R., AIChE J., **4**, 269 (1959).

61 Van Leer, R.A., Paulaitis, M.E., J. Chem. Eng. Data, **25**, 257 (1980).

62 Johnston, K.P., Eckert, C.A., AIChE J., **27**, 773 (1981).

63 Krukonis, V.J., Kurnik, R.T., J. Chem. Eng. Data, **30**, 247 (1985).

64 Wu, J., Pan, Q., Rempel, G.L., J. Appl. Polym. Sci., **85**, 1938 (2002).

65 West, B.L., Kazarian, S.G., Vincent, M.F., Brantley, N.H., Eckert, C.A., J. Appl. Polym. Sci., **69**, 911 (1998).

66 Koros, W.J., Paul, D.R., J. Polym. Sci.: Polym. Phys. Ed., **16**, 1947 (1978).

67 Tsujita,l Y., Progress in Polymer Science, **28** (9), 1377 (2003).

68 Berens, A.R., Polymer Engineering and Science, **20** (1), 95 (1980).

69 Bondar, V.I., Kamiya, Y., Yampol'skii, Y.P., J. Polym. Sci., Polym. Phys. Ed., **34**, 369 (1996).

70 Flory, P.J., Principles of Polymer Chemistry, Cornell Univ. Press, Ithaca, N. Y., (1953).

71 Huggins, M.L., Physical Chemistry of High Polymers, Ch. 5, Wiley, New York, (1958).

72 Nairn, J.A., Polymer Characterization, Univ. of Utah, 2003. <Hhttp://www.eng.utah.edu/~nairn/classes/mse5473/Characterization.pdfH>

73 Young, R.J., Lovell, P.A., Introduction to Polymers: 2nd Ed., Chapman & Hall, London (1991).

74 Faupel, F., Thermodynamics of Melts and Solutions, Christian-Albrechts Univ. zu Kiel, 2004. <Hhttp://www.tf.uni-kiel.de/matwis/matv/polymersi.htmlH>

75 Sperling, L.H., Introduction to Physical Polymer Science: 2nd Ed., Wiley, New York (1992).

76 Barbari, T.A., Conforti, R.M., Polym. Adv. Tech., **5**, 698 (1994).

77 Fleming, G.K., Koros, W.J., Macromolecules, **19**, 2285 (1986).

78 Barbari, T.A., Conforti, R.M., J. Polym. Sci., Polym. Phys. Ed., **30**, 1261 (1992).

79 Suwandi, M.S., Stern, S.A., J.Polym Sci., Polym. Phys. Ed., **11**, 663 (1973).

80 Kamiya, Y., Naito, Y., Bourbon, D., J. Polym. Sci., Polym. Phys. Ed., **32**, 281 (1994).

81 Prigogine, I., Molecular Theory of Solutions, North-Holland, Amsterdam (1957).

82 Sanchez, I. C., Lacombe, R. H., J. Phys. Chem., **80** (21), 2352 (1976).

83 Vrentas, J. S., Vrentas, C. M., Macromolecules, 24, 2404 (1991).

84 Panayiotou, C., Vera, J. H., Polym. J., **14**, 681 (1982).

85 Conforti, R. M., Barbari, T. A., Vimalchand, P., Donohue, M. D., Macromolecules, **24**, 3388 (1991).

86 Sanchez, I. C., Lacombe, R. H., Nature, **252**, 381 (1974).

87 Rodgers, P. A., Sanchez, I. C., J. Polym. Sci., **31**, 273 (1993).

88 Hariharan, R., Freeman, B. D., Carbonell, R. G., Sarti, G. C., J. Appl. Polym. Sci., 50, 1781 (1993).

89 Sanchez, I. C., Lacombe, R. H., Macromolecules, **11** (6), 1145 (1978).

90 Kiszka, M. B., Meilchen, M. A., McHugh, M. A., J. Appl. Polym. Sci., **36**, 583 (1998).

91 Pope, D. S., Sanchez, I. C., Koros, W. J., Fleming, G. K., Macromolecules, **24**, 1779 (1991).

92 Kilpatrick, P. K., Chang, S.-H., Fluid Phase Equilibria, **30**, 49 (1986).

93 Quach, A., Simha, R., J. Appl. Phys., **42**, 4592 (1971).

94 Olabisi, O., Simha, R., Macromolecules, **8**, 206 (1975).

95 Sanchez, I. C., Lacombe, R. H., J. Polym. Sci., Polym. Phys. Ed., **15**, 71 (1977).

96 McKinney, J. E., Goldstein, M., J. Res. Nat. Bur. Stand. A, **78**, 331 (1974.

97 Walker, T. A., Colina, C. M. , Gubbins, K. E., Spontak, R. J., Macromolecules, **37**, 2588 (2004).

98 Condo, P. D., Johnston, K. P., J. Polym. Sci.: Part B: Polym. Phys., **32**, 523 (1994).

99 Wang, W.-C. V., Kramer, E., Sachse, W., J. Polym. Sci., Polym. Phys. Ed., 20, 1371 (1982).

100 Chiou, J. S., Barlow, J. W., Paul, D. R., J. Appl. Polym. Sci., **30**, 2633 (1985).

101 Banerjee, T., Lipscomb, G. G., J. Appl. Polym. Sci., **68**, 1441 (1998).

102 Crank, J. The Mathematics of Diffusion, 2nd ed.; Clarendon Press: Oxford, 1975.

103 Vincent, M.F., Processing of Polymers using Supercritical CO2. PhD Thesis, Georgia Institute of Technology, 1997.

104 Edwards, D. A. J. Polym. Sci.: Polym. Phys. Ed., 34, 981 (1996).

105 Sicardi, S.; Manna, L.; Banchero, M. J. Supercrit. Fluids, 17, 187 (2000).

106 Santos, W. L. F.; Porto, M. F.; Muniz, E. C.; Povh, N. P.; Rubira, A. F. J. Supercrit. Fluids, 19, 177 (2001).

107 Edwards, S.F., Pithia, K.D., Physica A, **215**, 270 (1995).

108 Sun, X., Liu, H., Li, G., Liao, X., He, J., J. Appl. Polym. Sci., **93**, 163 (2004).

109 Lee, S.-T., Ramesh, N.S., Campbell, G.A., Polym. Eng. Sci., **36** (19), 2477 (1996).

110 Joshi, K., Lee, J.G., Shafi, M.A., Flumerfelt, R.W., J. Appl. Polym. Sci., **67**, 1353 (1998).

111 Lee, S.-T., Foam Nucleation in Gas-Dispersed Polymeric Systems, in Foam Extrusion: Principles and Practice, S. -T. Lee, Editor. 2000, Technomic: Lancaster, Basel.

112 Shafi, M.A. and Flumerfelt, R.W., Chem. Eng. Sci., **52** (4), 627 (1997).

113 P. L. Ku, Adv. Polym. Tech., **8** (2), 177 (1988).

114 Fontaine, M., Champagne, B., Perpète, E.A., André, J.-M., http://www.chimie.fundp.ac.be/cta/expo2/Mich1.pdf

115 Hildebrand, J., Scott, R., The Solubility of Non-Electrolytes, 3rd edn., Reinhold, New York (1949).

116 Coleman, M.M., Serman, C.J., Bhagwager, D.E., Painter, P.C., Polymer, **31**, 1187 (1990).

117 Small, P.A., J. Appl. Chem. **3**, 71 (1953).

118 Johnston, K. P., Peck, D. G., Kim, S., Ind. Eng. Chem. Res., **28**, 1115 (1989).

119 Giddings, J.C., Meyers, M.N., McLaren, S., Keller, R.A., Science, **162**, 67 (1968).

120 Wissinger, R.G., Paulaitis, M.E., J. Polym. Sci.: Polym. Phys. Ed., **25**, 2497 (1987).

121 Garcia-Leiner, M., Lesser, A.J., J. Appl. Polym. Sci., **93**, 1501 (2004).

122 Kazarian, S.G., Vincent, M.F., Bright, F.V., Liotta, C.L., Eckert, C.A., J. Am. Chem. Soc., **118**, 1729 (1996).

123 Hildebrand, J.H., Prausnitz, J.M., Scott, R.L., Regular and Related Solutions, Reinhold, New York, (1970).

124 Miyoshi, T., Takegoshi, K., Terao, T., Macromolecules, **30**, 6582 (1997).

125 Miyoshi, T., Takegoshi, K., Terao, T., J. Mag. Resonance, **125**, 383 (1997).

126 http://www.psigate.ac.uk/newsite/reference/plambeck/chem1/p01101a.htm

127 Han, X., Koelling, K., Tomasko D., Lee, L.J., Ohio State Univ. CAPCE Newsletter, **2** (2), 2 (2000).

128 Chen, L., Sheth, H., Kim, R., Polym. Eng. Sci., **41** (6), 990 (2001).

129 Chow, T.S., Macromolecules, **13**, 362 (1980).

130 Lee, M., Park, C., Tzoganakis, C., Polym. Eng. Sci., **39** (1), 99 (1999).

131 Lee, M., Tzoganakis, C., Park, C., Adv. Polym. Tech., **19**, 300 (2000).

132 Fox, T. G. Flory, P. J., J. Am. Chem. Soc., **70**, 2384 (1948).

133 Fox, T. G. Flory, P. J., J. Appl. Phys., **21**, 581 (1950).

134 Colucci, D. M. McKenna, G. B., Filliben, J. J., Lee, A., Curliss, D. B., Bowman, K. B., Russell, J. D., J. Polym. Sci., Polym. Phys. Ed., **35**, 1561 (1997).

135 Rehage, G., Oels, H.-J., High Temp.-High Press. **9**, 545 (1977).

136 Kauzmann, W., Chem. Rev. **43**, 219 (1948).

137 Angell, C.A., J. Res. Natl. Inst. Stand. Tech., **102**, 171 (1997).

138 DiMarzio, E. A., Gibbs, J. H., J. Chem. Phys., **28** (5), 807 (1958).

139 DiMarzio, E. A., Gibbs, J. H., Fleming, P. D. III, Sanchez, I. C., Macromolecules, **9**, 763 (1976).

140 Hilden, L. R., Morris, K. R., J. Pharm. Sci., **93** (1), 3 (2004).

141 Adam, G., Gibbs, J. H., J. Chem. Phys., **43**, 139 (1965).

142 Laschitsch, A., Bouchard, C., Habicht, J., Schimmel, M., Rühe, J., Johannsmann, D., Macromolecules, **32**, 1244 (1999).

143 Kumar, V., Suh, N.P., Polym. Eng. Sci., **30**, 1323 (1990).